UNIVERSITÀ CAMPUS BIO-MEDICO DI ROMA

FACULTY OF ENGINEERING

DOCTORAL THESIS

Inertial Sensing for Human Activity Recognition and Personal Indoor Localization

A thesis submitted in fulfilment of the requirements for the degree of

Doctor of Philosophy

in

Biomedical Engineering

Author:
Eng. Francesca DE CILLIS

Supervisor:
Prof. Roberto SETOLA
Coordinator:
Prof. Giulio IANNELLO

March 18, 2016

.

In the last few years, the interest in tracking people's habits and behaviour found even more interest among the scientific and industrial community. Monitoring people conditions, understanding their necessities and demands represent key values in a wide variety of fields. Nevertheless, healthcare, assistance and safety are possibly the fields that most actively leverage the knowledge gained from the analysis of the human behaviour. For these reasons, the automatic recognition of human physical activities, commonly referred to as Human Activity Recognition (HAR), has emerged as a key research area in the fields of human-computer interaction, mobile and ubiquitous computing.
Depending on the specific application domain, the inference of human behaviour could be assessed in different ways; however, the revolution that have undergone the class of inertial sensors in the last decades, has elected on-body inertial sensing to be the most prevalent monitoring technology in the HAR field. Integrating accelerometers, gyroscopes and compasses, the inertial sensor is able to measure physical quantities thus tracking body motion, in principle, without restrictions.
Despite the proven research interest among the topic, on-body inertial sensors HAR applications are still far from being mature. There is indeed a number of open challenges that spans from signal processing and sensor fusion to the improvement of existing algorithms and expansion to unexplored application areas.

The objective of this work consists into improving the current state of the art in the inertial-based HAR field.
As the first research focus, the dissertation examines the current state of the art in the field of HAR systems for gait assessment. Walking represents one of the most important daily activity and has significant influence on the quality of life. At the same time, it represents the function at the basis of several HAR application fields (healthcare, safety & security, sport and entertainment). In this context, we presents a pervasive solution for gait patterns classification that uses data retrieved from a waist-mounted inertial sensor. The proposed algorithm has been conceived to operate continuously for long term applications. In contrast to classic approaches that use a large number of features and sophisticated reasoners, our solution is able to assess 4 different gait patterns (standing, level walking, stair ascending and descending) by using only 3 features and a light classifier.

A leading HAR application field strongly related to the gait assessment is the personal Indoor Localization and Positioning (ILP) field. Tracking the pose of a user moving into indoor environments may indeed be useful in several contexts (special population care, key building management, retail industry, etc.), but is definitively crucial in case of emergencies. Given this demand, the second goal of this work is devoted to illustrate the HIPS, an hybrid indoor positioning system. Integrating inertial navigation and exteroceptive sensors, the HIPS is able to overcome typical limitations arising from the individual implementation of a single approach, providing a user position estimate with a room-level accuracy.

Apart from tracking human conditions, detecting anomalous behaviour represents another key-research area in the HAR field. Concerning healthcare, a typical example of such applications is represented by fall detection systems. Falls can potentially cause severe physical injuries and can reduce the independence of older individuals through dramatic psychological consequences. These findings called for the development of pervasive and easy-to-use assistive devices for fall detection.
The third and last goal of this work is indeed devoted to illustrating the FALLEN, an algorithm that uses accelerometer and gyroscope data retrieved from a waist-mounted inertial sensor for detecting falls. Integrating acceleration and gyroscope data, FALLEN

enables to overcome the limitations of classic approaches and allows differentiating falls from typical daily activities, increasing the overall system's accuracy without affecting the computational load.

Contents

Part I

Background & Motivations

Chapter 1

Introduction

This chapter provides an introduction to the thesis by briefly explaining the context in which the present work has been carried out, exposing the current challenges and stating the goals of the research. In this setting, the main contributions are presented and the organization of the material is outlined.

1.1 The human activity recognition

During the last 20 years, a tremendous interest in the evaluation of people's habits and daily routines has awakened [1]. The analysis of human behaviour has been demonstrated to be of key value to better understand people's necessities and demands. This understanding is of utility in a wide variety of fields, from education, medicine or sociology, security and safety to gaming or other kinds of industries with a demonstrated potential impact on society.
Nevertheless, health-care, assistance, wellness and safety are possibly the fields that most actively leverage the knowledge gained from the analysis of human behaviour. Here, the use of this information is, for example, devised for people's health empowerment or safety. Promoting healthier lifestyles (e.g., encouraging exercising), preventing unhealthy habits (e.g., tobacco use or unwholesome food), detecting anomalous behaviours (e.g., fall detection) or tracking conditions (e.g., mobility worsening due to ageing in healthcare or the first aid staff localization in unknown indoor environments for security applications) are different applications which may profit from the inference of human behaviour.
For these reasons, the automatic recognition of human physical activities, commonly referred to as Human Activity Recognition (HAR), has emerged as a key research area in human-computer interaction, mobile and ubiquitous computing in the last few years. One goal of the HAR systems is to provide information on a user's behaviour that allows computing systems to pro-actively assist users with their tasks [1].

The inference of human behaviour and activities could be performed in different ways and the methodology used depends on the specific application domain. For example, in the medical field the mobility-related activities monitoring for people affected by chronic diseases, as stated in [2], could be assessed by the use of questionnaires, interviews or a diary. However, these methods are mostly retrospective and contain a subjective judgement which leads to a certain amount of imprecision causing limited reliability.
A suitable alternative to self-assessment methods is represented by the use of specific sensors and devices. From a historical point of view, the computer vision has been the forefront of this application domain. A large number of researchers investigated machine recognition methods of gestures and activities from still images and video

in constrained environments or stationary settings. Nevertheless, structured environments limit the monitoring areas/time and are not well-suited for continuous applications [1].
Efforts to recognise activities in unconstrained daily life settings caused a shift towards using inertial sensors worn on the body, such as accelerometers or gyroscopes. Advances in sensor technology now allow for form factors and battery lifetimes suitable for long-term recordings, computing, and continuous interaction on the move. On-body sensing extends the potential application areas of activity recognition beyond instrumented rooms and promises to provide smart assistance and interfaces virtually anywhere and at any time by observing activities from the user's perspective.
At the end of the 90's, researchers performed the first feasibility studies on activity recognition using body-worn sensors [3]. Bouten et al. [4] were pioneers in remote monitoring of physical movement by conceiving a device comprised of a single tri-axial accelerometer and a data processing unit which could be used to assess physical movement via human body accelerations. Their work established a significant relationship (r = 0.89) between accelerometry and energy expenditure, which became the impetus for the wearable sensor revolution that followed.
The continuing success of activity recognition motivated steps towards more challenging and application-oriented scenarios [1].
Several real-world domains were identified that would clearly benefit from activity recognition, such as the industrial sector (for monitoring activities in automotive production facilities [5, 6], for tracking human in unknown indoor environment and/or robotics platform in industrial settings and assist human-robot interaction[7]), office scenarios, the sports & entertainment sector [8], healthcare.
Specifically, the Activities of Daily Living (ADLs) [9] attracted a great deal of interest. Monitoring daily activity to support medical diagnosis, for rehabilitation, or to assist patients with chronic impairments were shown to provide key enhancements to traditional medical methods. Early assistance to encourage humans to adopt a healthy lifestyle was regarded as another important goal. This led to a vast exploration of related human activities, (e.g. brushing teeth, hand washing, food intake, medication [1], indoor localization or transportation routines [10].
Recently, activity recognition made its debut as a key component in several consumer products. For example, game consoles such as the *NintendoWii* or the *Microsoft Kinect* rely on the recognition of gestures or even full body movements to fundamentally change the game experience. While originally developed for the entertainment sector, these systems have found additional applications, such as for personal fitness training and rehabilitation, and also stimulated new activity recognition research. Finally, some sports products such as the Philips *DirectLife* or the *Nike+* running shoes integrate motion sensors and offer both amateur and professional athletes feedback on their performance.
All of these examples underline the significance of human activity recognition in both academia and industry. Despite considerable advances in inferring activities from on-body inertial sensors and in prototyping and deploying activity recognition systems, developing HAR systems that meet application and user requirements remains a challenging task.

1.2 Current trends in the HAR field

HAR normally makes use of sensors on and around the subject to register their movements, while expert systems employ the monitored data to detect the performed activities. Although different methods and tools have been used both in academia and industries for HAR, on-body sensing proves to be the most prevalent monitoring technology.
On-body or wearable activity recognition systems normally consist of a set of sensors attached to the person's body that deliver signals (data streams) of diverse modalities [11]. Undoubtedly, one of the most important device family are inertial sensors (accelerometers, gyroscopes) that are commonly combined together as Inertial Measurement Units (IMU). Due to many positive characteristics, such as lightweight, small-size, low power consumption, portability and low-cost, inertial sensors have become widely used.
In the HAR field, particular attention is devoted to the problem of gait analysis since walking ability represents one of the most important vital functions that has significant influence on the quality of life.
Table 1.1 illustrates some of the main HAR application scenarios.

TABLE 1.1: Typical HAR application scenarios.

MEDICAL APPLICATION	- Monitoring & Diagnosis; - Rehabilitation; - Correlation between movement and emotions; - Child and elderly care;
HOME MONITORING AND ASSISTED LIVING	- Tracking, monitoring and emergency help; - Assistance for people with cognitive disorders; - Assistance for people with chronic conditions;
SPORTS AND LEISURE APPLICATIONS	- Daily sports activities; - Sports performances; - Quality of the activity performed.
SECURITY & SAFETY	- biometry; - indoor positioning for first aid staff, patients with Parkinson disease.

Inertial sensors can measure single or multi-point motion trajectories of single or multiple body segments of the subject during gait. During the measurement period, uni/multivariate signals are acquired that provide instantaneous information on measured quantity (i.e., spatial accelerations and angular velocity when using tri-axial sensors). In this manner, subject's gait can be assessed in terms of gait parameters that can be interpreted in several ways, depending on the specific application field which the analysis is devoted.
Furthermore, it should be mentioned that the development of inertial sensor-based human HAR approaches emerged simultaneously with the wide occurrence of ubiquitous smart devices, especially Smart-Phones (SPs) and tablets. Nowadays, integration of inertial sensors in smart devices has become a standard.
As stated in [12], there is a large pool of potential users that possess, carry and use smart devices on a daily basis. In 2012, In-Stat reported that by end of 2015, 65% of the U.S. population will own a tablet or a smart-phone having inertial sensors integrated [12]. It can be assumed that actual number has surely overreached these expectations.
Second, inertial sensors as a part of smart devices are powerful tool and are not longer strictly limited to support simple and trivial task only (i.e., tilt estimation) as it was

primarily intended at their appearance due to several limitations (energy efficiency, computational power, data transfer bandwidth and cost, storage) that were partly or fully overcome recently with the latest achievements in the field of pervasive computing. Inertial data acquired by sensors in ubiquitous smart devices can be used in order to assess users motion in advanced manner, including localization as one of the most intriguing challenges recently, as well as activity recognition and advanced motion analysis including gait. Such approaches have been examined in several areas, mostly in sports (i.e., step count and gait speed estimation), clinical applications (assessment of user's health state based on gait abnormalities, fall detection, etc.) and security (personal indoor positioning system). Thus, the assumption that gait recognition relying on inertial data acquired by using ubiquitous smart devices has become reasonable and has been addressed by many research groups recently [12].
Nowadays, with appearance of ubiquitous devices, including sensors, smart devices (SPs, tablets) as well as small and wearable single-board computing systems, pervasive computing has become indispensable in this context. One of the most important aspects of pervasive computing is inter-connectivity and inter-operability of ubiquitous devices. Such concept is also known as Internet of Things (IoT) with main purpose of integrating intelligent devices, technologies on several levels, including data, communication, decision-making and application level. IoT goes hand-in-hand with cloud computing, represented as the computation paradigm of the future. In this manner, connectivity is the most important issue that needs to be resolved. However, last-generation ubiquitous devices, including their performance and autonomy, ensure efficient data processing and communication with cloud system that relies on the bandwidth and cost of data transfer. Thus, such paradigm is expected to become completely feasible in the next feature since trends show that ratio bandwidth-cost is growing significantly.

Considering these factors, inertial sensors as a significant part of ubiquitous devices should strengthen their role as they can be applied for more complex tasks that are performed continuously. In this context, the approaches that allow for advanced motion analysis based on inertial data should be taken into careful consideration.
The rising attention gained from the field of inertial sensor-based HAR systems is also

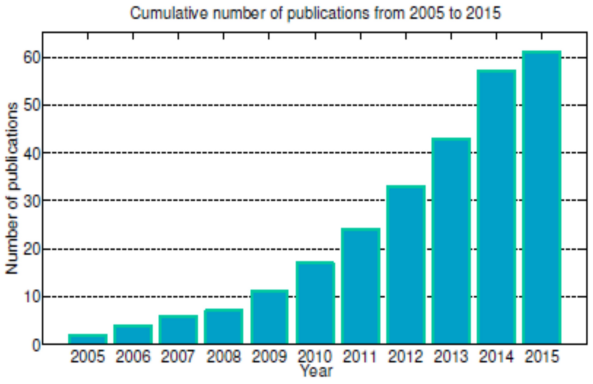

FIGURE 1.1: Number of papers in the area of inertial sensor-based HAR systems published in the last decade (Source [12]).

demonstrated by the increasing number of scientific publication on the topics. Figure 1.1 shows the cumulative number of publications in last decade on the inertial-based HAR systems topic (as stated by Sprager et al. in [12], please note that for 2015 only the first half of year is considered). It can be concluded that the inclination in the number of

papers is tightly connected with the popularity and wide usability of inertial sensors, especially as a significant part of smart devices. These ubiquitous devices hand-in-hand with the willingness of the users for their frequent use is a strong foundation for the wide applicability of HAR in the practical purposes.

1.3 Research challenges in HAR systems

Although activity recognition shares many methodological challenges with other fields, such as pattern recognition, computer vision, natural language processing or speech recognition, it also faces a number of unique challenges and requires a dedicated set of computational methods that extend on those developed in these fields. For example, computer vision and speech recognition can lend themselves on clear problem definitions, and focus on a well-defined and fixed sensing system, i.e., a defined number and type of cameras or microphones.
In contrast, HAR offers more degrees of freedom in terms of system design and implementation. In the HAR field, there is no common definition, language or structure of human activities that would allow formulating a clear and common problem statement (which activity has to be recognised, how a specific activity is characterised, etc.). For some applications, such as long-term behavioural monitoring, relevant activities can often not even be clearly defined upfront. To mention that human activity may be highly diverse upon different subjects and its recognition therefore requires careful selection of several heterogeneous specific features able to overcome the aforementioned limitation in HAR systems.
Apart from the activities to be classified and the specific technology on which the HAR system is based on, according to [1] in this section the main research challenge in the HAR field are illustrated.

1.3.1 Common research challenges

Intra-Class Variability. The first challenge that HAR shares with general pattern recognition is to develop recognition systems that are robust to intra-class variability. Such variability occurs because the same activity may be performed differently by different individuals. Intra-class variability can also occur if an activity is performed by the same individual. Several factors can effect the performance of the activity, such as stress, fatigue or the emotional or environmental state in which the activity is performed.
To address this issue one can either increase the amount of training data or develop person-independent features that are robust to this variability. Nevertheless, person independent systems may require a large number of features, contributing to both system complexity and computational burden. For these reasons, the design of the HAR system has to be subject to a delicate trade-off between using a highly specific and discriminative feature set, and a feature set that is more generic and therefore potentially less discriminative, but also more robust across different individuals.

Inter-Class Similarity. An inverse challenge is given by classes that are fundamentally different but that show very similar characteristics in the sensor data. Such close similarity can often only be resolved by using additional cues captured by different sensor modalities or by analysing co-occurring activities [1].

The NULL Class Problem. Typically, only a few parts of a continuous data stream are relevant for HAR systems. Given this imbalance of relevant versus irrelevant data, activities of interest can easily be confused with activities that have similar patterns but

that are irrelevant to the application in question, the so called NULL class. The NULL class problem is an active area of research. Several approaches have been proposed in literature for identifying the NULL class [1]; some of them exert the signal variance or make the use of thresholding approach to filter out outliers from the raw signal.

1.3.2 Challenges specific to HAR

Definition and Diversity of Physical Activities. The first challenge specific to the design of HAR systems is to develop a clear understanding of the definition of the activities under investigation and their specific characteristics. Human activities are highly complex and diverse and an activity can be performed in many different ways, depending on different contexts and for a multitude of reasons.
In addition, while state-of-the-art systems achieve decent performance on many activity recognition tasks, research so far mainly focuses on recognising "which" activity is being performed at a specific point in time. In contrast, only little work investigated means to extract qualitative information from sensor data that allow one to infer additional activity characteristics, such as the quality or correctness of executing an activity. Qualitative assessment is indeed more challenging to perform automatically and has so far only been demonstrated for constrained settings, such as in sports [1]. For general activities or physical behaviours, activity recognition research is still far from reaching a similar understanding.

Class Imbalance. A related challenge is that of modelling different activity classes in the face of considerable class imbalance. For many activity recognition problems, such as for long-term behavioural monitoring, only few activities occur often (e.g., walking, sitting, etc.), while most activities occur rather infrequently (e.g., brushing teeth, falling, etc.).

Ground Truth Annotation. Another challenge for supervised HAR recognition tasks is the collection of annotated or "ground truth labelled" training data. Ground truth annotation is an expensive and tedious task, as the annotator has to perform the annotation in real-time or to skim through the raw sensor data and manually label all activity instances post-hoc. In addition, motion data recorded from an accelerometer or gyroscope, is often more difficult to interpret than data from other sensors, such as cameras.
In daily life settings, ground truth annotation is a far more difficult problem. Researchers have investigated different techniques to address this problem, including daily self-recall methods, experience sampling [1], as well as reinforcement or active learning, all of which involve the user.

Data Collection and Experiment Design. Finally, there are also experimental challenges associated with data collection and the evaluation of HAR systems in real-world environments. One challenge is to collect data sets on which HAR systems can be evaluated. This challenge arises from the fact that, in contrast to other research fields such as speech recognition or computer vision, the research community in activity recognition has not yet started a joint effort to collect rich and thus more general-purpose data sets of human physical activity, nor has it agreed on the scientific value of collecting them. This challenge is intensified because data collection may focus on quite diverse requirements, such as high data quality, large numbers of modalities or sensors, long-term recordings, or large numbers of participants. Using standard data sets is crucial for reproducible research and is becoming increasingly important in HAR as a research discipline. Second, to properly design and conduct a HAR experiment is also more

difficult than it may at first seem. Researchers are faced with a trade-off between unobtrusiveness and ease of use of the sensors; the time required to prepare, conduct, and maintain the experiment; and the logistics and costs for participants, experimenters, and the equipment.

1.3.3 Application challenges

Variability in Sensor Characteristics. A practical challenge for implementing HAR in real world applications is caused by the sensing equipment, more specifically the variability in sensor characteristics. This variability may have internal and external causes. Internal causes are hardware features (sampling rate, resolution), crude assembling (i.e., axis misalignments) that may contribute to errors.
External causes may include changes in the operating conditions. Some sensors are particularly sensitive to the environment, such as magnetometers that are sensitive to ferromagnetic influences. Finally, portable devices containing sensors, such as mobile phones, may be used in different ways or carried at different locations on the body. Sensor displacement and changes in sensor orientation can be detected if they cause obvious differences in the recorded signals. Subtle deviations over time, such as signal drift, are much more difficult to identify.

Technology limitations. Many challenges arise from bringing machine learning to smart devices. Most of the known machine learning algorithms to date have been designed to run on powerful computers and do not adapt well to resource constrained devices such as SPs. It is important to design mobile sensing applications for SPs while meeting the phone user experience requirements, e.g., the ability to make and receive calls, an acceptable battery duration and the trade-off between inference responsiveness, and phone resource usage[1]. It is also necessary to identify new approaches that are less resource demanding and suitable for the limited resources available on SPs.

Privacy and Security. Sensitive user information should be retrieved without invading users private life and should be transmitted and stored with strong cryptography which requires computational power.
One way to meet this requirement without affecting computational burden, is to operate as much as possible on the smart device for feature extraction, without exposing the raw data to the external world and communicating only the features or the result of the inference to external entities. Nevertheless, running feature extraction on the smart device implies the need to identify features that require low computation (compared to the complex features extracted on server machines), yet are effective to produce accurate machine learning models. These observations, combined with the facts that battery capacity increase is slower than smart devices computation growth, and that wireless transmission is one of the main causes of battery drain, demand frameworks that rely on split techniques that distribute and trade-off local (on the device) versus remote (on the server) computation.

1.4 Research goals & contributions

The main objective of this work is to improve the current state of the art in the inertial-based HAR field.

[1]Inference responsiveness refers to the time needed to compute the inference labels, while resource usage is a parameter that quantifies the impact of the mobile sensing application on the smart-phone CPU, RAM, and battery life

The first goal has been devoted to the development of an algorithm for gait patterns classification by means of a waist-mounted inertial sensor. As stated, in the inertial-sensing HAR field a great emphasis is devoted to the problem of gait analysis. Walking indeed represents one of the most important activity that has significant influence on the quality of life and represents, at the same time, the function at the basis in several HAR application fields (healthcare, safety & security, sport and entertainment).
Specifically, the proposed solution for gait assessment has been conceived for long term applications to operate continuously. Stated that smart devices represent the elected running platforms for HAR systems in the next future, during the algorithm design several methodologies have been contemplated in order to meet power saving strategy and to limit computational burden. In contrast to typical approaches proposed in literature that use a quite large number of features and sophisticated classifier, the proposed solution is able to assess 4 different gait patterns (standing, level walking, stair ascending and descending) by using only 3 time-domain features and a light classifier.

A leading HAR application field strongly related to the gait assessment is represented by the personal Indoor Positioning and Localization (ILP) field. In general, an indoor localization system is devoted to track the pose (i.e., position and orientation) of a user moving in the environment. The estimate of the user pose can be processed and made available either to the user itself or to position-based services such as navigating, tracking, or monitoring.
Over the past decade, ILP systems have gained great attention among the scientific community. Localization and tracking support is indeed useful in many contexts [13] (special population care, key building management, retail industry, personal service, etc.), but may be crucial into emergency applications: being aware about his/her position is essential for a first responders operating in large unknown indoor environments.
Although several ILP systems have been proposed in literature, to date there is not an out-of-box solution able to solve the indoor localization and tracking problem. Given this demand, the second goal of this work is devoted to illustrate the Hybrid Indoor Positioning System (HIPS), an hybrid indoor positioning system developed in collaboration with the Italian Fire Corps within two European research project.
Integrating inertial navigation and exteroceptive sensors pre-installed into the environment, the HIPS is able to overcome typical limitations arising form the individual implementation of a single approach and provides a user position estimate with a room-level accuracy. In the proposed approach, we use specific passive beacons (RFID passive tags) that do not require for power supplying and present good performances also in real-operating scenarios, yielding the system suitable for emergency applications.

Apart from tracking human conditions, detecting anomalous behaviour represents another key-research area in the HAR field. Provides suitable solutions able to identify unintended and unintentional actions may prove extremely useful in specific application domain. Concerning healthcare, a typical example of such applications is representing by fall detection systems. As sporadic human activity, falls are usually isolated event, nevertheless the prevalence of falls is very common among the elderly and increases with age. Falls can potentially cause severe physical injuries and can reduce the independence of older individuals through dramatic psychological consequences. Moreover, most dramatic effects resulting from falls are usually related with long lying periods (i.e., remaining on the floor for prolonged periods after a fall) which lead to an increased risk of pneumonias, pressure ulcers and even death.
Although a number of fall-detection algorithms and methods do currently exist, none of these solutions is universally accepted. These findings called for the development of

pervasive and easy-to-use assistive devices for fall detection.
The third and last goal of this work is indeed devoted to illustrating the FALLEN (FALL dEtecioN algorithm), an algorithm that uses accelerometer and gyroscope data retrieved from a waist mounted IMU for detecting falls. Typical inertial-based solutions for fall detection commonly use the solely accelerometer data and are not able to effective discriminate between falls and typical ADLs presenting similar acceleration patterns (e.g., running or lying on the back). Integrating acceleration and gyroscope data, FALLEN enables to overcome the aforementioned limitations and allows differentiating falls from typical ADLs, increasing the overall system's accuracy without affecting its computational load.

1.5 Outline of the work

This dissertation is organized in two parts. Part I contains the background material to the research focus presented in Part II.
In Part I, Chapter 2 presents a general overview about the inertial-sensing HAR methods. The chapter opens illustrating the typical activities under investigation in the HAR field, distinguishing them according to different taxonomies proposed in literature. After a brief description about activities, the chapter continues presenting different methods commonly implemented in HAR systems. Focusing on those exerting the use of inertial sensing, following sections provide general remarks about the so-called Activity Recognition Chain (ARC). In general, an ARC is a sequence of signal processing, pattern recognition and machine learning techniques that implements a specific activity recognition system behaviour. It consists of several stages or phases: data acquisition, signal pre-processing, signal segmentation, feature selection & extraction, classification. Aim of the last part of the Chapter 2 is to give a general overview about the main methodologies proposed in literature, according to the current state-of-the-art in the inertial sensing HAR field.

Part II is devoted to the ADL detection & classification and consists of the Chapter 3 and 4, and 5.
Chapter 3 concerns with the classification of periodic ADLs (i.e., walking). Specifically, it discusses about the DETECT (DEcision TrEe for gait patterns ClassificaTion), our proposed solution for the gait assessment. The chapter starts illustrating current trends and research challenges in the field of inertial sensing gait analysis that motivate us to the design and implementation of DETECT. Then, a comprehensive description about the main features of each stage of DETECT according to the ARC follows. The chapter closes with a discussion about the results inferred from experimental trials and future developments.

Chapter 4 concerns with ILP tasks. Specifically, the chapter aims at presenting the current state of the art in the ILP field and our solution, the HIPS. After a comprehensive overview about different methodologies for ILP systems proposed in the last few years, the first part of the chapter is devoted to illustrates the main drawbacks of current solutions and the leading requirements of an ILP system specifically conceived for emergency applications. Then, the HIPS architecture is illustrated and the different part composing the system are described.
The core of the HIPS is the *Tracking System*: this is based on a prediction-correction schema, according with the commonly approach used in robotics, where both proprioceptive and exteroceptive sensors are jointly used for localization and tracking purposes.

The chapter illustrates the main peculiarities of both the *prediction* and *correction* phase. The algorithms implemented and main experimental results are described and commented.

Chapter 5 is devoted to the identification of sporadic activities, such as falling. It presents the main features about FALLEN, our proposed algorithm for falls detection. The chapter starts with a brief description about the current state of the art in the fall detection field, trying to highlight main concerns and open issues. The chapter carries out with FALLEN main features in relation to all the stage of the ARC, and closes showing some experimental results achieved during the testing phase.

Finally, Chapter 6 concludes the dissertation.

Chapter 2

Inertial-Based HAR systems: a general overview

This chapter presents a general overview about the inertial-sensing HAR methods. Section 2.1 illustrates typical activities under investigation in the HAR field, distinguishing them according to different taxonomies proposed in the literature. Section 2.2 presents different methods commonly used in academia and industry for the implementation of HAR systems, focusing on those exerting the use of inertial sensing.
Sections 2.3 provides the general outline of the so-called Activity Recognition Chain (ARC), that represents the set of machine learning techniques commonly used in the inertial-sensing HAR field for the implementation of a specific activity recognition system. Each stage of the ARC is then described, providing an overview of the most commonly used techniques; specifically, data acquisition and pre-processing are presented in Section 2.3.1, segmentation methodologies are illustrated in Section 2.3.2, features selection & extraction procedures are described in Section 2.3.3 and classification approaches are provided in Section 2.3.4.
The chapter closes with a brief overview about the inertial sensing platform, providing basics about the working principles of each sensor integrated into the platform and technical specifications about inertial sensors used for data collection during trials.

2.1 Human activities taxonomies

Apart from the specific activity and the technology used, HAR systems aim to correctly classifying input data into underlying activity categories. A first challenge in the design of HAR systems consists in the definition of the activity to be classified. Several taxonomies have been proposed in the literature for the categorization of human activities. The nature of the proposed approaches for activities classification, usually depends on the specific context in which the human activity is analysed. To note that in this section are mentioned only those categorizations useful for the purpose of this work. A full dissertation on the topic can be found in [14, 15, 16, 17, 18].
A straightforward categorization for activities pertaining inertial-based HAR systems is that proposed by Vrigkas et al. in [14]. Here, depending on their complexity human activities are categorized into: (i) gestures, (ii) atomic actions, (iii) human-to-object or human-to-human interactions, (iv) group actions, (v) behaviours, and (vi) events. Figure 2.1 illustrates the decomposition of human activities according to their complexity.
Gestures are considered as primitive movements of the body parts of a person that may correspond to a particular action of an individual [19]. Atomic actions are movements of a person describing a certain motion that may be part of more complex activities [20]. Human-to-object or human-to-human interactions are human activities that involve two or more persons or objects [21]. Group actions are activities performed by

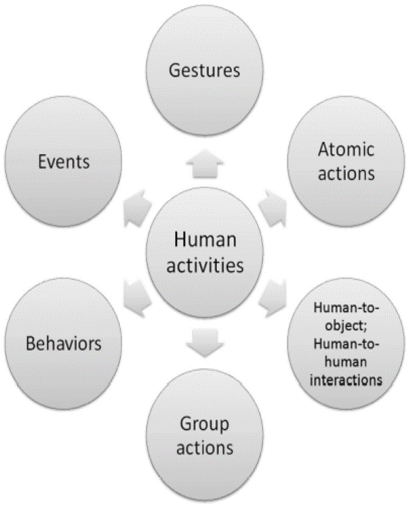

FIGURE 2.1: Categorization of human activities (Source [14]).

a group or persons [22]. Human behaviours refer to physical actions that are associated with the emotions, personality, and psychological state of the individual [23]. Finally, events are high-level activities that describe social actions between individuals and indicate the intention or the social role of a person [24].
Focusing the attention on atomic actions, an important class of activities in healthcare and assisted living are the so-called Activities of Daily Living (ADLs). The ADLs acronym is commonly used in several applications domains as an umbrella term relating to self care, comprising those activities or tasks that people undertake routinely in their every day life. Originally proposed by Katz et al. in 1963, they have evolved into a standard set of activities used by physicians and care-givers as a measure to estimate the physical well-being of elderly patients, as well as their need for assisted living. The core set of ADLs consists of the activities bathing, dressing, toileting, transferring, continence, and feeding. The set of ADLs is complemented by the so-called Instrumental ADLs.
More specifically, activities can be subdivided into personal care or Basic ADLs (BADLs) and domestic and community activities, IADLs. Hall et al. [25] suggested that the BADL term *"is typically restricted to activities involving functional mobility (ambulation, wheelchair mobility, bed mobility and transfers) and personal care (feeding, hygiene, toileting, bathing and dressing)"*. Whilst an early definition of IADL comes from Katz [9] who stated that "*...instrumental activities of daily living functions are concerned with a person's ability to cope with her/his environment in terms of such adaptive tasks as shopping, cooking, housekeeping, laundry, use of transportation, managing money, managing medication and the use of the telephone"* [26].
Still referring to ADLs taxonomy, an alternative categorization approach is proposed in [1], where ADLs are classified depending on their specific nature in *periodic* and *sporadic* activities. In this context, *periodic activities* are those actions that exhibit periodicity (such as walking, running, rowing, biking, etc.), while *sporadic activities* are those that occur sporadically, that is interspersed with other activities or gestures (e.g., brushing teeth, falling, answering at the phone, etc.).
Although the categorization between ADL and IADL is purely formal, the activities classification into periodic and sporadic has an impact on the HAR system design. The activity recognition process may presents different peculiarities for the so-called ARC,

depending on the specific nature of the activity under investigation.

2.2 HAR methods

As for the human activities classification, several classification criteria have been proposed in the literature for HAR methods. A general classification criterion proposed by Vrigkas et al. in [14] categorized the HAR methods into two main categories: (i) uni-modal and (ii) multi-modal activity recognition methods, according to the nature of sensor data the method employs. According to [14], each of these two categories is further split into sub-categories depending on how human activities are modelled. A hierarchical classification of HAR methods on the light of this taxonomy is depicted in Figure 2.2.

Uni-modal methods represent human activities from data of a single modality (such as

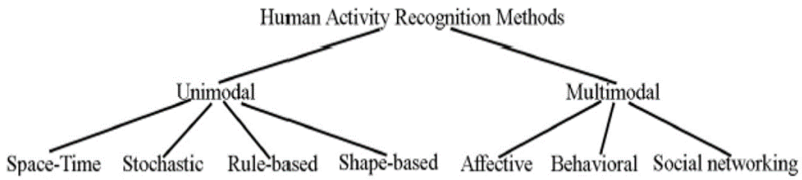

FIGURE 2.2: Hierarchical categorization of human activities recognition methods (Source [14]).

images, acceleration, etc.) while multi-modal methods combine features collected from different sources. Inertial-based HAR system belong to the first category, so further analysis are limited to uni-modal methods. For a complete dissertation on the topic, one can refer to [14] and related works.

Concerning uni-modal methods, they can be further categorized as: (i) space-time, (ii) stochastic, (iii) rule-based, and (iv) shape-based methods.

Space-time methods involve activity recognition methods, which represent human activities as a set of spatio-temporal features. Stochastic methods recognize activities by applying statistical models to represent human actions. Rule-based methods use a set of rules to describe human activities. Shape-based methods efficiently represent activities with high-level reasoning by modelling the motion of human body parts.

To note that rule-based and shaped-based methods are widely used in computer vision for HAR by means of still images and/or videos.

Concerning wearable solutions, the approaches definitely more widespread are the space-time methods. Apart from human activities to be classified, space-time methods for inertial-based HAR systems present some typical phases that contribute to set-up the ARC [11, 1, 12, 27]. A complete discussion about the ARC steps and their main characteristics for inertial-based HAR systems is presented in next sections.

2.3 The activity recognition chain: a state-of-the-art

In general, an ARC is a sequence of signal processing, pattern recognition and machine learning techniques that implements a specific activity recognition system behaviour. In general, an ARC bears strong similarity to general-purpose pattern recognition systems but also has a number of specific requirements and constraints [1]. Typical ARC phases are: data acquisition, pre-processing, segmentation, features extraction

and classification. Figure 2.3 outlines the main steps of the general ARC.
Input to the ARC are streams of sensor data acquired using single/multiple body-worn

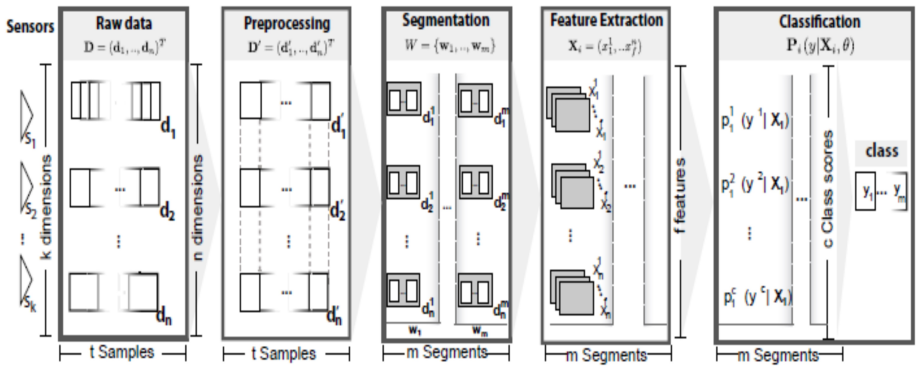

FIGURE 2.3: The typical ARC work-flow for wearable-sensors HAR systems: data acquisition, signal preprocessing and segmentation, feature extraction and selection, and classification. Raw signals (D) are first processed (D_0) and split into m segments (W_i) from which feature vectors (X_i) are extracted. Signal is then classified with specific labels, accordingly to the feature vector (X_i).

inertial sensors. The sensor data is first preprocessed to filter out signal variability or artefacts. The processed data is then segmented into sections of interest that are likely to contain an activity or gesture. Afterwards, features that capture the activity characteristics are extracted from the signals within each segment. In training mode, the extracted features and corresponding ground truth class labels are used as input to train a classifier model in the training stage. To note that the classification mode can be executed in two different modalities depending on the nature of the classification algorithm. If supervised classification algorithms are used, the features and a previously trained model are used to calculate a score for each activity class and to map these scores into a single class label in the classification stage. Unsupervised classification doesn't require a dedicated training step; in this context, activities classification is inferred directly from the sensor data.

The great interest gained by the inertial-based HAR field in the last few years has been chased by several solutions for the ARC problem, proposed by academic and industrial researches all around the world. For the same activities under investigation, several methods for each step of the ARC have been proposed and the corresponding literature is extremely broad.
For these reasons, next sections would provide a general overview on the topic. Without going into details, we illustrate current trends in the inertial-sensing HAR attempting to reasoning the selected option for the proposed solutions.
For a complete dissertation, please refer to [1, 27, 28, 3, 29, 12, 30]

2.3.1 Data acquisition and pre-processing

In the first stage of a typical ARC, raw data is acquired using one/several sensor/s attached to different locations on the body. Sensor/s placement represent the first design choice in a HAR system. Wearable sensors placement has indeed a direct effect on the measurement of bodily motions; nevertheless the ideal sensor location for a specific

application is still a subject of much debate [27]. Figure 2.4 illustrates typical sensors position in a HAR system.

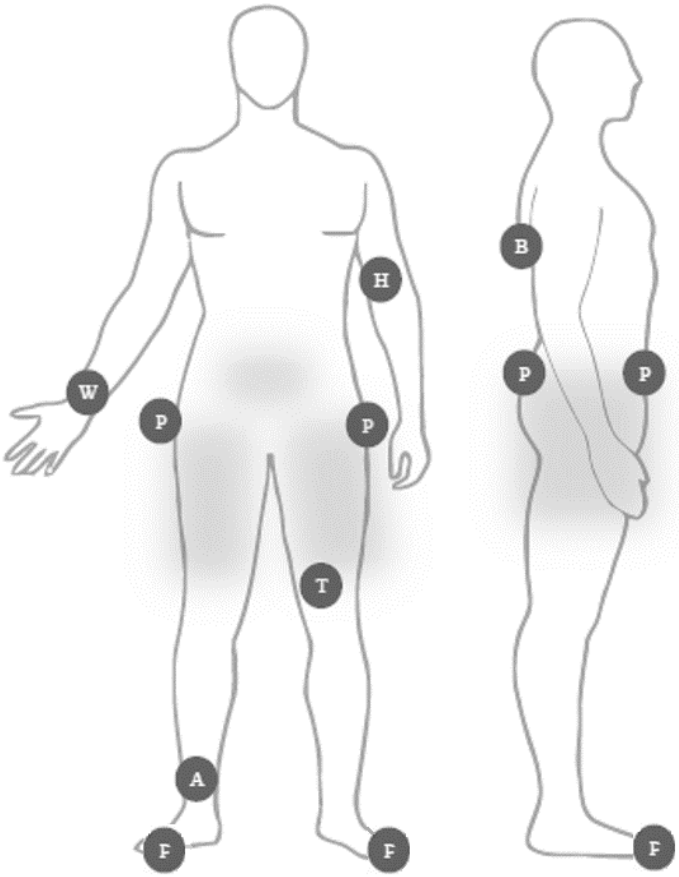

FIGURE 2.4: Typical sensor placements in inertial-sensing HAR systems. Shaded area represent the most frequently body district selected for potential sensors placement. Circles determine sensing positions that were used by typical experimental protocols that assumed controlled measuring conditions with these sensors usually firmly attached. B = back, H = arm, W = wrist, P = pelvis/pocket, T = thigh, A = ankle, F = foot. (Source [12]).

Wearable sensors can be placed on different body segments and districts. Specifically, one or more IMU/s and/or Smart-Phones (SPs) can be placed on the sternum, lower back [31], waist [32], [33], rear hip, neck, wrists, knees, and lower legs [28]), kept in a pocket [34] or on hand [29]. Waist-placement of the wearable sensors can better represent most human motions since they are then close to the center of mass of the human body [27]. Various studies have combined multiple accelerometers attached at different locations of the body. The majority of these studies highlight that the placement of many sensors can become burdensome for the wearer, leading us to focus on determining both the minimum number of sensors as well as their relevant placement, while still ensuring a sufficiently high activity recognition rate. Indeed, this rate decreases with the number of wearable accelerometers [27].
Although the type, the number and the placement of the sensors are important for ensuring relatively high rates of human activities recognition, some issues may be related to acceptance of such kind of sensors. For these reasons, it is usually preferable limiting

the number of sensors as well as selecting a comfortable device placement in order to promote the acceptance by the user.
Figure 2.4 illustrates an overview about the most used sensors placements for human activity recognition.

Once the platform is placed, the system is able to collect data continuously. Since some sensors can provide multiple values (e.g. an acceleration sensor provides a 3-D acceleration vector), or multiple sensors are jointly sampled, vector notation is used to describe the sensor's output:

$$s_i = (d_1, d_2, d_3, \cdots, d_t) \tag{2.1}$$

for $i = 1, \cdots, k$, where k denotes the number of sensors and d_i the multiple values at a time t. Each of the sensors is sampled at regular intervals, which results in a multivariate time series. Often, however, the sampling rates of different types of sensors can differ. For example, acceleration sampling rate usually relies between $10Hz \div 100Hz$, but sensors can also change their sampling frequency for several reasons (e.g., for power saving or due to requirements of the operating system). In any case, t may differ across $s_i(t)$ and synchronisation across multi-modal sensor data becomes a central technical issue.
Moreover, raw sensor data can be corrupted by artefacts caused by a variety of sources. The aim of the preprocessing stage is to synchronise and to remove such artefacts, and to prepare the acquired signals for feature extraction. It is important to note that this preprocessing is supposed to be generic, i.e., it should not depend on anything but the data itself. It should not, for example, be specific to any particular person. The preprocessing stage transforms the raw multivariate and non-synchronous time series data into a pre-processed time series D':

$$D' = \begin{pmatrix} d_1'^1 & \cdots & d_1'^t \\ \vdots & \ldots & \vdots \\ d_n'^1 & \cdots & d_n'^t \end{pmatrix} = (\mathbf{d_1'}, \ldots, \mathbf{d_n'})^T \tag{2.2}$$

where $d_1'^1$ corresponds to one dimension of the preprocessed time series, n to the number of total data dimensions, and t to the number of samples. The transformation aims to enhance the robustness of the extraction by applying signal processing algorithms that reduce noise or filter out artefacts. At the same time, these algorithms need to preserve those signal characteristics that carry relevant information about the activities of interest. Preprocessing of acceleration signals may involve calibration, unit conversion, normalisation, re-sampling, synchronisation, or signal-level fusion [1].
Several approaches have been proposed in the literature to filter out potential disturbances and outliers in the acceleration signals. Almost always, high frequency noise in acceleration data needs to be removed [28]. Therefore, non-linear, low-pass median, Laplacian, and Gaussian filters can be employed for removal of high-frequency noise. In some cases, gravitational acceleration has to be extracted from accelerometer data in order to analyse only useful dynamic acceleration. For this purpose, high-pass filters can be used to distinguish body acceleration from gravitational acceleration. Representation of raw data while preserving useful information is the key to efficient and effective solutions and it affects the overall performance and computation time of activity recognition systems.

2.3.2 Segmentation

After filtering, accelerometer data are usually partitioned into segments of data to capture the dynamics of the signal. The second stage of the ARC, the segmentation, corresponds to the process of dividing sensor signals into smaller data segments. Each data segment $p_i = (t_1, t_2)$ is defined by its start time t_1 and end time t_2 within the time series. The segmentation stage yields a set of segments P containing a potential activity x:

$$P = \{p_1, \ldots, p_m\} \tag{2.3}$$

Segmenting a continuous sensor stream is a difficult task. Humans perform activities fluently and consecutive activities blur into each other rather than being clearly separated by pauses. Another problem arises from the definition of an activity. Often, the exact boundaries of an activity are difficult to define.
In the literature, various methods exist to approach the problem of segmentation. Please refer to the review papers [11, 28, 1, 35] for a complete dissertation on the topic.
According to [11], most of the segmentation techniques could be categorized into three groups, namely *activity-defined windows*, *event-defined windows* and *sliding windows*.
The *activity-defined* windowing procedure consists of a partitioning of the sensor data stream based on the detection of activity changes. Initial and end points are determined for each activity, prior to explicitly identifying the specific activities. In the literature, diverse methods have been proposed to identify activity-transition points. For example, changes between activities could be identified through the analysis of variations in the frequency characteristics. This analysis has been performed by using wavelet decomposition [36, 37] to detect frequency changes for walking activities from a continuous record, by means specific heuristic methods [37] that differentiates among static and dynamic actions or in an off-line fashion for activities of a long duration [11]. Less obtrusively methods concern the use of external cues for the identification of the activity performed.

The *event-defined* approach consists of locating specific events, which are further used to define successive data partitioning. Since the events may not be uniformly distributed in time, the size of the corresponding windows is not fixed. As for the activity-defined approach, the events could be also identified through external mechanisms. The registration of these events could be, for example, performed through a stopwatch. Nevertheless, this kind of approach is restricted to laboratory settings or recognition under expert supervision, which is found to be of little use in real settings. Both activity-defined and event-defined methods are particularly interesting for spotting purposes; however, the size of the window normally determines that a subsegmentation process is required.

The *sliding window* approach, hereafter referred to as *windowing*, is the most widely employed segmentation technique in activity recognition. Its implementational simplicity and lack of preprocessing determines the windowing approach as ideally suited to real-time applications. To mention that the sliding window approach has been proven to be especially beneficial for the recognition of periodic (e.g., walking, running) and static activities (e.g., standing, sitting) and of questionable utility for the detection of sporadic activities. Sporadic activities may require indeed a more sophisticated segmentation process given their complex and interspersed nature.
In sliding windows, the signals are split into windows of a fixed size and with (Fixed size Non-overlapping Sliding Window, FNSW [35]) or without inter window gaps (Fixed size Overlapping Sliding Window, FOSW [35]). In the FNSW approach (see picture (a) in Figure 2.5), the end point of segmentation window N is the starting point

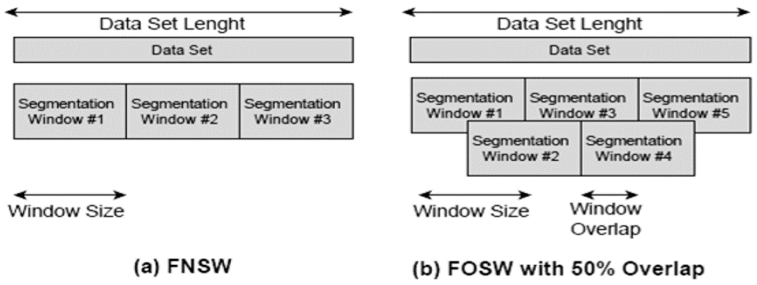

FIGURE 2.5: FNSW and FOSW approaches, respectively. (Source [35]).

for the window $N + 1$. The amount of windows generated (W_{FNSW}) for a given data set size is given by:

$$W_{FNSW} = \frac{S}{S_W} \tag{2.4}$$

S is the total number of signal samples, S_W is the amount of samples for each window defined as $S_W = fr * W_{size}$, where fr is the acquisition/re-sampling data rate and W_{size} is the selected window size.
The FOSW segmentation technique allows data overlap (see picture (b) in Figure 2.5 showing FOSW with an overlap of 50%). Depending on the percentage overlap, more or less data overlaps from window N into N + 1. The overlap between adjacent windows is also referred to as a window shift. A 0% overlap corresponds to the FNSW segmentation method, while an overlap of 100% would yield to a static window as it would not be shifted and the data would always be segmented at the exact same point. The number of segmentation windows (W_{FOWS}) generated can be computed as follows:

$$W_{FOSW} = \frac{S}{S_W - S_W * \frac{o\%}{100}} \tag{2.5}$$

with $o\%$ being the percentage overlap values. Typical overlapping parameters used in the literature are 25, 50, 75, and 90 [35, 11].

An overlap between adjacent windows is tolerated for certain applications; however, this is less frequently used. Concerning the window size, there is no clear recommendation in the literature. Several authors tested a range of 32 different sizes in the range of 0.5 to 24 s [35]. The use of longer window sizes (60 s [38] and 74 s [39]) is usually associated with the aim to only include single ADLs in each window to achieve the best classification results. Nevertheless, some authors supported the opinion that indicates a decrease in accuracy for window sizes above 8 s [35]. Furthermore, the authors belief is that most ADLs will only take a short amount of time and a maximum of 24 s should be sufficient to include at least two ADLs.

2.3.3 Features selection & extraction

In general, features can be defined as the abstractions of raw data and the purpose of feature extraction is to find the main characteristics of a data segment that accurately represent the original data. The transformation of large input data into a reduced representation set of features, usually referred to as *feature vector*, is called feature extraction. The feature vector includes important cues for distinguishing various activities and features are then used as inputs to classification algorithms [28].

TABLE 2.1: Main features used in the inertial-based HAR systems field. Source [28].

TYPE	FEATURE
TIME-DOMAIN	Mean
	Variance, Standard Deviation (SD), Mean Absolute Deviation (MAD)
	Root Mean Square (RMS)
	Zero crossing rate
	Derivative
	Peak count & amplitude
	Sign
FREQUENCY-DOMAIN	Discrete FFT coeffient
	Spectral centroid
	Spectral energy
	Spectral entropy
	Frequency range power
TIME/FREQUENCY DOMAIN	Wavelet coefficients
HEURISTIC	Signal Magnitude Area (SMA)
	Signal Magnitude Vector (SMV)

The total number of features extracted from the data (i.e., the length of the feature vector) form the so-called feature space. Generally speaking, the more clearly each activity can be separated in the feature space, the higher the achieved recognition performance. Ideally, features corresponding to the same activity should be clustered in the feature space, while features corresponding to different activities should be far apart. At the same time, the feature vector need to be robust across different people as well as to intra-class variability of an activity. Depending on the type of activities, these features may be extracted on over-segmenting windows (for repetitive activities) or on windows covering the entire activity or gesture (for non-repetitive activities) [1].
In general, regardless of the activities under investigation, relevant features are often unknown a priori. Usually, many candidate features are introduced to better represent the domain. Unfortunately many of these may be either partially or completely irrelevant/redundant to the target concept. In many applications, the length of the feature vector may be so large as to affect the classification process. Reducing the number of irrelevant/redundant features may drastically reduces computational time and burden of the classification step, yielding a more general concept [40]. As stated in [1], the higher the dimensionality of the feature space the more computationally intensive the classification. Particularly for real-time processing on embedded systems, the objective is to minimise memory, computational power, and bandwidth requirements. It is therefore important to use a minimum number of features that still allow the ARC to achieve the desired target performance.
Depending on the specific activity, several feature have been proposed in the literature. A rather widespread categorization method states features classification depending on the specific nature of the belonging domain. According to [28], Table 2.1 presents the most widely used features.

Time-domain features

Time-domain features include basic waveform characteristics and signal statistics [28]. They are directly derived from the data segment and the specific feature selected strictly

depends on the nature of the activity under investigation.
For example, Veltink et al. in [41] examined the mean and standard deviation, of the accelerometer signal to determine periods of static and dynamic activity. With the same purpose, variance and covariance of the acceleration vector have been widely used in the literature. Further mathematical operands and statistical features such as skewness, kurtosis, and eccentricity of the accelerometer signal have been largely employed in several works (see [42] for a survey on the topic) for discriminating specific dynamics activities, such as walking up and down stairs.

Frequency-domain features

Frequency-domain features focus on the periodic structure of the accelerometer signal [28]. In the HAR field, several data analysis has involved the use of frequency spectrum analysis and the examination of dominant frequencies using the Fast Fourier transforms (FFT). These traditional spectral analysis methods are able to compute the frequency components of a signal. Fourier analysis is a global tool providing a description of the overall regularity of a signal and copes with naturally occurring sinusoidal behaviour [42]. Other common computation tools in the frequency domain are the spectral energy (to distinguish sedentary activities from vigorous activities [43]) and the spectral entropy (to help discriminating the activities with similar energy values, as in [44]).

Time-frequency domain features

Time-frequency domain features are used to investigate both time and frequency characteristics of complex signals. Also known as Multi-Resolution Analysis (MRA) [42], this kind of investigation aims to overcome the shortfalls of frequency analysis. The Fourier transform is indeed not able to provide the time at which the different signal frequency components occurred. The MRA is a more comprehensive tool able to analyse the accelerometer signal in more detail (in both time and frequency). Time – frequency analysis is important especially in analysing non-stationary signals, i.e. where the frequency content changes over time. An example of a non-stationary signal includes the acceleration pattern during human movement, where varied accelerations with sharp high-frequency transients are present at certain time instances. As its name suggests, MRA analyses the signal at different frequencies with different resolutions. As human movement is generally associated with low frequencies (e.g., approximately 2.5 Hz for walking), MRA can be considered to be ideally suited for translating accelerometer data into comprehensive clinical terms (quantitative and qualitative data). Wavelet analysis with the Continuous and Discrete Wavelet Transform (CWT, DWT) are two such MRA techniques. Application of wavelet coefficient for HAR applications are illustrated in [42, 28, 37, 45, 32, 46, 33, 47, 48].

Heuristic features

Heuristic features are the features which have been derived from a fundamental understanding of how a specific movement would produce a distinguishable sensor signal [28]. The Signal Magnitude Area (SMA) of the acceleration signal have been widely used to discriminate between period of activity and rest in several works [35]. Yang et al. [43] use SMA to identify static and dynamic activities.

Alongside SMA, also the Root Sum of Squares (RSS, or Signal Magnitude Vector, SMV) of a tri-axial accelerometer output has been largely employed in the HAR field. For example, Bourke et al. [49] in their study of fall detection reached a very high detection accuracy by means of a threshold algorithm based on the acceleration SMV.
To mention that inter-axis correlation has been demonstrated to be especially useful for discriminating between activities that involve translation in just one dimension. Bao et al. [50] use the correlation between axes and achieve good results for distinguishing cycling from running.

2.3.4 Classification

In the classification step of the ARC, the selected features are used as inputs for the classification and recognition methods. Research in machine learning and computational statistics developed a large variety of inference methods.
In a machine learning context, patterns are to be discovered from a set of given examples or observations denominated *instances*. Such input set is called the *training set*. In the HAR field, each instance is a feature vector extracted from signals within a time window. Depending on the learning process, the examples in the training set may or may not be labelled, i.e., associated to a known class (e.g., walking, running, etc.). Labelled training data set are usually referred to as *ground truth*. In some cases, labelling data is not feasible because it may require an expert to manually examine the examples and assign a label based upon their experience. This process is usually tedious, expensive, and time consuming in many data mining applications [30, 1]. Table illustrates the most used approaches proposed in the literature for HAR systems. A brief description about the main peculiarities of the leading algorithm follows. For a comprehensive disquisition on the theme, please refer to [30, 1].

TABLE 2.2: Classification algorithms used by the state-of-the-art HAR systems. Source [30].

TYPE	CLASSIFIER
Decision tree	C4.5 and ID3
Bayesian	Naïve Bayes and Bayesian Networks
Instance Based	k-Nearest Neighbors
Neural Networks	Multilayer Perceptron
Domain transform	Support Vector Machines
Fuzzy Logic	Fuzzy Basis and Function and Fuzzy Inference System
Regression methods	MLR, ALR
Markov models	Hidden Markov Models and Conditional Random Fields
Classifier ensembles	Boosting and Bagging

Decision trees. These methods build a hierarchical model in which nodes map attributes and edges represent the possible attribute values. Each branch from the root to a leaf node is a classification rule. C4.5 is perhaps the most widely used decision tree classifier and is based on the concept of information gain to select the attributes that should be placed in the top nodes.

Bayesian methods. These algorithms calculate posterior probabilities for each class using estimated conditional probabilities from the training set. The Bayesian Network (BN) classifier and Naïve Bayes (NB, which is a specific case of BNs)

are the principal exponents of this family of classifiers. A key issue in Bayesian Networks is the topology construction, as it is necessary to make assumptions on the independence among features. For instance, the NB classifier assumes that all features are conditionally independent given a class value, yet such assumption does not hold in many cases.

Instance Based Learning (IBL). Methods that classify an instance based upon the most similar instance(s) in the training set. For that purpose, IBL define a distance function to measure similarity between each pair of instances. This makes IBL classifiers quite expensive in their evaluation phase as each new instance to be classified needs to be compared to the entire training set. Such high cost in terms of computation and storage, makes IBL models not convenient to be implemented in a mobile device.

Support Vector Machines (SVM), Artificial Neural Networks (ANN). These methods have also been broadly used in HAR although they do not provide a set of rules understandable by humans. Instead, knowledge is hidden within the model, which may hinder the analysis and incorporation of additional reasoning. SVMs rely on kernel functions that project all instances to a higher dimensional space with the aim of finding a linear decision boundary (i.e., a hyperplane) to partition the data.

ANNs replicate the behaviour of biological neurons in the human brain, propagating activation signals and encoding knowledge in the network links. Besides, ANNs have been shown to be universal function approximators. The high computational cost and the need for large amount of training data are two common drawbacks of neural networks.

Ensembles of classifiers combine the output of several classifiers to improve classification accuracy. Some examples are bagging, boosting, and stacking. Classifier ensembles are clearly more expensive, computationally speaking, as they require several models to be trained and evaluated.

Ensembles of classifiers. They combine the output of several classifiers to improve classification accuracy. Some examples are bagging, boosting, and stacking. Classifier ensembles are clearly more expensive, computationally speaking, as they require several models to be trained and evaluated.

As stated in [1], the choice for a particular inference method is subject to a trade-off between computational complexity and recognition performance. With a view to classification on embedded systems with limited resources, the goal is to minimise computational complexity and memory requirements, while still achieving high recognition performance. Feature selection allows to identify contributing features during training and hereby reduce computational complexity during classification. Therefore, inference methods are typically selected depending on the type of activity and the complexity of the feature space. They may also be selected based on other factors such as latency or on-line operation and adaptation. Depending on the mode of operation of the ARC, either the training or the classification stage is active to further process the extracted features.

2.4 The inertial measurement unit

In this work of thesis, the inertial measurement unit (commonly referred as IMU) is used throughout the text as the main source of information. This section aims to provide the reader with a background of the working principles of each sensor integrated into the IMU and the technical specifications about inertial platforms used for data collection during trials.

2.4.1 Sensors

The term IMU identifies a class of devices that generally comprise a pair of tri-axial accelerometer and gyroscope into a single sensing unit. A fully equipped IMU often also includes a tri-axial magnetometer in the same package. In this latter case, either the terms magnetic-IMU, M-IMU or IMMU (Inertial and Magnetic Measurement Unit) are found in the literature. To mention that throughout the text, we use the term IMU to refer either to IMU and M-IMU.
An IMU is capable of measuring inertial quantities (acceleration and angular velocity) and the magnetic flux vector which, in absence of magnetic field perturbations, measures the direction of the Earth magnetic north. Since the advent of Micro Electro-Mechanical Systems (MEMS) technology in the 1990s, a trend in miniaturization of the individual sensor components (driven by the requirements of the automotive and aeronautical industries) have brought to market devices that are cheap ($20 - 100\$$) and so small ($< 4mm^3$) to be integrated on single chip.
On the one hand, current IMUs are low cost, small and lightweight and are now suitable for a number of new applications (e.g. wearable devices). On the other hand, although the performance of MEMS is improving rapidly, compared to traditional technology, MEMS devices have reduced performance in terms of accuracy and bias stability.
The following sections briefly describe the working principle of each sensor and the mathematical models used to describe the behaviour of MEMS sensors included in an IMU. Further details can be found in [51, 52, 53].

MEMS accelerometer

Micro-machined silicon accelerometers use the same principles as mechanical and solid state sensors. There are two main classes of MEMS accelerometer. The first class consists of mechanical (i.e: devices which measure the displacement of a supported mass) manufactured using MEMS techniques. The second class consists of devices which measure the change in frequency of a vibrating element caused by a change of tension. MEMS accelerometers are small, light and have low power consumption and start-up times. Their main disadvantage is that they are not currently as accurate as accelerometers manufactured using traditional techniques, although the performance of MEMS devices is improving rapidly.

In mechanical MEMS accelerometers, the core of the sensor consists of a suspended proof mass connected to the sensor's basement through a spring-damper link. When the sensor is subjected to an acceleration along its sensitive axis the proof mass tends to resist the change in movement owing to its own inertia. As a result, the mass moves relatively to the sensor housing in the opposite direction than the direction of the movement. The displacement is proportional to the applied force. Figure 2.6 shows a typical mechanical accelerometer.

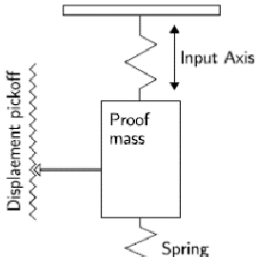

FIGURE 2.6: A mechanical accelerometer (Source [51]).

An accelerometer measures the external specific force ($\vec{f}$) applied to its proof mass, which is related to acceleration ($\vec{a}$) as:

$$\vec{a} \propto \vec{f} + \vec{g} \tag{2.6}$$

where $\vec{g}$ denotes the Earth's gravitational acceleration.

For a generic MEMS tri-axial accelerometer, the following measurement model can be used to describe the output from the sensor ($\vec{a_m}$), when an external specific force ($\vec{f_r}$) is applied to its proof mass:

$$\vec{a_m} = T_{acc}\ K_{acc}\ (\vec{f_r} + \vec{b}_{acc} + \vec{\nu}_{acc}) \tag{2.7}$$

$$T_{acc} = \begin{pmatrix} 1 & -\alpha_{y,z} & \alpha_{z,y} \\ 0 & 1 & -\alpha_{z,x} \\ 0 & 0 & 1 \end{pmatrix} \tag{2.8}$$

where T_{acc} is a matrix that take into account cross-coupling errors (i.e., errors arising from manufacturing imperfections which determine non-orthogonality of the sensor axes), $K_{acc} = diag\{s^x_{acc}, s^y_{acc}, s^z_{acc}\}$ represents a 3×3 diagonal gain matrix which considers for scale factors (i.e., it relates the sensor output to the physical quantity to be measured); $\vec{b}_{acc} = [b^x_{acc}, b^y_{acc}, b^z_{acc}]^T$ is the fixed bias vector and $\vec{\nu}_{acc}$ represents the vector of the stochastic measurement noise.
Specifically, the bias vector term represents the displacement from zero on the accelerometer output when the sensed specific force ($\vec{a_m}$) is null. The magnitude of the bias term is independent of any motion to which the accelerometer may be subjected and it is commonly expressed as a fraction of the full scale of the accelerometer. To mention that $\vec{b}_{acc}$ and $\vec{\nu}_{acc}$ are type of errors that usually affect accelerometer.

TABLE 2.3: A summary of typical error sources in MEMS sensors. (Source from [51])

ERROR TYPE	DESCRIPTION
BIAS	A constant bias in the accelerometer's output signal
WHITE NOISE	White noise with some standard deviation
TEMPERATURE	Temperature dependent residual bias
CALIBRATION	Deterministic errors in scale factors, alignments and gyro linearities
BIAS INSTABILITY	Bias fluctuations, usually modelled as a bias random walk

For MEMS devices angle random walk (noise) and uncorrected bias errors are typically the error sources which limit the performance of the device, however the relative

importance of each error source depends on the specific device being used. Table 2.3 illustrates the main sources of error for MEMS accelerometers.For a complete dissertation about the topic, please refer to [51, 52, 53].

MEMS gyroscope

Almost all MEMS gyroscopes devices are based on the measurement of the Coriolis force acting on a vibrating structure. When a mass (m) is moving with a linear velocity ($\vec{v}$) and its reference frame is rotated with an angular velocity ($\vec{\omega}$), a Coriolis force ($\vec{f_c}$) given by the following equation is observed:

$$\vec{f_c} = -2m\ (\vec{\omega} \times \vec{v}) \tag{2.9}$$

Many vibrating element geometries exist, such as vibrating wheel and tuning fork

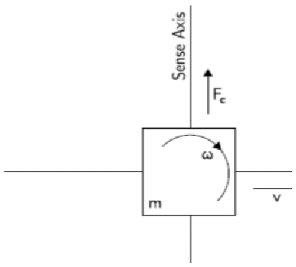

FIGURE 2.7: A MEMS gyroscope (Source [51]).

gyroscopes. The simplest geometry consists of a single mass which is driven to vibrate along a drive axis, as shown in Figure 2.7. When the gyroscope is rotated, a secondary vibration is induced along the perpendicular sense axis due to the Coriolis force. The angular velocity can be calculated by measuring this secondary rotation.

A gyroscope is a sensor capable of measuring its own angular velocity, or rate of turn ($\vec{\omega}$). A suitable model to describe sensor output ($\vec{\omega}_m$) as a function of applied angular velocity ($\vec{\omega}_r$) is:

$$\vec{\omega_m} = T_{gyro}\ K_{gyro}\ (\vec{\omega_r} + \vec{b}_{gyro} + \vec{\nu}_{gyro}) \tag{2.10}$$

where the different terms shown in equation 2.10 have the same meaning as the those illustrated in equation 2.7 and Table 2.3 for MEMS accelerometers.

MEMS magnetometer

A tri-axial magnetometer provides a measure of the local magnetic flux vector. Under unperturbed conditions, it is sensitive to the Earth's magnetic field and plays the role of a digital compass in the IMU ensemble. A similar model to that describing the other MEMS sensors can be used for a tri-axial magnetometer.
In this context, the local magnetic flux component ($\vec{m}_r$) can be expresses as:

$$\vec{m}_m = K_{compass}\ \vec{m}_r + \vec{b}_{compass} + \vec{\nu}_{compass} \tag{2.11}$$

where $\vec{m}_m^i$ is the sensor output, $K_{compass}$ represents the compass gain matrix, that takes into account for scale factors and cross-coupling errors, $\vec{b}_{compass}$ is the fixed bias vector and $\vec{\nu}_{compass}$ represents the vector of the stochastic measurement noise.

Typical source of errors in compasses are the same as illistrated in Table 2.3 for MEMS accelerometer.
To mention that MEMS magnetometers are very sensitive to ferromagnetic perturbations; specifically, the entity of the error strictly depends upon the nature of the ferromagnetic material in the environment. For more details about environmental perturbations affecting compasses please refer to [51, 52, 53].

2.4.2 Calibration

The process of IMU calibration pertains to the estimation of the deterministic sources of error, introduced in the previous section, that characterize each sensing element. The basic idea is to compare the sensor output with known values generated using calibration instruments.
Off-the-shelf IMUs are typically factory calibrated, nevertheless, it is good practice performing periodic calibrations on the platform before data collection.
Several procedures involving [54] or not [55] external equipment and/or specific software applications [56] can be used for identifying calibration parameters.
Next sections presents some common procedures used to perform parameters estimation, that have been used for experimental trials. To mention that the accelerometer and gyroscope calibration has been performed accordingly to the procedure illustrated in [55], while for the magnetometer calibration has used the method proposed in [57].
Note that explaining each steps of the calibration procedures is beyond the scope of this work. For a complete dissertation about the methodologies, please refer to [55, 57].

Calibration procedure for accelerometer and gyroscope

As stated in the previous section, for the calibration of accelerometer and gyroscope clusters we use the procedure proposed by Tedaldi et al. in [55].
This procedure only requires to collect IMU data with the simple scheme described in the flow chart reported in Figure 2.8.
After an initial initialization period with no motion, the operator moves the IMU in

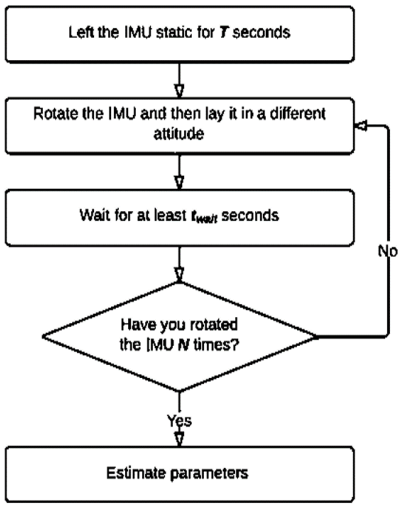

FIGURE 2.8: Flow chart of the calibration procedure for accelerometer and gyroscope (Source [55]).

different positions, in order to generate a set of distinct, temporarily stable, rotations. The collected dataset is used to calibrate the scale and the misalignments factors for both the accelerometers and gyroscopes triads, while estimating the sensor biases.
The procedure exploits the basic idea of the multi-position method for accelerometers calibration: in a static position, the norms of the measured accelerations is equal to the magnitudes of the gravity plus a multi source error factor (i.e., it includes biases, misalignment, noise,...). All these quantities can be estimated via minimization over a set of static attitudes. After the calibration of the accelerometer triad, gravity vector positions measured by the accelerometers is used as a reference to calibrate the gyroscope triad. Integrating the angular velocities between two consecutive static positions, the gravity positions in the new orientation is estimated. The gyroscopes calibration is finally obtained minimizing the errors between these estimates and the gravity references given by the calibrated accelerometers.

Specifically, the calibration of the accelerometers triad requires the estimation of the following unknown parameter vector according to the error model described in Section 2.4.1:

$$\theta_{acc} = [\alpha_{y,z}, \alpha_{z,y}, \alpha_{z,x}, s^x_{acc}, s^y_{acc}, s^z_{acc}, b^x_{acc}, b^y_{acc}, b^z_{acc}] \tag{2.12}$$

We can rewrite the equation 2.7, as follows:

$$\vec{a}_m = h(\vec{a_r}, \theta_{acc}) = T_{acc}\, K_{acc}\, (\vec{f_r} + \vec{b}_{acc}) \tag{2.13}$$

where in the equation 2.13 the measurement noise has been neglected thanks to the fact that in the calibration procedure, the signal is averaged in static intervals.
As illustrated in the Figure 2.8, the IMU is moved in a set of M distinct, temporarily stable, rotations. At the end of the procedure, M acceleration vectors $\vec{a}^k_r$ can be extracted, that average the accelerometers readings in a temporal window inside each static interval. The cost function used in [55] to estimate accelerometers parameters is:

$$\mathbf{L}(\theta_{acc}) = \sum_{k=1}^{M} (\parallel \vec{g} \parallel^2 - \parallel h(\vec{a_r}, \theta_{acc}) \parallel^2)^2) \tag{2.14}$$

where $\parallel \vec{g} \parallel$ is the actual magnitude of the local gravity vector that can can easily recovered from specific public tables (e.g., knowing latitude, longitude and altitude of the location where we are performing the calibration).
In order to minimize equation 2.14, in the proposed procedure it is used the Levenberg-Marquardt (LM) algorithm. Please refer to [55] for further reading.

In order to calibrate the gyroscope triad, it can assume the system as bias-free simply averaging the static gyroscope signals over a suitable initial period of no motion.
For the gyroscope calibration, the accelerometers output is used as known references. For this reason, the calibration parameters θ_{acc} computed through the equation 2.14 are used during the procedure.
For the gyro calibration, the operator Ψ is defined. It takes as input a sequence of n gyroscopes readings $\vec{\omega}^i_r$ and an initial gravity versor $\vec{u}_{acc,\,k-1}$ (i.e., a unit vector representing the gravity direction) given by the calibrated accelerometers, and return the final gravity versor $\vec{u}_{gyro,k}$ computed using the gyroscopes measurements between the $k-1-th$ and the $k-th$ static intervals:

$$\vec{u}_{gyro,k} = \Psi[\vec{\omega}^i_r, \vec{u}_{acc,\,k-1}] \tag{2.15}$$

Ψ can be any integration algorithm that computes the final orientation through integrating the input angular velocities.
The unknown parameter vector we need to estimate to calibrate the gyroscope is:

$$\theta_{gyro} = [\beta_{y,z}, \beta_{z,y}, \beta_{z,x}, s^x_{gyro}, s^y_{gyro}, s^z_{gyro}, b^x_{gyro}, b^y_{gyro}, b^z_{gyro}] \tag{2.16}$$

and the corresponding cost function can be defined as:

$$\mathbf{L}(\theta_{gyro}) = \sum_{k=2}^{M} \parallel \vec{u}_{a,k} - \vec{u}_{gyro,k} \parallel^2 \tag{2.17}$$

where M is the number of static intervals, $\vec{u}_{a,k}$ is the acceleration versor measured averaging in a temporal window the calibrated accelerometer readings in the $k-th$ static interval, and $\vec{u}_{gyro,k}$ is the acceleration versor computed using the equation 2.15 (i.e., integrating the angular velocities between the $k-1-th$ and the $k-th$ static intervals). Also in this case, the minimization of the functional cost in equation 2.17 is obtained using the LM algorithm.
Typical output obtained from the procedure are shown in Section 2.4.3 and 2.4.3.

Calibration procedure for the magnetometer

The calibration of the compass has been preformed according to the procedure illustrated in [57].
This methodology can be used to determine the offset and the scale factors value by simply rotating by $360\,\mathrm{deg}$ the platform, that is placed on a flat surface, with respect to the vertical axis (i.e., the $\vec{g}$ axis).
In absence of potential disturbances, out-layers and errors the procedure should provide a circle around the origin, as illustrated in Figure 2.9. Nevertheless, errors and

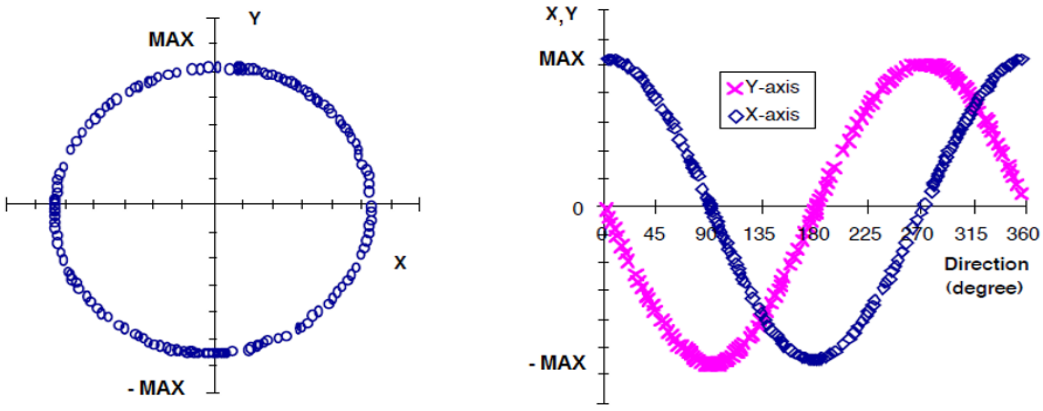

FIGURE 2.9: Ideal output for a compass with no interferences, for a rotation of $360\,\mathrm{deg}$ in the xy plane. (Source [57]).

disturbances affecting the measures contribute to provide an ellipsoid with the origin shifted with respect to the origin.
According to the equation 2.18, the magnetic flux measured with respect to the $i-th$ axis:

$$m^i_m = s^i_{compass} \cdot m^i_r + b^i_{compass} \tag{2.18}$$

where $s^i_{compass}$ and $b^i_{compass}$ represent the scale factor and the bias with respect to the $i-th$ axis, respectively.
The objective of the procedure described in [57] is devoted to the estimation of scale factors and biases for each axis, by simply carrying out the above mentioned rotation in each plane and by computing:

$$s^i_{compass} = \frac{max(\vec{m}^j_r) - min(\vec{m}^j_r)}{max(\vec{m}^i_r) - min(\vec{m}^i_r)} \tag{2.19}$$

$$b^i_{compass} = s^i_{compass} \cdot \left(\frac{max(\vec{m}^i_r) - min(\vec{m}^i_r)}{2} - max(\vec{m}^i_r) \right) \tag{2.20}$$

where $\vec{m}^i_r$ and $\vec{m}^j_r$ are the measured magnetic vector flux in the ij plane during the rotation.

2.4.3 Experimental set-up

In this section we present the general features of the inertial platforms used to collect data. Specifically, collected data have been used for both training and validating the proposed algorithms.
As stated, tests have been performed using different sensors. To note that algorithms proposed in Chapter 3, 4, 5 are general and they are not constrained to a specific device or brand. The simultaneously use of more devices for data collection have been proposed for cross validation purposes and for checking potential benefits arising from the use of a specific platform.

The InvenSense MPU-9150

The InvenSense MPU-9150 is a System in Package that combines the MPU-6050 chip (which contains a 3-axis gyroscope and 3-axis accelerometer), an on-board Digital Motion Processor for processing motion-fusion algorithms and the AK8975 3-axis digital compass.
Both gyroscope and accelerometer are user-programmable and present a full-scale range of $\pm$ 250 dps, $\pm$ 500 dps, $\pm$ 1000 dps, and $\pm$ 2000 dps and of $\pm$ 2g, $\pm$ 4g, $\pm$ 8g, and $\pm$ 16g respectively, while the one of the compass is $\pm$ 1200μT.
MPU-9150 integrates a 110 mAh rechargeable battery providing 24 hours of activity.
Data from sensors can be acquired both remotely via Bluetooth and by wire using a dedicated software application. A radio module embedded in the MPU-9150 (BT2.1 + EDR compliant) allows remote data capture up to 10 m distance. A micro-USB connector allows wired connectivity. A 256 Mbit serial flash interfaces sensors to the Mobile Control Unit through an SPI interface. Figure 2.10 shows the circuit boards and the reference frame of the tri-axial accelerometer. Table 2.4 shows the main results inferred from the calibration procedure exposed in Section 2.4.2 for accelerometer and gyroscope, and in Section 2.4.2 for the compass.

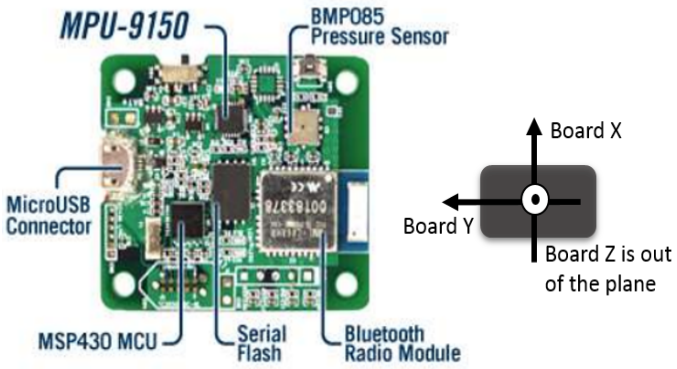

FIGURE 2.10: The MPU-9150: circuit board and reference frame of the tri-axial accelerometer.

TABLE 2.4: Accelerometer, gyroscope and magnetometer calibration parameters for the InvenSense MPU-9150 using the procedure illustrated in [55, 57].

ACCELEROMTER		GYROSCOPE		MAGNETOMETER	
α_y, z	0.0073	β_y, z	0.0112	/	/
α_z, y	-0.0067	β_z, y	-0.0089	/	/
α_z, x	-0.0057	β_z, x	0.0017	/	/
s^x_{acc}	1.0478	s^x_{gyto}	0.8975	$s^x_{compass}$	1.0082
s^y_{acc}	0.9990	s^y_{gyro}	0.9873	$s^y_{compass}$	0.9987
s^z_{acc}	1.0068	s^z_{gyro}	1.0056	$s^z_{compass}$	1.0567
b^x_{acc}	-0.0045	b^x_{gyro}	-0.0013	$b^x_{compass}$	-0.0987
b^y_{acc}	-0.0098	b^y_{gyro}	0.0099	$b^y_{compass}$	-0.0089
b^z_{acc}	0.0056	b^z_{gyro}	0.0113	$b^z_{compass}$	0.0012

The Nexus5

The availability on the market of smart devices at low price and with good technical specifications, has led us to the use of a SP for data collection.
The selected SP is a LG Nexus 5 (see Figure 2.11) equipped with Android OS v. 5.0.1. It integrates the Qualcomm MSM8974 Snapdragon 800 chipset with a quad-core 2.3 GHz Krait 400 CPU and the 6-axis MPU-6515 MEMS featuring tri-axis accelerometer and tri-axis gyroscope. The MPU-6515 presents the same operation ranges of the MPU-9150. Data logging from SP has been performed using the Sensor Insider Pro Android app [58] (see Figure 2.12) that enables to import data directly in MATLAB for further analysis. Table 2.5 illustrates the calibration parameters retrieved from the procedures exposed in Section 2.4.2 and 2.4.2.

FIGURE 2.11: The Nexus5 by Google: SP and reference frame of the tri-axial accelerometer.

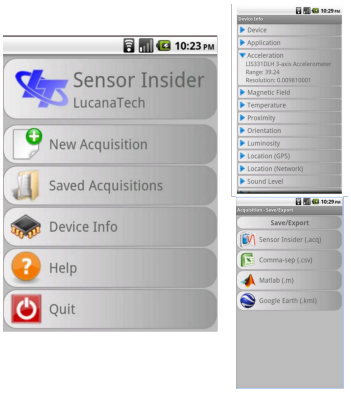

FIGURE 2.12: The Sensor Insider Pro app.

TABLE 2.5: Accelerometer, gyroscope and magnetometer calibration parameters for the Nexus5 using the procedure illustrated in [55, 57].

ACCELEROMTER		**GYROSCOPE**		**MAGNETOMETER**	
α_y, z	-0.0089	β_y, z	-0.0072	/	/
α_z, y	-0.0751	β_z, y	0.0097	/	/
α_z, x	0.0089	β_z, x	-0.0065	/	/
s^x_{acc}	0.9989	s^x_{gyto}	1.0078	$s^x_{compass}$	1.0092
s^y_{acc}	1.0098	s^y_{gyro}	0.9998	$s^y_{compass}$	0.9998
s^z_{acc}	0.9968	s^z_{gyro}	1.0076	$s^z_{compass}$	1.0065
b^x_{acc}	-0.0057	b^x_{gyro}	0.0015	$b^x_{compass}$	0.0112
b^y_{acc}	0.0065	b^y_{gyro}	-0.0079	$b^y_{compass}$	-0.0095
b^z_{acc}	-0.0019	b^z_{gyro}	0.0038	$b^z_{compass}$	-0.0015

Part II

ADLs Detection & Classification

Chapter 3

Periodic ADLs Detection & Classification using Inertial Sensing

This chapter presents the DETECT, a multi-level adaptive decision tree for gait patterns classification by using data collected from a waist-mounted inertial sensor.
Specifically, sections 5.1 and 5.2 present the current state-of-the-art in the field of gait assessment by means of inertial sensing and the motivation that led us to the design of DETECT.
Next sections (3.3.1 and 3.3.2) illustrate main remarks about the human locomotion, during the level walking and stair patterns.
According to the general outline of the ARC, the following sections aim at providing the main features about the DETECT: preprocessing 3.4.1, segmentation 3.4.2, features selection 3.4.3, and classification 3.4.4. Section 3.5.1 and 3.5.2 show the experimental set-up, data collection and results achieved during trials.

3.1 Background & motivations

A typically active lifestyle is associated with a decreased risk of suffering various chronic diseases and health conditions such as diabetes mellitus, cardiovascular disease, hypertension, certain cancers, obesity, and premature death [59]. The ability to monitor levels of physical activity enables sufficient feedback regarding compliance to suggested exercise regimes in prevention treatments, chronic disease management, rehabilitation management and health promotion programs in general [47].
At the same time, monitoring and assessing daily activity play key roles in the evaluation of the quality of life of those who have limited mobility, such as elderly people. ADLs assessment has become a clinical de facto instrument to check daily functional status of older people both in clinical and home environment [60]. Especially for those living independently at home, ADLs assessment represents a useful clinical approach for long-term analysis of functional independence in elderly.

In the ADLs field, walking is definitely one of the most common and most important of these activities. Assessing different gait patterns (i.e., standing, flat walking, walking up/down stairs, running, etc.) can provide valuable information regarding an individual's mobility, energy expenditure and stability during locomotion [61]. The continuous monitoring of these factors may act as a good predictor of a wide range of health-related behaviour in seniors and an effective tool to detect risks of/preventing falls in elderly. As well as in diagnosis and prevention, gait assessment is crucial for clinicians also for monitoring disease progression and assessing the outcome of therapies [31].
Traditional gait assessment methods are based on clinical observations. However, it

has the drawbacks of being qualitative, whereby decisions were based on the subjective judgement of clinicians, and also on time-consuming processes.
Significant technical and intellectual progress has been made in the area of gait analysis over the past few decades. Ground Reaction Force (GRF) measurements, ElectroMyoGraphy (EMG) and Video-Based (VB) analysis have been investigated as feasible solutions for automatic gait patterns detection and classification.
For comprehensive gait analysis, these techniques are usually integrated in ad-hoc gait laboratories. Nevertheless, diseases prevention/early diagnosis and/or gait disorders monitoring require continuous and long-term analysis of patients walking activities. In addition, it has been demonstrated [31] that a subject's level of mobility estimated from quality of gait within controlled environment is usually not reliable. Gait parameters derived from a gait laboratory may not reflect natural gait behaviour of each individual observed in everyday life. Measures of gait in daily life could provide more reliable mobility assessment.
These findings call for the development and use of assistive devices for continuous and long-term automatic gait patterns detection and discrimination. One major problem concerning the above-mentioned techniques (GRF, EMG and VB) is that they have deficiencies that hinder pervasive solutions. Although rather efficient, these methods are usually costly, require the use of professional devices, could need maintenance and may have bounded maximum distance between the sensor and the base, limiting the detection area within small indoor environments.
A feasible solution able to overcome such limitations is the accelerometry. Alone or usually integrated in IMUs and SPs, linear tri-axial accelerometers fixed on the body have been used as effective wearable tools for data collection, without limiting the subject. As stated in Chapter 1, compared with classical gait analysis techniques, accelerometer-based systems present many advantages including small size, lightweight, low cost, low power consumption, easy usability and minimum interferences with user's activities [31]. All these factors contributed to make accelerometry a practical, inexpensive and reliable method for monitoring ambulatory motion in free-living subjects [32].

As a part of HAR systems, gait assessment solutions based on accelerometry follow the same course of actions of the typical ARC (see Chapter 2). In this context, several procedures have been proposed in literature for translating accelerometry data into useful clinical information. Typical techniques for features extraction use simple mathematical operators [62, 63] (i.e., means, standard deviations, signal magnitude vector, etc.) and/or statistical indexes [64], [65] (such as, skewness, kurtosis, eccentricity, etc.). Other approaches are based upon the frequency spectrum analysis of the raw accelerometer data [61], [45], [66], [67] or combine time-frequency features by using the MRA approaches, such as CWT or DWT [47].
Once features have been extracted, ADLs assessment is performed using simple or more complex artificial intelligent-based classifiers for gait pattern detection.
Despite the proven effectiveness about some of the aforementioned approaches for features extraction and classification, actually there is no off-the-shelf solution for daily gait patterns monitoring that uses accelerometry. The limited power and computational load typically from mobile platforms are almost unsuitable with most of them.
Aside from the technique, classical methods for gait analysis may require a quite large number of time and/or frequency domain features. The feature vectors length is extremely variable and depends on the specific application.
Current accelerometry-base gait assessment solutions usually require $15 \div 45$ features (e.g., the number of features is 15 in [46], 20 in [47], 33 in [32], [31], 45 in [34]), but

the features vector length may be also greater (e.g., 57 in [59]). Nevertheless, high dimensions features vectors may usually require time and power consuming extraction procedures.
To overcome these limitations, some researches attempted reducing the features vector size (e.g., in [33] authors use 5-features vector); however, despite these efforts a remarkable detection accuracy is usually associated with a sophisticated classifier that require a high computational burden [28].
Among the ARC phases, the classification is usually in charge for the most of the energy expenditure (i.e., computational time and complexity). To date, Naïve Bayesian classifiers [68], [69], artificial neural networks [70], support vector machine, nearest neighbour algorithms [71], hidden Markov models [72] and Gaussian mixture models [73] represent the most widely used machine learning approaches for gait assessment. Although their potential high classification rates, finding a way for reaching best results with minimum power consumption still represent an open issue [28].
According to the current research challenges in the HAR field illustrated in Chapter 1, the new advent of the mobile era calls for pervasive solution able to perform long-term monitoring while limiting memory requirements and power consumption. All these facts contribute to get more challenging the implementation of these solutions on mobile platforms, thwarting their use in daily applications.

3.2 Research goals & contributions

As it emerged from the previous section, feature selection & extraction and classification represent the most critical phases in the design of a HAR systems.
The selection of suitable features is an important factor towards practical HAR. The exact number and type of features is a design decision and the selection process is usually driven by experimental results and/or experience. At the same time, as stated in Section 5.1, the classification algorithm is liable for time and power consumption. Limiting the number of features while using a light and effective classifier should match the needed requirements of time and power saving strategy. This is the paradigm behind the proposed solution, the DETECT (DEcision TrEe for gait patterns ClassificaTion). DETECT is a multi-level Decision Tree (DT) for continuous, long-term gait patterns detection and classification. In the proposed approach, gait assessments is performed using time-domain statistical and heuristic features extracted from data retrieved by means of a waist-mounted tri-axial accelerometer. Several factors contribute to differentiate DETECT from other solutions:

- Unlike classical approaches that usually exploit a quite large number of features, DETECT is able to identify four different gait patterns (standing, flat walking, walking up/down the stairs), using only 3 features (1 time-domain statistical feature and 2 heuristic features);
- Heuristic features implemented in DETECT are newly conceived; they have been specifically designed for discriminating between close-related gait patterns (i.e., stairs ascending/descending) and dynamic gait patterns in mixed dynamic tracks, using minimal computational resources;
- The DETECT classification accuracy combined with time and power saving strategies for features extraction and classification contribute making DETECT ideal for the implementation on mobile platform for daily gait assessment applications.

The effectiveness of the proposed solution has been proven by means of extensive trials. Tests have been performed by users presenting different anthropomorphic features; mixed gait patterns tracks and different walking terrains have been also investigated.

3.3 Bio-mechanics of the human locomotion

Before going into details with the main algorithm peculiarities, it is worth dwelling on the bio-mechanics of the human locomotion. A clear understanding about the nature of the human locomotion and how these movements results in terms of the accelerometer signal is an essential task in the design of a HAR system for gait assessment.

Next sections briefly describe the main peculiarities of the human gait during walking and stairs climbing /descending, giving also some practical examples about the typical behaviour of the accelerometer signal during these activities for a user equipped with a waist-mounted inertial sensor.

3.3.1 The walking gait cycle

In bio-mechanics walk refers to the medical term which describes the human locomotion. Each person has a pattern of walking different from any other individual, and it is described in term of the *gait cycle*. Specifically, the gait cycle is the time period or sequence of events or movements during locomotion in which one foot contacts the ground until the same foot contacts again the ground, and involves forward propulsion of the centre of gravity of the human body.
Although in this context the gait cycle is referred to the level walking, this term is generally used for representing typical human locomotion activity on level ground, stairs and slopes. The bio-mechanics and the various phases, except for some peculiarities, are almost the same for each of the afore-mentioned gait patterns.

Concerning the level walking, Prof. Sandra J. Shultz describes gait as [74] "*...someone's manner of ambulation or locomotion, involves the total body. Gait speed determines the contribution of each body segment. Normal walking speed primarily involves the lower extremities, with the arms and trunk providing stability and balance. The faster the speed, the more the body depends on the upper extremities and trunk for propulsion as well as balance and stability. The legs continue to do the most of the work as the joints produce greater ranges of motion trough greater muscle responses. In the bipedal system, the three major joints of the lower body and pelvis work with each other as muscles and momentum moves the body forward. The degree to which the body's center of gravity moves during forward translation defines efficiency. The body's center moves both side to side and up and down during gait.*"

The gait cycle is a repetitive pattern involving *steps* and *strides*. A step is one single step, a stride is a whole gait cycle. The step time is the time from one foot hitting the floor to the other foot hitting the floor. The step width can be described as the mediolateral space between the two feet. A single gait cycle is also known as a stride.
The sequences for walking that occur may be summarized as follows [75]:

- registration and activation of the gait command within the central nervous system;
- transmission of the gait systems to the peripheral nervous system;
- contraction of muscles;
- generation of several forces;

- regulation of joint forces and moments across synovial joints and skeletal segments;
- generation of ground reaction forces.

The human gait-cycle can be divided in two phases:

- double limb support period;
- single limb support period.

These periods are identified by start and stop events. The first event begins when the first foot strikes and ends when the other foot's toe-off. The second one starts with the opposite foot toe-off and ends with opposite foot strikes.

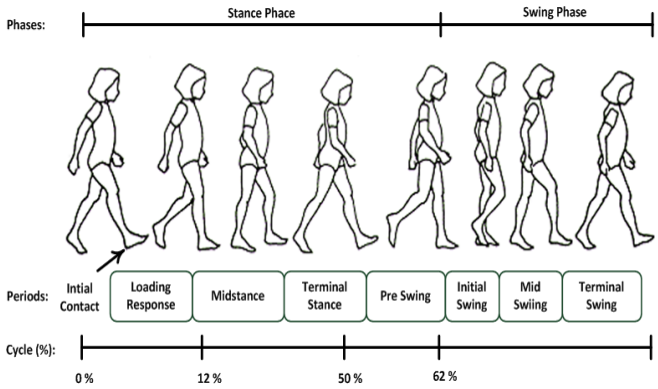

FIGURE 3.1: The gait cycle.

An alternative classification of gait involves that the cycle of the walk is split into two main phases [76, 74]:

- the *stance phase*. It represents the time interval in which the foot is in contact with the ground. Occupies about 60% of the cycle of the walk. Stance phase begins with the heel strike, that is the moment when the heel begins to touch the ground but the toes do not yet touch, and ends with the *toe-off* phase, also named the *propulsive phase*. More specifically, in the *stance* phase it is possible to identify five sub-phases:
  - *heel strike*, also known as *initial contact*. It is a short period which begins when the foot touches the ground and is the first phase of the double support period. A flexion of the hip and a full extension in the knee is observed. The ankle moves from a neutral position into a plantar flexion. After this, knee flexion begins and increases, just as the plantar flexion of the heel increased.
  - In *foot flat*, or *loading response* phase, the body absorbs the impact of the foot by rolling in pronation. The hip moves slowly into extension, caused by a contraction of the adductor magnus and gluteus maximus muscles. The knee flexes and the ankle plantar flexion increases.
  - In *midstance* the hip moves from flexion to extension, by contraction of the gluteus medius muscle. The knee reaches maximal flexion and then begins to extend. During this phase, the body is supported by one single leg. At this moment the body begins to move from force absorption at impact to force propulsion forward.

  - *Heel off* begins when the heel leaves the floor. In this phase, the body weight is divided over the metatarsal heads.
  - In the *toe-off / pre-swing* phase, the hip becomes less extended. The knee is flexed and plantar flexion of the ankle increases. In toe-off, like the name suggests, the toes leave the ground.

- the *swing phase*. It is the phase between the toe-off phase and the heel-strike phase, in which the foot is not in contact with the ground. It occupies about 40% of the cycle. In the swing phase, we can recognize two extra phases , the *acceleration* and the *declaration*. The *acceleration* phase goes from *toe-off* to *mid-swing*, while the *declaration* goes from *mid-swing* to *heel strike*.
  In the *acceleration* phase, the swing leg makes an accelerated forward movement with the goal of propelling the body weight forward. The *declaration* phase brakes the velocity of this forward body movement in order to place the foot down with control. Between these two phases, the mid-swing phase occurs. In this phase, both feet are under the body, with the heel next to each other. In details, during the swing phase, we can identify:

  - *early swing* or *acceleration*: the hip extends and then flexes due to contraction of the iliopsoas muscle, with lateral rotation. The knee flexes and the ankle goes from plantar flexion to dorsiflexion, to end in a neutral position.
  - *mid-swing*: the hip flexes (by contraction of the adductors) and the ankle becomes dorsiflexed due to a contraction of the tibialis anterior muscle. The knee flexes but then extends due to contraction of the sartorius muscle.
  - *late swing* or *declaration* phase begins with hip flexion, a locked extension of the knee and a neutral position of the ankle.

3.3.2 The stair gait cycle

As stated, the bio-mechanics and the phases pertaining stair pattens are almost the same with respect to the level walking pattern. During stair ascent and descent, lower

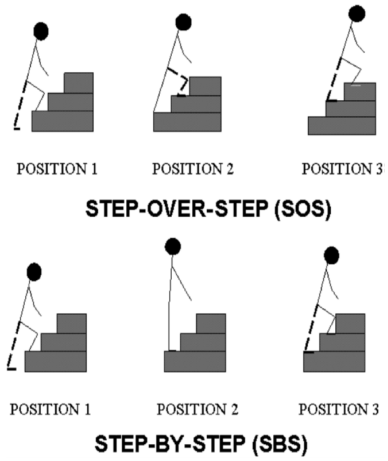

FIGURE 3.2: A schematic illustrating the gait cycles of SOS (normal reciprocal stepping pattern) and SBS stepping (placement of both feet on the same step before ascending or descending) patterns during the stair ascent ambulation. Source [77].

limbs move indeed in a cyclical pattern similar to that of the level walking.

Nevertheless, stair patterns are usually more demanding than level walking. Stair ambulation is performed with ease by healthy individuals; however, it is more difficult to perform for those with decrements in motor function, balance problems, or reduced lower-limb function [77].
Generally, healthy individuals use a traditional Step-Over-Step (SOS) gait pattern during stair ambulation; however, patients, older adults, and disabled populations may be forced to adjust their stair patterns for the reasons previously explained. Therefore, those populations with decrements in motor function often adopt alternate gait patterns, such as a Step-By-Step (SBS) pattern (placing both feet on the same step before ascending or descending) that deviate from the traditional SOS gait pattern [77]. Figure 3.2 illustrates the stair ascent gait cycle during SOS and SBS.
These deviations in stair gait patterns result in higher energy costs, lower efficiency, and an increased risk of falling; specifically this taxonomy among stair patterns has been introduced here since in the design phase it drove the selection of specific heuristic feature for the stair patterns assessment (see Section 3.4.3).

As for level walking, the gait cycle for both stair ascent/descent is divided into two phases: the *stance phase* (or *support phase*) and the *swing phase*. As stated in [78], each phases is characterized by a distinct time length spent in the swing and stance phases. Specifically, in the stair ascent pattern the stance phase deals with the 66% of the whole gait cycle, while the swing phase takes the remaining 34%; in the stair descent pattern, the cycle percentage pertaining to both the phases is the same as the level walking (60% stance, 40% swing).
Figure 3.3 illustrates the main phases pertaining with stair patterns. In terms of the

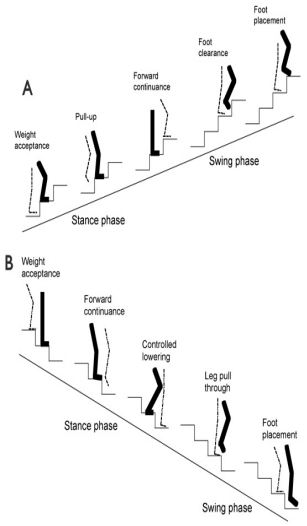

FIGURE 3.3: A schematic of the ascent (top figure) and descent cycles of SOS stair negotiation. Main phases for the stair ascending: weight acceptance, pull-up, forward continuance, foot clearance, foot placement. Phases for the stair descent pattern: weight acceptance, forward continuance, controlled lowering, leg pull through, foot placement. Source [79].

SOS stair climbing, the stance and swing phases are further subdivided into three sub-phases during support and two sub-phases during swing.

- For the stance phase during stair ascent, the sub-phases are:

  - *weight acceptance*, that represents the initial movement of the body into an optimal position to be pulled up;
  - *pull up*, that is the main progression of ascending from one step to the subsequent step;
  - *forward continuance*, in this phase the complete ascent of a step has occurred and continued progression forward occurs.

- The swing phase is subdivided into two specific sub phases:
  - *foot clearance*, this phase consists in the bringing the leg up and over to the next step while keeping the foot clear of the intermediate step;
  - *foot placement*, that is the simultaneous lifting of the swing leg and leg positioning for foot placement on step.

The main phases of the SBS stair descent pattern are illustrated in Figure 3.3.

- The stance phase in stair descending is divided into three specific sub-phases:
  - *weight acceptance*;
  - *forward continuance*, that consist in the commencement of single leg support while the body begins to move forward;
  - *controlled lowering*, it is the major portion of progression when descending from one step to the next in the SOS stair ascending.

- The swing phase during the stair descent pattern is subdivided into two specific sub-phases:
  - leg pull through, in which the swing ling in pulled forward;
  - foot placement.

3.3.3 Sensor placement

From an anatomical point of view, as illustrated in previous sections, the gait cycle[1] involves movement in each part of the leg and the whole body moves during ambulation. Specifically, as mentioned by Prof. Schultz [74] in the pelvic region there is an anterior-posterior (horizontal plane) and a superior-inferior (sagital plane) displacements (see Figure 3.4). These displacements are typical for each gait patterns, but may be more explicit in some patterns with respect to the others (e.g., stair patterns versus level walking).

Especially in the indoor localization field, a popular option concerns with putting the inertial sensor directly on the user's foot. Nevertheless, this design choice is usually not compliant with users requirements because of the constraint to get sensors in a position hard to fit and monitor.

With the growing popularity of the SPs as sensor for data logging, the issue related to sensor positioning underwent to further impetus which led to the common practice to put the sensor on the trunk (i.e., arm, pocket, waist). It is worth mentioning that signals retrieved from sensors can greatly vary depending on the sensor's placement. HAR systems conceived for a foot-placed sensor may not work a for waist-mounted

[1] In this context, with the term gait cycle we are referring to the cyclical pattern typical from the ambulatory motion in all the afore-mentioned patterns.

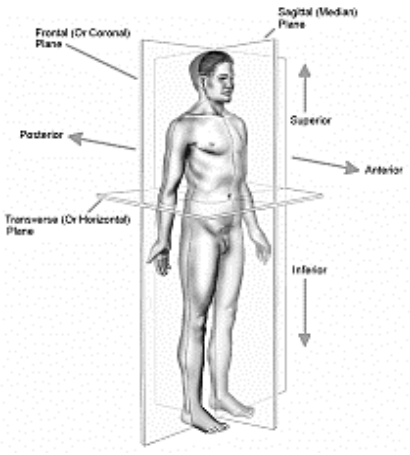

FIGURE 3.4: Typical anatomical planes (frontal or coronal plane, transverse or horizontal plane, sagittal or median plane) and directional terms (Anterior-Posterior, AP, in the sagittal plane, Superior-Inferior, SI, in the horizontal plane) as applied to the human organism.

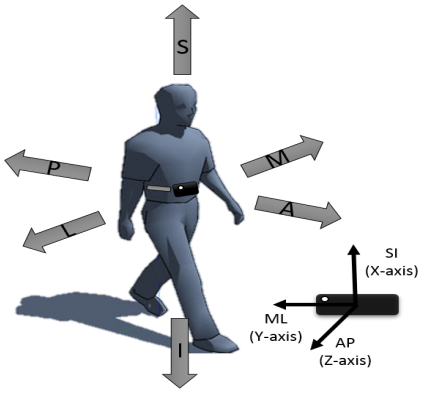

FIGURE 3.5: Local IMU coordinate frame and body-fixed coordinate frame poses. The local IMU frame orthogonal axes (x,y,z) are aligned along with the Superior-Inferior (SI), the Medio-Lateral (ML) and the Anterior-Posterior (AP) directions of the body segment, respectively.

one. The main features for all the stages of the ARC for gait pattern recognition strictly depends on this design option.

In this dissertation, the inertial sensors was assumed to be on the waist of the subject. Several reasons drove this design choice:

- it is easy-accepted by users, also for long time period;
- given its proximity to the Center Of Mass (COM) of the human body, this location is well suited for detecting body accelerations that result from typical ambulatory movement;
- it is perfectly compliant with current trends in the inertial sensing HAR field;
- ubiquitous devices (i.e., SPs and tablet) are even more used in everyday life for several tasks. During their use, devices are usually positioned in the trunk (i.e., in a hand, in a pocket) nearby the COM. This design choice make easier relaxing this constraint in future works.

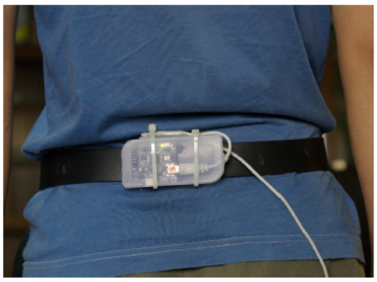

FIGURE 3.6: User wearing a waist-mounted IMU.

To mention that during trials the inertial sensor is clipped to a fastened belt on the waist of the subject, as illustrated in Figure 3.6.
Figure 3.7 illustrates the typical acceleration signal retrieved from and individual equipped with a tri-axial accelerometer (as illustrated in Figure 3.5) during level walking. The

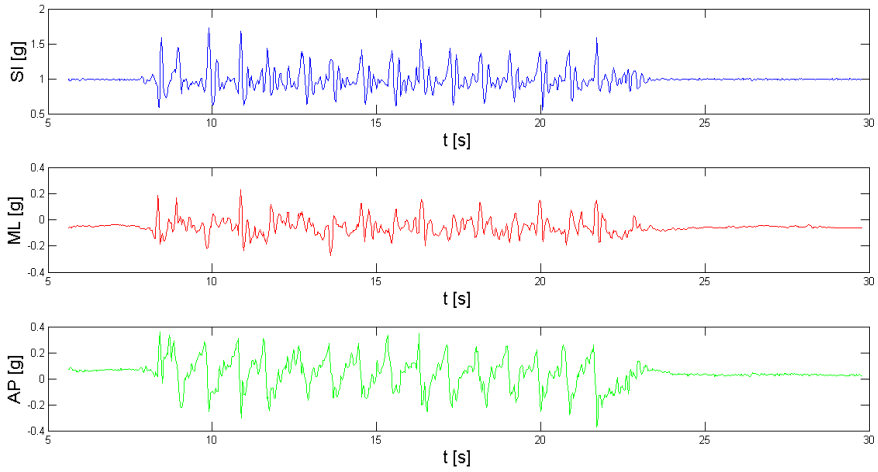

FIGURE 3.7: SI, ML and AP acceleration component retrieved from a user equipped with a waist-mounted tri-axial accelerometer during level walking. Acceleration signal is expressed in g ($1g = 9.81\frac{m}{s^2}$).

trend that typically occurs in the acceleration data during level walking and stair ascending is illustrated in Figure 3.8. Specifically, in this trial the user equipped as in the previous test has performed 3 steps and has climbed a 11-steps stair.

3.4 The DETECT

In these sections, we provide a general overview about the ARC steps involved in the DETECT[2]. It is worth mentioning that during the design phase, several approaches have been implemented for all the stages of the ARC (pre-processing, segmentation, feature extractions and classification). The selection of a specific methodology and its peculiar features has been fostered by results achieved during trials.

[2]Hereinafter, we often use DETECT to refer to the DT. However, notice that DETECT represents the whole algorithm, including all stages from the typical ARC.

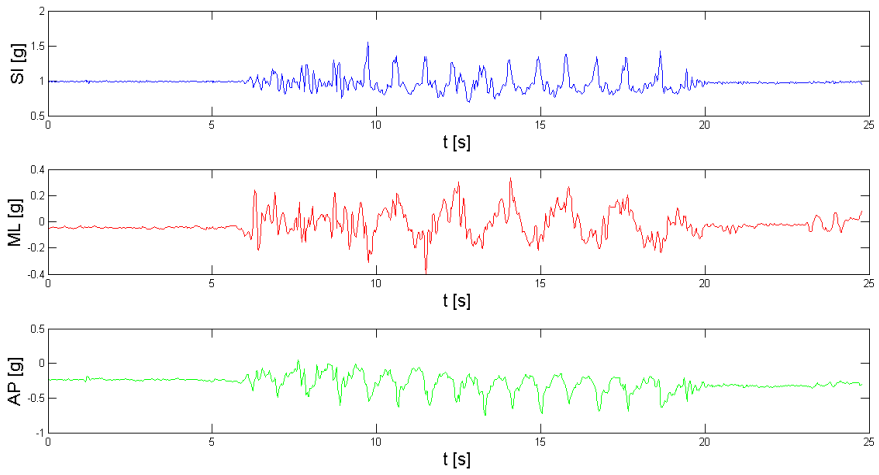

FIGURE 3.8: SI, ML and AP acceleration component retrieved from a user equipped with a waist-mounted tri-axial accelerometer during level walking and stair climbing. Acceleration signal is expressed in g ($1g = 9.81\frac{m}{s^2}$).

Before illustrating the ACR stages, it is appropriate providing a brief preliminary description about the implemented classification algorithm. Stated that the classification is the procedure usually in charge for most of the energy expenditure (see Chapter 2, and Section 5.1), several factors and planning options led us to design and implement a multi-level DT for gait assessment.
These classification algorithms are indeed usually less complex and require the lowest computational power compared with other classic machine learning approach. Stated that SPs are becoming the main platform for human activity recognition due to their unobtrusiveness, low/none installation cost, and easy-to-use, DT algorithms represent a suitable option for long-term HAR solutions. Figure 3.9 depicts the layout of a generic

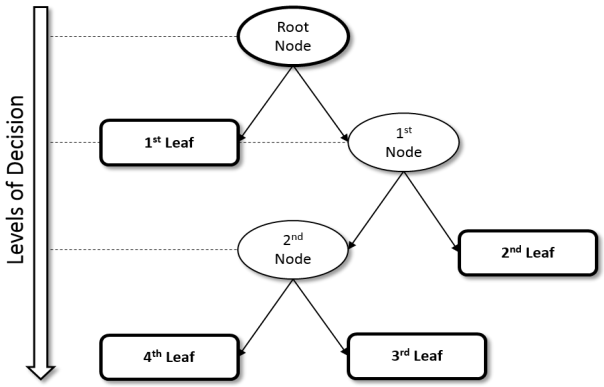

FIGURE 3.9: Outline of a general DT. The starting node (*root node*) has no incoming edges; all other nodes have exactly one incoming. Node with outgoing edges are called *internal* or *test nodes*, while node lacking in outgoing branches are called *leaf* or *terminal nodes*. Decision rules within inner nodes are mutually exclusive and are applied one after another; as a result, starting from the root node each item follows a unique path till to a leaf node, representing the class which the item belongs.

DT. In general, DTs typically consist on tree-like models arranged in nested hierarchies of branches where segments or branches are called nodes. Terminal nodes (*leaves*) represent classes in which the dataset should be ranked, while inner or test nodes concern with a set of logical conditions acting like splitting criteria for data classification. In most of the cases, the splitting criteria are univariate, which means that an internal node is split according to the value of a single attribute.

Figure 3.10 outlines the DETECT. Triangles represent decision nodes, while squares are leaf nodes. The DETECT is arranged in four levels (Lev. 0 - Lev. 3). Each level corresponds to a splitting criterion. Decision rules are univariate and compare the value assumed by the dataset within specific thresholds or ranges. The dataset is represented by the features extracted from accelerometer data; thresholds and ranges hailed from a detailed analysis about experimental results get from specific inference trials. Main peculiarities about thresholds, splitting criteria and trials are illustrated in Table 3.1. As illustrated in Figure 3.10 and Table 3.1, the first level of DETECT (Lev. 0)

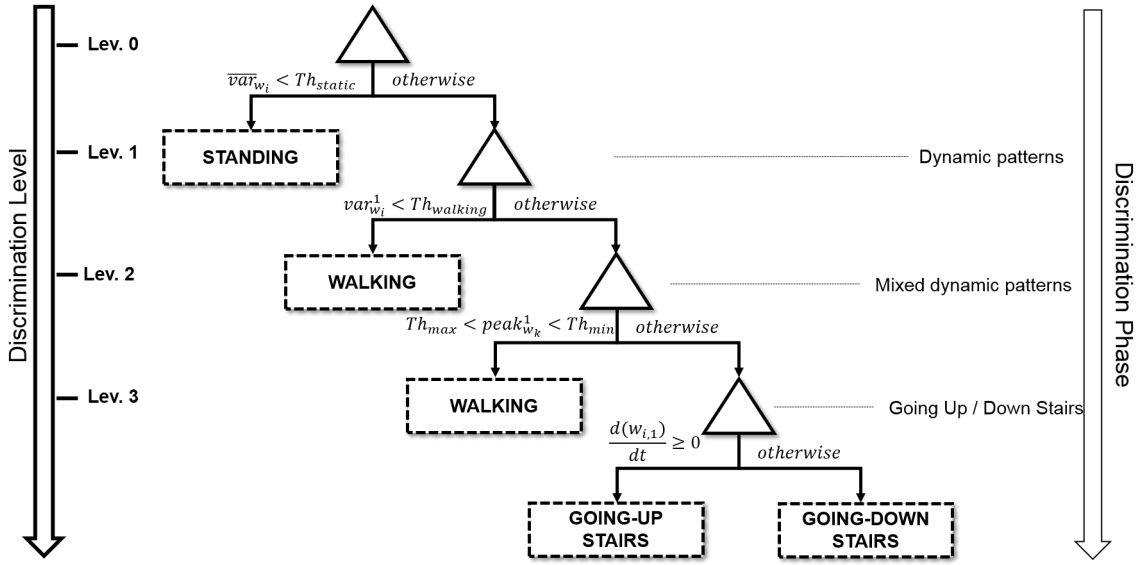

FIGURE 3.10: Top–down structure of the DETECT. Square leaves represent patterns labels (Standing, Walking, Going Up/Down Stairs) while triangular branches represent splitting nodes leading to the pruning (patterns classification) or to the growing (further classification) phase.

is in charge of discriminating between static (standing) and dynamic pattern/s (level walking and going up/down stairs). The second level (Lev. 1) assesses dynamic patterns into level walking and mixed-dynamic gait patterns (level walking and going up/down the stairs). In Lev. 2, mixed-dynamic gait patterns are further split into level walking and stair patterns. Finally, in the last DETECT level (Lev. 3), the classification between going up and going down the stairs is performed.
To note that the first two splitting criteria of DETECT concern with a statistical feature (variance). Branching rules from Lev. 0 to Lev. 1 lie on thresholds get from peculiar trials. Concerning Lev. 2 and Lev. 3, the achievement of suitable classification rates between stairs patterns requires the use of heuristic features as splitting rules.

To mention that system performances (i.e., pattern classification accuracy) have been expressed in term of *Accuracy Rate (AR)*, Mis-Classification Rate (MCR) and *confusion matrices*.
In general, AR and MCR are expressed in terms of True Positive (TP)/False Negative

TABLE 3.1: DETECT main peculiarities: type and nature of each splitting criterion, corresponding test node and trials used to define the branching rule. TRIAL I: turnover of mixed standing and level walking patterns; duration about 2 minute. TRIAL II: typical gait locomotion. Turnover of mixed standing, level walking, going up and down the stairs; typical test duration about 5 minute. To avoid any potential constraints, several users performed the tracks on different paths and walking terrains.

CRITERION	FEATURE	TEST NODE	TRIAL
Th_{static}	statistical variance	Lev. 0 static pattern (standing) - dynamic patterns (lwalking, going up/ down stairs)	TRIAL I
$Th_{walking}$	statistical variance	Lev. 1 dynamic pattern (walking) - mixed static /dynamic patterns (standing, walking, going up/down stairs)	TRIAL II
Th_{max}, Th_{min}	heuristic	Lev. 2 dynamic pattern (walking) - mixed dynamic patterns (going up/down stairs)	TRIAL II
$\frac{da_x}{dt}$	heuristic	Lev.3 dynamic pattern (going up stairs) - dynamic pattern (going down stairs)	TRIAL II

(FN) and True Negative (TN)/False Positive (FP) rates.
Specifically, TP (FN) happens when a pattern occur and (but) the algorithm detects it (another pattern). FP (TN) happens when the system (does not) detects a pattern and it did not occur.
Given the above, AR and MCR are defined as follows:

$$AR = \frac{TP + TN}{P + N} MCR = \frac{FP + FN}{P + N} = 1 - AR \tag{3.1}$$

where $P = TP + FN$ represents the number of tests with positive outcome, while $N = TN + FP$ is the number of the ones with negative result.
Other metrics commonly used in classification problems are the sensitivity or True Positive Rate (TPR),

$$TPR = \frac{TP}{P} = \frac{TP}{TP + FN} \tag{3.2}$$

the specificity (SPC) or true negative rate:

$$SPC = \frac{TN}{N} = \frac{TN}{TN + FP} \tag{3.3}$$

and the precision or Positive Predictive Value (PPV):

$$PPV = \frac{TP}{TP + FP} \tag{3.4}$$

For a complete lists about metrics, please refer to [1].

Confusion matrices are commonly used in classification problems to represent the system performances in a compact way. In general, a confusion matrix summarises how many instances of the different activity classes got confused, i.e., misclassified by

	PREDICTED Label 1	PREDICTED Label 2	...	PREDICTED Label i	...	PREDICTED Label N
TRUE Label 1	$AR_1\%$	$MCR_{(1-2)}\%$	....	$MCR_{(1-i)}\%$	....	$MCR_{(1-N)}\%$
TRUE Label 2	$MCR_{(2-1)}\%$	$AR_2\%$	....	$MCR_{(2-i)}\%$	....	$MCR_{(2-N)}\%$
....	....	....	....	....	....	....
TRUE Label i	$MCR_{(i-1)}\%$	$MCR_{(i-2)}\%$	....	$AR_i\%$	....	$MCR_{(i-N)}\%$
...	....	....	....	....	....	....
TRUE Label N	$MCR_{(N-1)}\%$	$MCR_{(N-2)}\%$	....	$MCR_{(N-i)}\%$	....	$AR_N\%$

FIGURE 3.11: Typical layout af a generic confusion matrix. Rows represent actual activity classes, while columns consist of classes predicted by the classifier. The classification accuracy is expressed in term of AR% and MCR%

the system. Typically, the rows of a confusion matrix show the number of instances in each actual activity class (defined by the ground truth), while the columns show the number of instances for each predicted activity class (given by the classifier's output). Each row of the matrix is filled by comparing all ground truth instances of the corresponding actual class with the class labels predicted by the system in terms of AR and MCR. Figure 3.11 illustrates the typical layout of a generic confusion matrix.

3.4.1 Preprocessing

As stated in Chapter 2, several procedures have been proposed in literature for accelerometer data pre-processing. In this work, to reduce the effect of disturbances, potential drifts, noises and outliers without affecting the computation time, a two-stage filter has been proposed.

Specifically, collected data are firstly sent to a Moving Average Filter (MAF) of fixed length to smooth-out high-frequency signal's fluctuations. Figure 3.12 shows the effect of the MAF on the raw signal by varying filter's length. It is worth noticing that best smoothing results without loss of information are achieved setting $l = 5 \div 30$. In the proposed solution the MAF's length is set to 20.

The processed data are then sent to a 5-th order band-pass Butterworth filter with lower and upper cut-off frequencies set to 0.5 Hz and 6 Hz, respectively (*bandwidth* = 5.5 Hz). Since for a regular human daily activity typical ADLs frequencies are between 0.4 and 5 Hz [18], the Butterworth filter bandwidth has been selected accordingly [80, 4].

3.4.2 Windowing

As segmentation technique, the sliding window approach has been selected in this study. As stated in Chapter 2, the partition of the filtered acceleration signals into a sequence of non overlapping consecutive windows is indeed perfectly compliant with the detection and classification of periodic ADLs, such as gait patterns.

The windows length have been selected according to literature and experimental results. Wang et al. in [80] state that the slowest and the fastest human movements take usually from 0.2 to 2.5 s, respectively. In order to capture in each window the activity

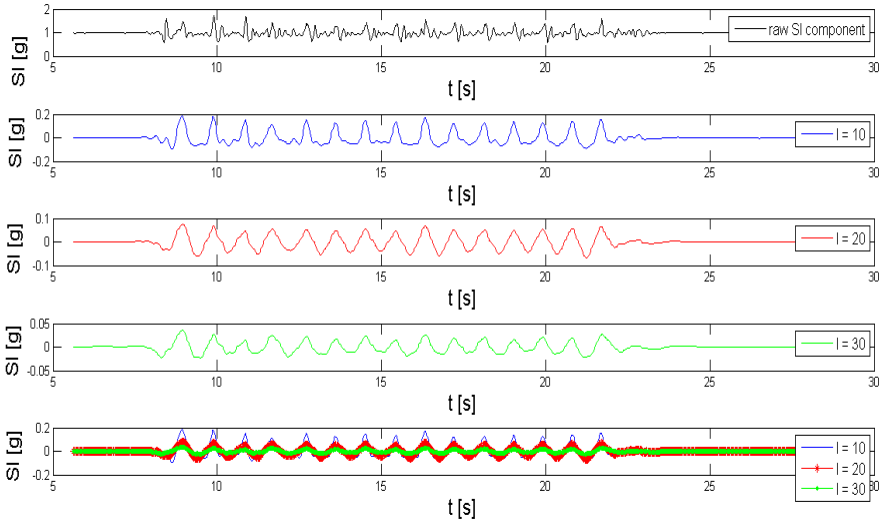

FIGURE 3.12: Effects of MAF's length on the raw SI acceleration component during level walking retrieved from a waist-mounted tri-axial accelerometer. Increasing in the MAF's length enhances the smoothing effect while decreases the signal's amplitude. Nevertheless, the signal's shrinking does not affect further analysis because preserves percentage ratios between peaks' amplitude that concerns with gait patterns classification.

under investigation (i.e., a stride), the window length (W_{size}) has been settled in $0.54s$, that is the typical duration of a single stride for an individual walking at normal speed [11]. It is worth mentioning that during the design phase, several window lengths have been tested and best results in the discrimination accuracy has been achieved by using the afore-mentioned option.

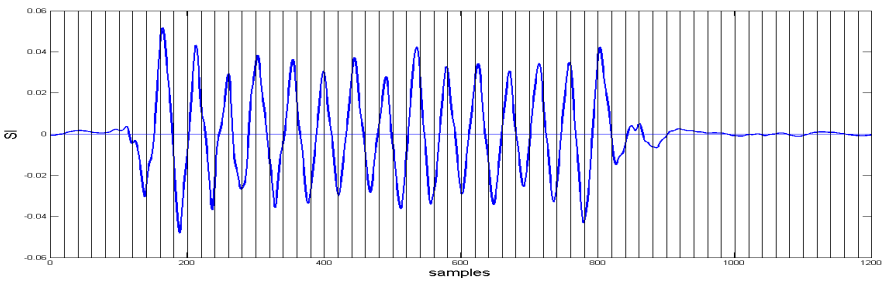

FIGURE 3.13: Filtered and segmented SI acceleration component of a user equipped with a waist worn IMU during level walking

Concerning the windows' overlap, different overlapping degrees have been attempted in trials. Figure 3.14 shows the same acceleration signal exposed to two different sliding window techniques: the FNSW and the FOSW (see Chapter 2).
Even if the overlap between consecutive windows has been considerably changed from 10% to 50% during trials, no increase in the classification accuracy has been observed accordingly, thus justifying the adoption of the FNSW approach.

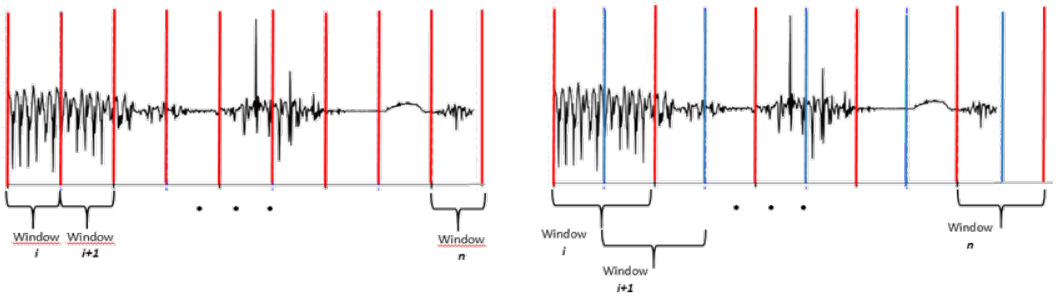

FIGURE 3.14: Acceleration signal exposed to two different sliding window approach: the FNSW without overlap (picture on the left) and the FOSW with an overlap degree of $o\% = 50\%$.

Using non-overlapping windows, the number of windows (N_w) for a collected trial with a total number of S samples, can be computed as:

$$N_w = \frac{S}{N_s} \tag{3.5}$$

where N_s is the amount of samples for each window. It can be defined as $N_s = facc * W_{size}$, with $facc$ the accelerometer acquisition frequency and $W_{size} = 0.54s$ the selected window size.

Before going further, it is worth mentioning that typical HAR systems, perform classification using features extracted from a single window. This procedure is extremely efficacious when gait patterns are clearly detached from each other in the accelerometry data, that is the user performing the trial uses standing for few seconds before/after has performed a specific pattern. In trials in which the user performs the patterns continuously, the classification based upon features extracted by a single window may prove ineffective. In order to increase the classification accuracy in continuous data stream, it is our belief the need to pay attention to potential unclear and ambiguous data arising from adjacent windows. Given the small window size commonly used in the HAR field, it is indeed reasonable assuming that a fair number of adjacent windows (i.e., $2 \div 3$) are associated with the same activity. Nevertheless, the segmentation may cause potential loss of information (i.e., an activity is split between adjacent window) or two patterns may occur in the same window, contributing to activity misclassification.
This is the reason why in the DETECT solution, we perform the feature extraction from both single windows and macro-windows, the so-called *motion segments*. A motion segments is essentially a set of unclassified consecutive windows arising from the Lev. 1 of the DT during the classification and have been introduced for avoiding misclassification in close-related patterns (such as stair ascending and descending) and mixed-dynamic patterns (such as level walking and stair patterns).
Concerning dynamic patterns, motions segments has been introduced to clear identify the level walking pattern with respect to short stretches of walk that can occur on landings between consecutive flights of stairs during stairs ascending/descending. During segmentation, two pattens may indeed occur in the same window, thus causing misclassification. Experimental results arising for the training phase showed that motion segments were able to mitigate this phenomenon.
In details, features extracted from each window are used for discriminating the corresponding activity in: standing (Lev. 0), level walking (Lev. 1) and mixed dynamic patterns. From Lev. 2, the classification is performed using motion segments. Adjacent

unclassified windows arising from Lev. 1 are grouped into several motion segments. Each motion segments undergoes to decision rules for further classification in: level walking (Lev. 2) and stair ascending/descending (Lev. 3).

3.4.3 Features

According to experimental data, we propose the use of time-domain features for gait patterns detection and classification: 1 statistical feature and 2 heuristic features.

Statistical feature

Time-domain features usually deal with statistical quantities directly extracted from accelerometer windowed data. As illustrated in Chapter 2, mean and standard deviation are generally used for discriminating between periods of static/dynamic activity (i.e., standing and ambulatory motion), while skewness, kurtosis, and eccentricity deal with further refinement to perceive different dynamic gait patterns (level walking, stair ascending and descending).
In this study, we use the mean *variance* for both discriminating between static/dynamic patterns and for identifying different dynamic gait patterns (i.e., level walking versus going up/down stairs). To mention that the variance has been computed for all the acceleration component by using data inferred from each windows.

For the sake of completeness, let assume $\vec{a} = [a_x, a_y, a_z]^T = \{a^k\}$ with $k = 1, 2, 3$ be the filtered acceleration components in the IMU's coordinate frame, corresponding to the SI, ML and AP component in the body reference frame, respectively.
Let be $a^k_{w_i} = \{a^k_{w_i,1}, \ldots, a^k_{w_i,j}, \ldots, a^k_{w_i,N_s}\}$ the set of N_s samples of the $k-th$ acceleration component within the $i-th$ window. The corresponding variance in the same window can be computed as follows:

$$var^k_{w_i} = \frac{\sum_{j=1}^{N_s}(a^k_{w_i,j} - \bar{a}^k_{w_i})^2}{N_s} \tag{3.6}$$

where $\bar{a}^k_{w_i}$ is the mean of the $k-th$ acceleration component within the window w_i.
Applying the equation 3.6 to acceleration data retrieved from a generic trial, we can obtain:

$$VAR = \begin{pmatrix} var^1_1 & var^2_1 & var^3_1 \\ \vdots & \ldots & \vdots \\ var^1_{n_W} & var^2_{N_w} & var^3_{N_w} \end{pmatrix} \tag{3.7}$$

where VAR is N_w x 3 matrix containing the variance of each acceleration component, computed for each window and N_w represent the total number of windows within the test. By averaging the elements of VAR by rows, we achieve:

$$\overline{VAR} = \begin{pmatrix} \overline{var_1} \\ \vdots \\ \overline{var_{N_w}} \end{pmatrix} \tag{3.8}$$

where $\overline{VAR}$ is the vector of the mean tri-axial acceleration variance, computed for each window.

Heuristic features

Results inferred from trials revealed that mathematical and statistical features in combination with DTs were rather inefficient in discriminating close-related dynamic patterns (such as negotiating step in stair ascending/descending) and/or for identifying different patterns when combined in mixed-dynamic tracks (level walking versus stair patterns).
Concerning mathematical features, classification results could be even worse if related with patients and/or elderly people. As stated in Section 3.3.2, stair ambulation is generally more demanding than level walking and individuals with motor impairments while performing stairs may prefer the SBS pattern rather than the more efficient SOS [77].
Nevertheless, this deviation in stairs patterns not only result in higher energy costs and lower efficiency, but it also leads to an alteration of the accelerometer signal behaviour typical from the stair patterns. As a results, traditional features may be ineffective in discriminating altered stairs patterns.
To overcome this gap and extend the usability of the proposed algorithm, we introduced heuristic features. In general, heuristic features represent hallmarks related to characteristic behaviours of the signal.

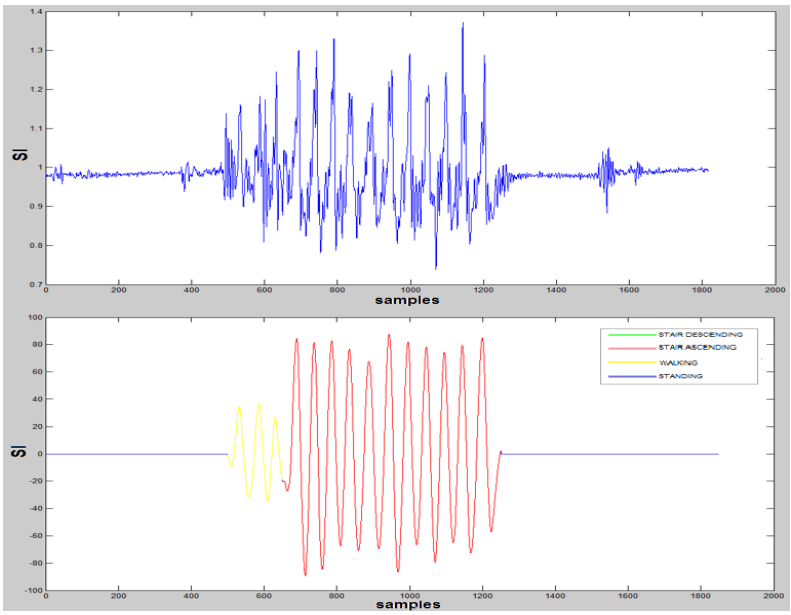

FIGURE 3.15: Raw (top figure) and filtered SI acceleration component during level walking (3 steps) and stair ascending (11 steps), for a user equipped with a waist mounted IMU.

In this work, for both features we focused on the peculiar trend exhibited by the SI acceleration component. Figures 3.15 and 3.16 show the raw (top picture) and the filtered SI acceleration component during level walking/stair ascending (Figure 3.15) and during stair ascending/descending (Figure 3.16), respectively.

In DETECT, the peak amplitude of the SI acceleration signal has been used for discriminating between level walking and stair patterns. As stated in Section 3.3, the COM moves both side to side and up and down during motion. Nevertheless, this periodic movement does not occur at a constant speed and the acceleration rapidly

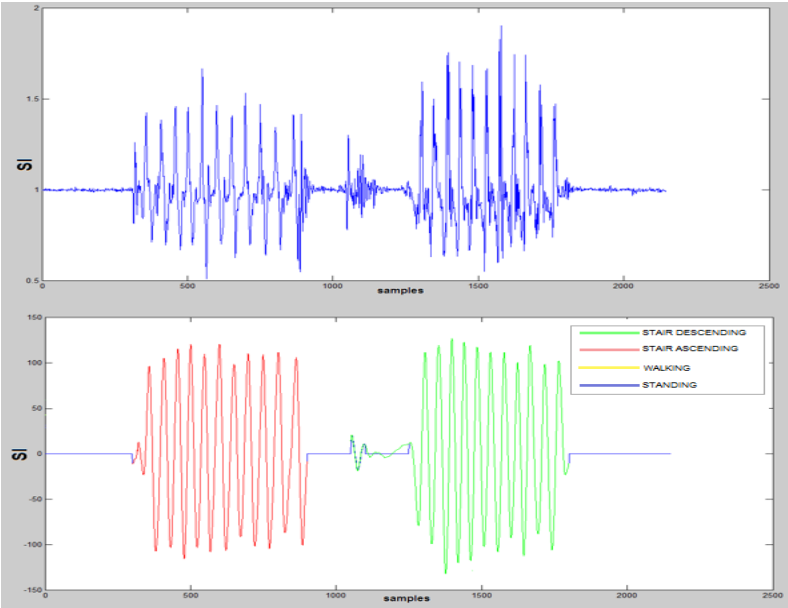

FIGURE 3.16: Raw (top figure) and filtered SI acceleration component during stair ascending (11 steps) and stair descending (11 steps), for a user equipped with a waist mounted IMU.

changes throughout gait phases (see Figure 3.15 and 3.16). The SI acceleration component shows almost the same trend both in level walking and stair patterns. The only clear differences concerns with the signal amplitude. Stair patterns are indeed more demanding than level walking (see Section 3.3.2) and the SI acceleration signal presents an higher amplitude because of the larger forces involved.
The comparison between the typical trends exhibited by the SI acceleration component in Figure 3.15) clearly show a gap in peaks amplitude between the two patterns. Although the SI span is a peculiarity and may slightly change among individuals, the relative ratio between SI peaks belonging to different patterns remains almost constant. This information can be easily use for assessing distinct patterns when combined in mixed dynamic tracks.

The discrimination among different stair patterns has been performed by analysing the SI signal during the early pull-up (forward continuance) stage in the stair ascending (descending) pattern. During this phases, the extensions (push-up) of the hip and the knee, as well as the flexion of the ankle, cause an iterated increasing (decreasing) in the SI amplitude, that influence the mutual position between first maximum (minimum) and minimum (maximum) peaks in the acceleration signal.
On this basis, a signal showing the peculiar behaviour illustrated by the top picture in Figure 3.17 is identified as a *stair ascent*, while a pattern showing the trend illustrated in the lower illustration in Figure 3.17 is classified as a *stair descent*. In other words, focusing on early peaks, the stairs ascending pattern typically presents a local maximum and a local minimum in sequence; the opposite behaviour is instead usually observed in the stairs descending pattern.

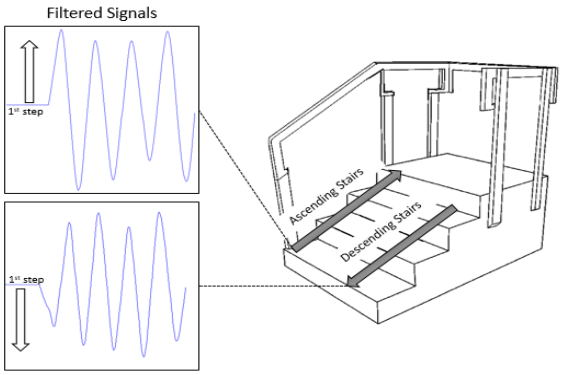

FIGURE 3.17: Typical behaviours of the SI acceleration component during stairs ascending and descending. Arrows illustrate the positive/negative trend of the first peak during the pattern.

3.4.4 Classification

Once the necessary information has been retrieved from the accelerometer signal, the extracted features as used as input vector to the reasoner for the patterns classification. As mentioned in previous sections, the inference method used in this work is a multi-level DT.
This section aims to illustrate the methodology implemented in each level of the DT, according to the DT layout illustrated in Figure 3.10 and the splitting criteria indicated in Table 3.1.

DETECT Lev. 0 - Static Pattern Identification

This level is in charge of discriminating between static (standing) and dynamic patterns (level walking and stair patterns). The splitting criterion concerns with the acceleration variance.
The $i-th$ window is identified as dynamic patterns if the corresponding mean acceleration variance is greater than a specific threshold Th_{static}:

$$\overline{var}_{w_i} \geq Th_{static} \tag{3.9}$$

otherwise it is assessed as the static pattern. Th_{static} (see (3.10)) is an experimental threshold inferred from results get from TRIAL I (see Table 3.1). This threshold has been defined as a percentage of the mean variance computed on the acceleration data during TRIAL I tests:

$$Th_{static} = \alpha \, \overline{var}_{TRIAL_I} \tag{3.10}$$

where $\alpha \in \mathbb{R}^+$, with $\mid \alpha \mid \leq 1$ and $\overline{var}_{TRIAL_I}$ is the mean acceleration variance computed on acceleration data collected during TRIAL I:

$$\overline{var}_{TRIAL_I} \frac{\Sigma_{i=1}^{N_w} \overline{VAR(i)}_{TRIALI}}{N_w}$$

Concerning the parameter α, the value selected for equation (3.10) is those maximizing the algorithm AR during tests performed according to TRIAL I.
Figure 3.18 illustrates the AR for the standing pattern classification as a function of α during TRIAL I tests performed by users presenting the anthropomorphic features

illustrated in Section 3.5.1. Figure 3.18 clearly shows as the AR for the static phase is maximum ($\simeq 100\%$) when $0.1 \leq \alpha \leq 0.5$. As illustrated in Section 3.5.2, $\alpha \simeq 0.3$ provides an high classification accuracy.

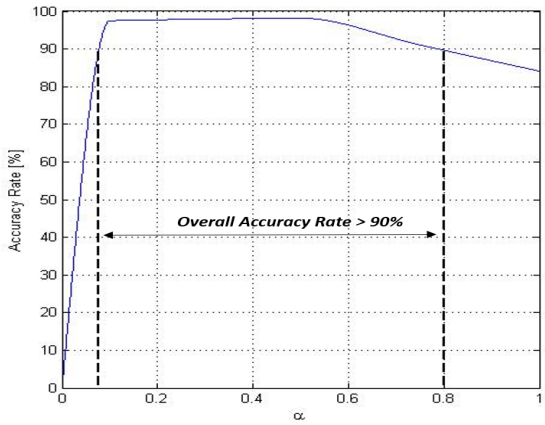

FIGURE 3.18: AR for the static pattern as a function of α during TRIAL I tests.

DETECT Lev. 1 - Walking Pattern Identification

Once the static pattern has been detected, dynamic gait patterns are then further classified into level walking pattern and mixed-dynamic patterns (level waking and stair patterns).
The level walking pattern identification is a two-stages process that concerns with Lev. 1 and Lev. 2 in Figure 3.10, respectively. The classification process concerning with Lev. 1 relies on a threshold-based process concerning the SI acceleration component, closed match with the strategy adopted in Lev. 0.
In details, the pattern concerning the $i-th$ window is mixed-dynamic if the mean variance of the SI acceleration component in the same window is greater than a specific threshold ($Th_{walking}$):

$$var^1_{w_i} \geq Th_{walking} \tag{3.11}$$

otherwise it is assessed as walking.
As in the previous case, $Th_{walking}$ (see (3.12)) has been statistically defined as a percentage β of the SI mean acceleration variance during a typical TRIAL II test:

$$Th_{walking} = \beta \, \overline{var^1}_{TRIAL_{II}} \tag{3.12}$$

where $\overline{var^1}_{TRIAL_{II}}$ has been computed as:

$$\overline{var^1}_{TRIAL_{II}} = \frac{\Sigma_{j=1}^{1}\Sigma_{i=1}^{N_w} VAR(i,j)_{TRIALII}}{N_w}$$

Figure 3.19 illustrates the AR for the discrimination of the level walking pattern as a function of β in TRIAL II tests.

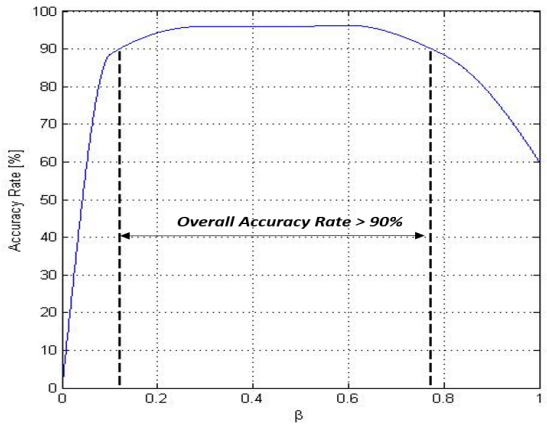

FIGURE 3.19: AR for the level walking pattern as a function of β during TRIAL II tests.

DETECT Lev. 2 - Stair Patterns Identification

In Lev. 2, mixed-dynamic gait patterns are then discriminate between level walking and stair patterns. In this stage, the classification is performed by using the motion segment by means two heuristic thresholds based on the peak amplitude of the SI acceleration component. To mention that thresholds are not fixed as in previous cases, but are adaptive and computed each time on the SI signal retrieved form motion segments.

For the sake of completeness, let be:

$$MotionSegments = \{motionSeg_1, \ldots, motionSeg_i, \ldots, motionSeg_n\} \tag{3.13}$$

the motion segments set, where the $i-th$ element of the setting can be expressed as $motionSeg_i = \{w_{i,1}, \ldots, w_{i,k}, \ldots, w_{i,m}\}$ with m the total number of windows composing the motion segment at issue.[3]
Concerning the $i-th$ motion segment, the $k-th$ window of $motionSeg_i$ is classified as level walking, if the first peak occurring in the same window fulfils the following condition:

$$Th_{min} < peak^1_{w_k} < Th_{max} \tag{3.14}$$

otherwise it is assessed as stair patterns. Th_{min} and Th_{max} are the two adaptive thresholds, defined within the motion segment $motionSeg_i$ under investigation, as follows:

$$Th_{min} = \frac{\sum_{i=1}^{N_{min}} peak^{1,min}_{motionSeg_i}}{N_{min}} \tag{3.15}$$

$$Th_{max} = \frac{\sum_{i=1}^{N_{max}} peak^{1,max}_{motionSeg_i}}{N_{max}} \tag{3.16}$$

where $peak^{1,min}_{motionSeg_i}$ and $peak^{1,max}_{motionSeg_i}$ represent the higher and lower peaks pertaining to the SI acceleration component within $i-th$ motion segment, respectively.

[3]Notice that the number of windows composing the different motion segment may vary and strictly depends on the patterns performed, that is from the classification outcomes arising from previous levels of DETECT.

DETECT Lev. 3 - Stairs Patterns Classification

Lev. 3 pertains to the stair patterns discrimination. The unclassified windows and motion segments arising form Lev. 2 are then identified into stair ascent/descent patterns by investigating the trend exhibited by the SI acceleration component within the first window of the motion segment under analysis.
As illustrated in Section 3.4.3, although the behaviour typical from the SI component is almost the same in both pattern (see Figure 3.16) the order in which the maximum and minimum peak occur at first step negotiation is a peculiarity of the specific pattern.
A straightforward analysis about the trend of the first derivative of the SI acceleration component within the first window of the motion segment allowed us to discriminating between the two stair patterns.

Let us indicate with $motionSeg_i = \{w_{i,1}, \ldots, w_{i,k}, \ldots, w_{i,m}\}$ the motion segment under analysis, where m is the total number of windows composing the motion segment at issue. This motion segment is classified as the stair ascending pattern if the time derivative of the SI acceleration samples pertaining the first window $w_{i,1}$ presents a positive trend:

$$\frac{d(w_{i,1})}{dt} \geq 0 \tag{3.17}$$

otherwise it is identified as the stair descent pattern, with $w_{i,1} = [a_{i,1}^{1,1}, \ldots, a_{i,1}^{1,N_s}]$.

3.5 System evaluation

To evaluate the performance of the proposed algorithm several experimental trials have been performed by users presenting different anthropomorphic features, equipped with a waist mounted IMU. To mention that the DETECT has been implemented using MATLAB.

Next sections provide a brief description about the tests performed for the system evaluation (Section 3.5.1) and main experimental results achieved (Section 3.5.2).

3.5.1 Data collection

The data collection as been performed using the InvenSense MPU-9150 (see Chapter 2) connected via Bluetooth to a laptop PC.
As mentioned in Section 3.3.3, the IMU unit was clipped to a fastened belt on the waist of the subject (see Figure 3.5). Potential vibration noise during motion has been reduced by adjusting the tightness of the belt fastening from medium to tight, depending on users' opinion.

Several experimental tests have been performed by a group of volunteers for the DETECT validation. Participants (25 subjects, 13 males, 12 females, average age 29.49 $\pm$ 7.75 years, average height 172.38 $\pm$ 6.76 cm, and average weight 70.46 $\pm$ 10.97 kg) were asked to perform two different trials-set. The first trial-set concerned with TRIAL I and TRIAL II described in Table 3.1 and results inferred from tests has been used in the system designing phase.
The second trial-set have been used for system validation and pertain to several experiments as described in Table 3.2.

Specifically, experiments *With Interruption of Motion (WIM)* were performed asking the subject to standing among different patterns; in experiments *With No Interruption of Motion (WNIM)*, the subject performed the test continuously, without pausing between

TABLE 3.2: Experiments performed by volunteers for DETECT validation.

Experiment	With Interruption of Motion(WIM)	With No Interruption of Motion (WNIM)
level walking	√	
stair ascent & stair descent	√	
mixed static-dynamic patterns	√	
level walking		√
stair ascent & stair descent		√
mixed static-dynamic patterns		√

patterns.
In details, the level walking test concerns in walking in straight line for about 2 minutes, the stair ascent & stair descent test pertains to going up and down the same stairs; finally, mixed static-dynamic patterns test combines all the patterns in the same trial for about 5 minutes. To mention that in WIM tests the individual performing the experiment uses to stop during the test among different patterns for about $5s$.

3.5.2 Experimental results

As stated in Section 3.4, system performances are presented in terms of confusion matrices.
Table 3.3 presents classification results achieved during WIM trail-set. As it is clear

TABLE 3.3: AR & MCR (%) confusion matrix for the four gait patterns (standing, level walking, stair ascending, stair descending) arising form data collected during WIM experiments.

	STANDING	WALKING	STAIR ASCENT	STAIR DESCENT
STANDING	100%	0	0	0
WALKING	0	100%	0	0
STAIR ASCENT	0	0	95,77%	4,23%
STAIR DESCENT	0	0	5,39%	94,61%

from Table 3.3, the DETECT is perfectly in charge for discriminating among different patterns. Standing and level walking are both perfectly identified (AR=100%); the AR tends to decrease in stairs patterns: stair ascent and descent may be misclassified. Nevertheless, the MCR between stairs patterns does not exceed the 6%, allowing us to get excellent overall results (AR is about 98%) also in long lasting experiment. Figure 3.20 illustrates the raw signal (top figure) and the classification outcome (bottom figure) in a WIM mixed static/dynamic patters experiment. The experiment path was arranged as follows: level walking, stair ascent (one flight of stairs), level walking, stair ascent (one flights of stairs), standing, stair ascent (one flight of stairs), level walking, standing, level walking, standing, level walking, stair descent (three flights of stairs), level walking stair ascent (two flights), level walking. Belonging to the WIM, apart from the

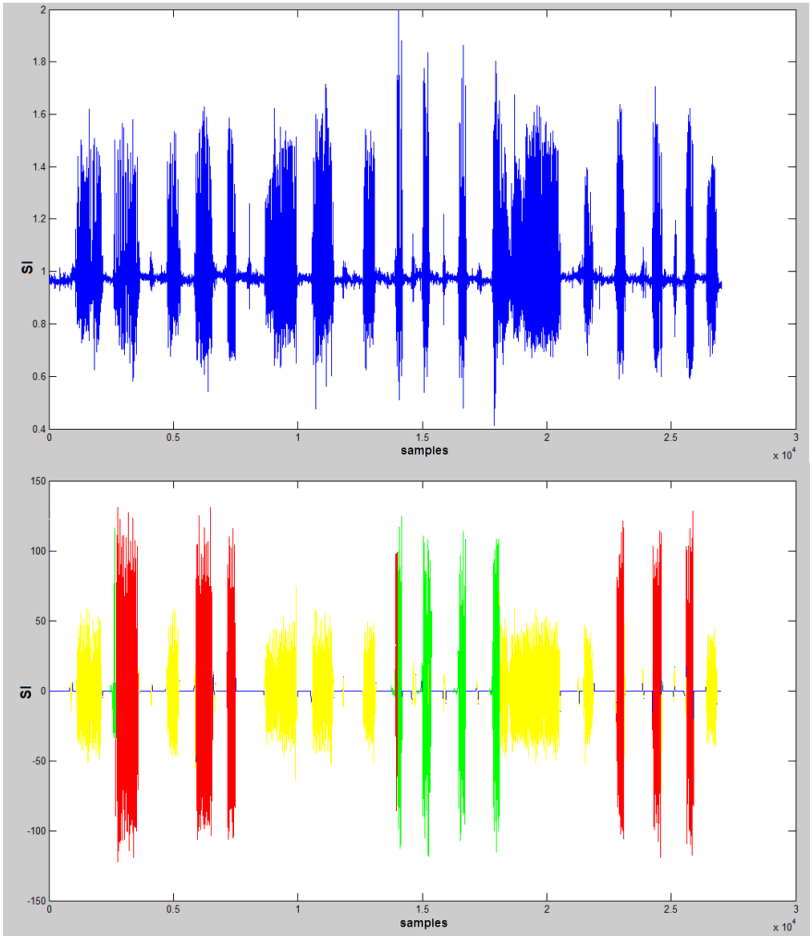

FIGURE 3.20: Patterns classification during a WIM mixed static/dynamic patters experiment. The top figure represents the raw SI acceleration component. The bottom figure illustrates the DETECT outcome: blue line refers to the standing, the yellow concerns with the level walking, red and green pertains with the stair ascent and descent respectively.

standing patterns explicitly stated, the user during the experiment uses to stand among different patterns. The total duration of the test was about 12 minutes.
As it is clear from Figure 3.20, all the discriminated patterns are perfectly compliant with the experiment path. According to the results showed in Table 3.3, misclassification occurred between stair ascent and descent. Nevertheless, the erroneous classification pertains only few sample, as illustrated in Figure 3.21 Considering the total number of samples collected, only the 4% of the total amount were wrongly classified.

Table 3.4 illustrates results get in WNIM tests. Results from WNIM experiments shows that the standing and the level walking patterns (apart from an almost negligible %) are perfectly discriminated. As in WIM experiments, stair patterns may be misclassified and the MCRs pertaining to WNIM exceed those in WIM.
In contrast with previous results, the stair patterns could be confused also with le level walking. Nevertheless, the AR for both stair patterns exceed the 80% providing an overall classification accuracy of 91% for the four patterns.
Figure 3.22 shows the results achieved during a WNIM mixed static/dynamic patters experiment. The experiment path was arranged as follows: level walking, stair ascent

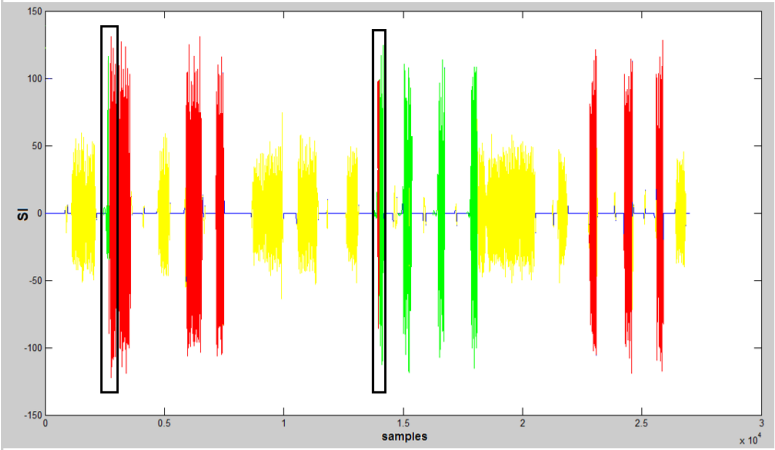

FIGURE 3.21: Patterns classification during a WIM mixed static/dynamic patters experiment: blue line refers to the standing, the yellow concerns with the level walking, red and green pertains with the stair ascent and descent respectively. Black boxes highlight misclassification.

TABLE 3.4: AR & MCR (%) confusion matrix for the four gait patterns (standing, level walking, stair ascending, stair descending) arising form data collected during WNIM experiments.

	STANDING	WALKING	STAIR ASCENT	STAIR DESCENT
STANDING	100%	0	0	0
WALKING	0	98,88%	1,12%	0
STAIR ASCENT	0	6,12%	82,87%	11,01%
STAIR DESCENT	0	7,13%	8,21%	84,66%

(two flights of stairs), level walking, stair descent (two flights of stairs). It is clear form the figure that the misclassification in the experiment concerns with the stair ascent and the stair descent: some samples belonging to stair patterns are classified as level walking (see the black boxes in Figure 3.22). Nevertheless, the overall classification accuracy for the experiment exceed the 94%.

A very interesting result concerns with long lasting experiment. Figure 3.23 shows a WNIM mixed static/dynamic patters experiment with a total duration of about 45 minutes. The experiments path is as follows: level walking, stair ascending (one flight), level walking, stair ascending (two flights), level walking, stair descending (two flights), level walking, stair descending (two flights), level walking, stair ascending (two flights), level walking, standing, level walking, stair ascending (two flights), level walking.

Despite the long duration of the experiment, the DETECT is able to discriminate all the patterns according to the experiment path. Misclassification among different patterns has been highlighted in Figure 3.23 by means black boxes. Considering all the samples within the experiment, the MCR does not exceed the 6%. This implies that the duration of the experiment does not affect the DETECT classification accuracy, demonstrating the validity of the proposed solution for long term applications.

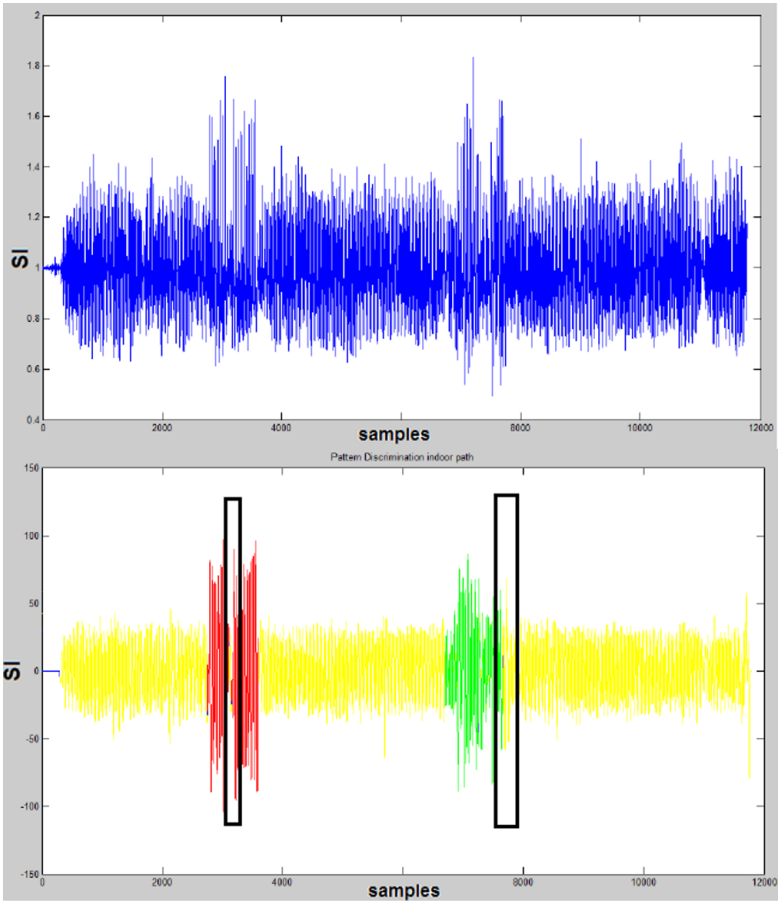

FIGURE 3.22: Patterns classification during a WNIM mixed static/dynamic patters experiment. The top figure represents the raw SI acceleration component. The bottom figure illustrates the DETECT outcome: blue line refers to the standing, the yellow concerns with the level walking, red and green pertains with the stair ascent and descent respectively. Black boxes highlight misclassification.

3.6 Conclusion

In this chapter, a waist-worn IMU combined with a decision tree algorithm is used to accurately estimate human gait patterns. We demonstrated that only three time-domain and heuristic features are sufficient to properly classify between standing, level walking and going up/down stairs.
The major advantage of the proposed solution is the prevention from additional algorithms for feature dimensionality reduction and the compliance of the proposed algorithm to applications that require patterns identification with low computation burden and complexity. Given the limited number of features exerted for patterns classification, the DETECT represent a perfect candidate for the implementation on mobile platforms.
Experimental results show that the maximum misclassification rate concerns with stair ascending and descending. The reason probably lies on the physiological variation of the accelerometer signal between different subjects.
Nevertheless, the DETECT presents an excellent overall classification accuracy that exceeds the 94% also in long-lasting experiment. This requirement yields our proposed

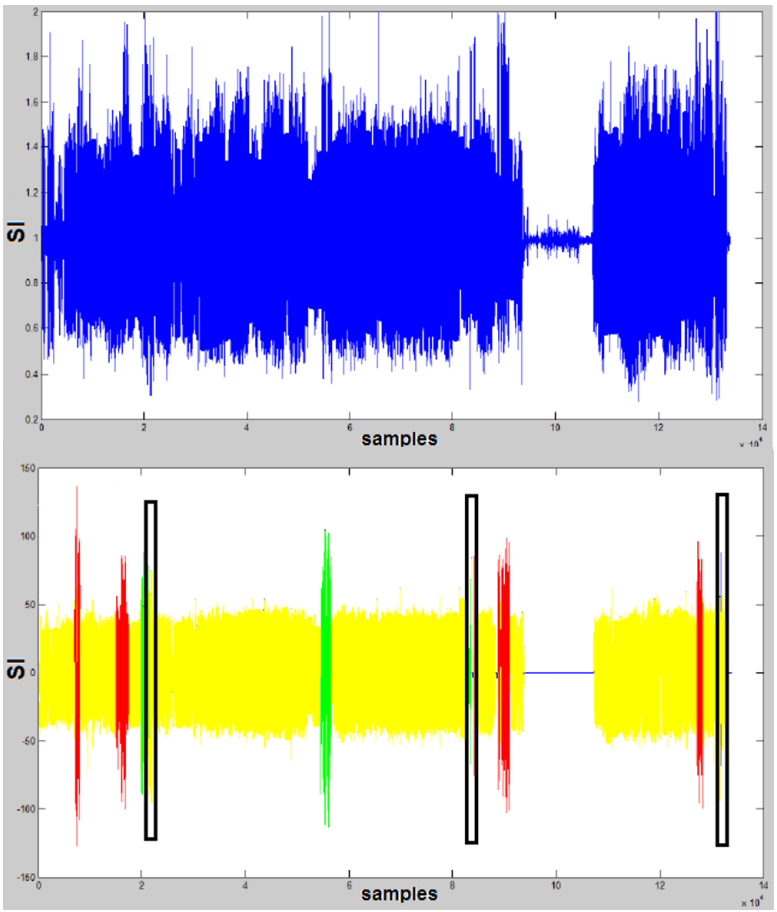

FIGURE 3.23: Patterns classification during a WNIM mixed static/dynamic patters experiment. The top figure represents the raw SI acceleration component. The bottom figure illustrates the DETECT outcome: blue line refers to the standing, the yellow concerns with the level walking, red and green pertains with the stair ascent and descent respectively. Black boxes highlight misclassification. The total duration of the experiments is about 45 minutes.

solution perfectly compliant with continuous, long-term daily applications in which the tracking activity of a user is required.

Chapter 4

Personal Indoor Localization

4.1 Introduction

Among HAR systems, a very promising category is represented by Indoor Positioning Systems (IPSs) for pedestrian. Indoor Location and Positioning (ILP) technology is considered the Next Big Thing, since it brings the power of Global Positioning System (GPS) and maps indoors, where people spend most of their time (working, shopping, eating, etc.) in different locations (malls, offices, campus, etc.). Over the past decade, IPSs have indeed become a focus of research and development, both in industries and academia.
Localization and tracking support is useful in many contexts [13] (special population care, key building management, retail industry, personal service, etc.), but becomes crucial in emergency response scenarios: being aware of team location is essential for a suitable rescue mission management.
For emergencies in large and complex indoor environments, first responders need to know their exact locations, possible escaping routes and potential risks (machinery, hazardous materials, etc.). From that, it can depend the life and the safety of rescuer and rescued persons. Properly localized and well informed about risks, rescuers can be better coordinated, commanded and guided reducing the possibility of disorientation and failure in victims localization.

Although a great deal of research efforts have been spent on these issues over the past years, actually there is not any off-the-shelf solution devoted to solve the indoor localization and tracking problem.
Current solutions mostly address the ILP problem by means of exteroceptive sensors. In such applications, systems require dedicated local infrastructures and/or customized mobile units. These systems typical use video [81], laser scanner [82] or wireless technologies (Wi-Fi [83], Zigbee [84], RFID (Radio Frequency IDentification) [85], ultrasound [86], Ultra Wide-Band (UWB) [87], Bluetooth [88], Pseudolite [13], infra-red [89]) for localization and tracking purposes. Depending on the positioning method they are based on, these systems can be ranked as active (i.e., the user is equipped with a specific device) or device-free systems.

A promising alternative to the afore-mentioned methods is represented by proprioceptive approaches, in which the user position is estimated by means of physical quantities measured directly within the user him/herself.
In this category, the most widespread methodology is definitively the inertial navigation. In such an approach, the user wears an inertial systems and the his/her pose (position and orientation) is defined using data retrieved from the platform (instantaneous acceleration, angular velocity, and local magnetic flux vectors), which are directly related to the motion of the body segment where the sensor is placed. Being internally

referenced and immune to interference and shadowing, inertial sensing can track body motion, in principle, without restrictions.

Both exeterocpetive and proprioceptive approaches present some limitations, that hinder the implementation of a pervasive IPS. Next sections aim to provide a general overview about the current state-of-the-art in the ILP field.

4.2 Related Work

Typical IPSs classification criteria take into account the sensor/s used (inertial platform, barometric altimeter, Doppler radar, UWB system, radio-based ranging, ultrasonic sensors, imaging sensors) by itself or in combination [90], stand-alone or powered-systems, the localization technique (i.e., triangulation, fingerprinting, Time Of Arrival [TOA] or the Time Difference Of Arrival [TDOA] methods, signal strength, data filtering and fusion, etc.), infrastructure-based or infrastructure-less systems, etc.
Next sections provide a survey on technologies and concepts for infrastructure-based/less positioning systems, showing their main up/downsides. Great emphasis will be devoted to IPS specifically conceived for emergency operations.

4.2.1 Infrastructure-less ILP systems

Infrastructure-Less IPSs (ILIPSs) track a person pose without any external references through the use of stand-alone, fully portable localization systems.
Typical ILIPS solutions consists in Inertial Navigation Systems (INSs), such as stand-alone IMU (or smart-phone) and/or Laser scanner, in case used in combination [91].
Common INSs use PDR approach and data retrieved from waist/foot-mounted IMUs or smart-phone. As users walk, their position is computed by double integrating the acceleration measurements while their orientation is retrieved from gyros data. Nevertheless, as stated in Chapter 2, inertial sensors are usually affected by biases and noises, whereby the single and double time integration causes that position and orientation errors grow unbounded along the path.
In order to reduce afore-mentioned errors, specific techniques have been proposed in the literature. Software components such as filtering, outlier detection, integration of INSs in hybrid positioning systems or with GIS (Geographic Information System) and topographical data play a major role for increasing the overall system performances [92].
In foot-mounted INSs for example, systems typically benefit from static periods for drift corrections (the so called zero-velocity update approach), that is performed during the stance phase, as the foot is stationary.
In waist-worn INSs, more sophisticated algorithms for navigation are required because the pelvis does not have similar zero-velocity points during the walking motion. In the waist-worn Pedestrian Dead Reckoning (PDR) approach presented in [93], accelerometer measurements retrieved from a waist-worn IMU are used to detect step events and to estimate step lengths. Concerning the orientation, simple numerical integration of the gyroscope data introduces drift errors and is not accurate for heading estimation. In order to reduce the pose-error, a quaternion-based Extended Kalman Filter (EKF) is proposed to estimate the full 3D attitude of the sensor module.
Alternative approaches to INSs [94], suggested the use of Laser scanners to solve the

indoor localization problem. The well-known 3D Simultaneous and Localisation Mapping (3D SLAM) technique used in robotics, allows estimating the 3D map and the six Degree Of Freedom (DOF) pose of a device/person through 3D point cloud matching methods (e.g., Iterative Closest Point [ICP]). However, the computational requirements for matching 3D point clouds are typically prohibitive for real-time implementations. More importantly, the 3D laser scanners needed for acquiring the point clouds are usually too large and heavy for a person to carry, thus making these systems inappropriate for use as a personal navigation aid.
Alternative methods for performing 3D SLAM employ cameras to map the environment based on visual landmarks. The main drawback of camera-based systems is the sensitivity to variable lighting conditions, which restricts their use as navigation aids for the visually impaired where reliability is paramount. Additionally, processing images and extracting visual features are typically computationally intensive tasks that are impractical to carry out on hand-held computing devices. Furthermore, the visual landmark (e.g., features) often used in these approaches may not be geometrically meaningful or interpretable for humans. Finally, extracting and matching visual landmarks in indoor environments can be challenging and unreliable due to insufficient texture.
The majority of the proposed systems for SLAM consider either 2D map and sensor motion, or restrict the sensor motion to planar surfaces and create a 3D map of the surroundings. However, these algorithms are not suitable for use on a personal navigation system since the motion of a human is not limited to a planar surface (e.g., when climbing stairs) [94].

Concerning emergency scenarios, several ILIPSs solution have been proposed over last years to provide high-performance deep indoor positioning system.
In 2004, the Personal Navigation System (PeNa) [95] of the PeLoTe project was designed to be a stand-alone localization solution. The position estimate has been achieved by the PDR algorithm and map-based localization. PDR includes step measurements (pedometer), magnetic sensors (compasses), inertial measurements (gyros and accelerometers) and a laser (used for map building and localisation). Although the PeNa is a fully portable system, the total weight of the system is approximately $14\ kg$ without the laptops and represents a proof-of-concept: the PeNa hardware is incompatible with both rescuer equipment and operating conditions.
A more recent example of IPS for emergency operations is the WASP [96] system, a Wearable Advanced Sensor Platform developed by Globe. This body-worn system integrates physiological monitoring and location tracking into a single system that collects, transmits and displays user data to a command station. The Physiological Status Monitoring (PSM) system tracks in real time fire-fighter heart rate, respiration, activity levels and other physiological factors. The PSM sensor is on a strap housed within a fire resistant T-shirt. The location tracking system is worn on a belt under the fire-fighter's turnout gear.
Although WASP represents a fully equipped, stand-alone system for ILP tasks, the lack of external references may influence the accuracy in the pose estimation especially in long-lasting mission. The extreme operating conditions typical from Search & Rescue applications (i.e., high temperatures, humidity rate, etc.) may indeed affect sensors performances. MEMS gyros are quite sensitive to temperature changes and may also exhibit non-linearities that cannot be easily modelled.
In [97], to increase the overall performance of the ILIPSs in operating condition, authors

described a framework for fusing building plans and PDR approaches. A novel implementation of map filtering, called the Backtracking Particle Filter (BPF), was evaluated with real PDR displacement data and a building plan as input. It was shown that the BPF can take advantage of long-range (geometrical) constraint information provided by various levels, effectively mitigating heading errors.

As stated, even if the rate of pose-error increase can be reduced, actually PDR systems still remain unreliable over long time intervals [91].

4.2.2 Infrastructure-based IPSs

Infrastructure-Based IPSs (IBIPSs) infer the user position and orientation information from known landmarks deployed into the environment.
Typical IBIPS signal technologies include Radio Frequency (RF) technology, ultrasound, infra-red, vision based systems and magnetic fields. The RF signal based technologies can be split into WLAN (2.4 GHz and 5 GHz band), Bluetooth (2.4 GHz band), UWB and RFID [94].
GPS can provide centimetre-level positioning accuracy in outdoor environments. However, Global Navigation Satellite Systems (GNSSs) have difficulties operating indoors, the signals being severely attenuated when propagating through walls and become too weak for standard GNSS receivers for ILP tasks. The AGNSS (Assisted GNSS) or AGPS (Assisted GPS) addresses this problem. AGPS is successfully used for localisation of mobile phones. A data link via mobile phone provides information of the satellite Ephemeris, Almanac, differential corrections and other relevant information that is normally obtained from the GNSS satellites directly [92]. As a consequence, the AGPS receiver can more easily lock on the satellites and obtain a fix position, assuming that some weak GNSS signals can be received. In order to make use of the weak satellite signals indoors, the low signal to noise ratio is improved by integration over multiple intervals, which on the other hand requires longer acquisition times.
The signal blockage due to obstructions and the low power of satellite signals can be also compensated by combining GNSS with a self-contained INS. The integrated system can provide continuous position, velocity and attitude solutions during a short outage of GNSS. However, the maximal outage time is limited, because the positional error of INS only has a drift that increases unfounded by the outage time of GNSS.
A new terrestrial, RF-based distance measurement technology offers promise of continuous signal coverage, even in difficult urban/suburban/indoor environments [98, 99]. The new LOCATA approach consists in a network of ground-based transceivers that cover an area with strong time-synchronised ranging signals. When a LOCATA receiver uses four or more ranging signals, it can compute a high accuracy position entirely independent of GPS or INS. However, a standalone LOCATA receiver has its own shortcomings: in some situations it may be difficult to achieve good dilution of precision (i.e., accuracy in the position estimation) due to logistical constraints of placing transmitters (to give a variation in elevation angle between the terrestrial transmitters and the receiver whose positions is to be determined), and as with GPS, multiple receivers/antennas are required to derive orientation information [94].
Focusing the attention on IBIPSs using other technologies than GPS, localization systems available on the market are currently based on LASER tracker, ultrasound solutions (Crickets, Active Bat, DOLPHIN), WLAN and Bluetooth technologies (Symeo, EKAHAU, MAGIC MAP, SIPS) [92]. Localization based on passive RFID technology offers great potential for commercial use due to the extensive installation of passive

RFID tags, the low cost of tags and the effortless maintenance required. The stability of RFID localization is better than other radio-based localization systems, such as WLAN or GSM localization, due to the relatively small reading range. Nevertheless, each specific technology has its own drawbacks such as low accuracy, sophisticated infrastructures, limited coverage area or inadequate acquisition costs.

Concerning systems specifically conceived for emergency operations, IBIPSs systems can be classified into two main categories: ad hoc IBIPSs, where localization/ tracking device are placed on-the-fly by first-responders, and pre-installed IBIPSs. To overcome the aforementioned IBIPSs limitations, the pre-deployed/ad-hoc network of sensors is usually integrated with the measures obtained from proprioceptive sensors (INS), in order to increase the overall system performance.

The LifeNet system, proposed by [100], provides the functionality of a traditional lifeline. It is based on a sensor network that first responders deploy on-the-fly during an intervention and a wearable system that provides them navigational support. The essential elements of LifeNet implementation are a wearable computer able to receive positioning information from the beacons integrated within the boots, a micro-display integrated in the breathing mask to present navigational information and the ultrasound beacons deployed on-the-fly during the mission. Instead of showing a map, the interface presents an egocentric representation of the user surroundings. The LifeNet beacons are implemented by RELATE bricks, which are essentially stand-alone mobile computers equipped with an 8bit PIC18 micro controller and 868 MHz TR1001 radio front-end. The main characteristic regarding LifeNet is that two bricks can determine the distance and the angle between them.
In EU Project LIAISON [101], a self-deployable passive network is considered. While progressing indoor, the first responders deploy passive RFID tags that are used to correct the large errors affecting MEMS performances by an EKF. This principle follows the idea told by the "Hop o'my thumb" story. In the FIRE project, the SmokeNet Wireless Sensor Network (WSN) is used to track first responders while operating in large building incidents and supply key information to all parties involved. Basically, SmokeNet allows first responders to quickly determine where in the building the fire started, how the fire is spreading and which evacuation routes are safe. The FIRE rescue architecture provides also several additional features. The information retrieved by SmokeNet are shown on the FireEye, an Head-Mounted Display (HDM). The same data are communicated to the electronic Incident Command System (eICS) software. Localization is performed by exploiting beacons motes that constantly broadcast static information.
The Hybrid Rescue Teams Localization System (HRTLS) [102, 103] considers hybrid team composed by both human operators and robots. Hybrid team uses pre-deployed RFID tags embedded in emergency signs, extinguishers and emergency lamps to correct PDR. PDR is performed using commercial smart phone equipped with an inertial sensor. The RFID tags are static, while first responders and robots wear the mobile readers. To validate the approach, tags providing information in about 2 m range are considered. The deployment effort is negligible, with a considerable cost in map maintenance. The localization system, however, is reliable, since it is based on an Bayesian adaptive filter able to solve both localization and SLAM when changes occur in the environment. The main goal of HRTLS is to create location awareness for both the supervisor and the rescuers inside the emergency area. HRTLS provides also several additional features: redundant communication channels are sketched in the architecture to share information between the hybrid team and the supervisor; inertial sensors are used to identify rescuers in distress. The major limitation of HRTLS stems in the

implementation: it has been tested only by simulation and still needs to be validated in a real emergency situation.

In conclusion, while GNSS have become the dominating system for open-sky, actually several systems share the indoor market; each having its own drawbacks. To overcome such limitations, the usage of signals that can penetrate building materials, or better, the combination of more than one IPS technique may probably overcome this problem in the near future [94].

4.3 Contributions

As illustrated in previous sections, even if several solutions have been proposed for solving the ILP problem, different drawbacks limit their widespread diffusion especially in emergencies.
For example, video and laser-scanner systems are almost unsuitable with emergency applications peculiarities because of their reliance on environmental lightning [90], the power supply requirement, the computational load demand for image and/or point cloud processing [94, 90], and the weight to be carried by the user [95].

Concerning the wireless category, although these systems are usually able to provide the localization of the user, some issues should be addressed. Apart from typical concerns affecting exteroceptive localization systems (e.g., non-line of sight, shadowing, interferences), it is crucial focusing that most of the wireless solutions use the trilateration for localization purposes. Since in the 2D space, a point needs the positional knowledge of at least three non-linearly spaced anchor nodes to be localized, the tracking and localization support into unknown indoor environments relies on the deployment of a huge number of anchors into known-fixed positions for a fitting area coverage.
In addition to potential issues arising from sensors deployment, these systems may be also not suitable for applications in emergency scenarios because of their need of dedicated power supply infrastructures. This latter limitation has been partially overcame by ILP solutions [104], [105] providing for the deployment on-the-fly of anchor nodes within the emergency area in ad-hoc positions by the rescuer team throughout the mission. Nevertheless, these solutions are usually quite expensive, require a considerable time for sensors deployment and, most importantly, they typically present limited penetration capabilities, making them merely ineffective for the exploitation in deep indoor and underground scenarios.

Nevertheless, INSs also present some limitations. First and foremost, these systems compute the user's position by using data retrieved from the inertial platform, including any superimposed sensors drift and/or noise; it implies that the estimation errors tend to grow unbounded. In addition, inertial sensors are not well-suited for determining absolute location: the computation starts from initial conditions, which inertial sensors cannot help defining (position, velocity), or disambiguate completely (orientation).

To overcome the limitations of both approaches, in this work we present the Hybrid Indoor Positioning system (hereafter, the HIPS) that integrates inertial navigation and RFID technology for assessing personal indoor localization and tracking in the 2D space.

In general the RFID technology exploits active receivers (i.e., RFID readers) installed into the environment and transponders (i.e., tags) attached to specific items to identify and track objects. Tags are indeed equipped with a built-in memory that is able to carry a limited amount of information about the object/person to be tagged.
The HIPS flips over the classic RFID approach: the environment is kitted out with pre-deployed RFID passive tags provided with information about their absolute geographical position. On the other side, the user is equipped with a waist-mounted IMU, an active RFID reader and a mobile unit for data collection.
The IMU, that integrates tri-axial accelerometer, gyroscope and magnetometer, provides for instantaneous acceleration, angular velocity and local magnetic field vectors. Using the PDR approach, the information collected from the IMU are processed to provide an estimate about the operator's relative pose (i.e., position and orientation).
The fusion between inertial navigation data and geo-referenced information about tags position results in the HIPS: the pose estimate from the inertial navigation is then eventually corrected by means of data retrieved from detected tags using a strategy specifically conceived within the HIPS.
In such a way, the HIPS is able reducing the drift error which the inertial system is affected providing a position estimation having a room-level accuracy by using a limited set of RFID tags. The number of tags required for the drift error compensation in support to inertial navigation is indeed considerably lower with respect to the one need for the position computation in typical wireless-based ILP applications.
Furthermore, HIPS uses passive tags and does not require for external power supplying. For facilitating the sensors deployment and a fitting area coverage, the HIPS framework envisages that passive tags are embedded into the emergency signs.
To mention that the HIPS has been design to operate in real operating scenarios and it is perfectly compliant with typical rescue missions requirements.
Although RFID does not require line of sight for communication and it can read several tags simultaneously even in adverse environmental conditions, the antenna radiation pattern and the tag detection area strictly depend on the environment layout (i.e., may cause multiple reflections), operating conditions (i.e., temperature, humidity, etc.) and the local proximity of metals and liquids. All these factors may contribute altering the local system's electromagnetic field thus causing a potential system performances degradation. In addition to the aforementioned issues, the information about systems performances provided by vendors are often inaccurate or usually not suitable for ILP applications.
In order to assess the typical shape of the tag radiation lobe both in static (i.e., the user is stationary) and dynamic (i.e., the user is moving into the environment) conditions, extensive experimental trials for the characterization of the RFID system adopted within the HIPS have been performed. Outcomes from experimental trials allowed us defining a suitable correction strategy for the user pose provided by the inertial navigation system, accordingly.

4.4 The Hybrid Indoor Positioning System

The HIPS is able to compute the position and the attitude (i.e. orientation) of a rescuer in the operating scenario with respect to a global reference frame. It has been specifically designed within the European research project REFIRE[1] to meet first responders requirements. It envisages the use of Mobile Terminals (MTs) carried by the rescuer and low-cost highly standardized Pre-Installed Location Devices (PILDs), as illustrated in Figure 4.1.

In the HIPS implementation, the MT consists of a sensory system (i.e., an inertial

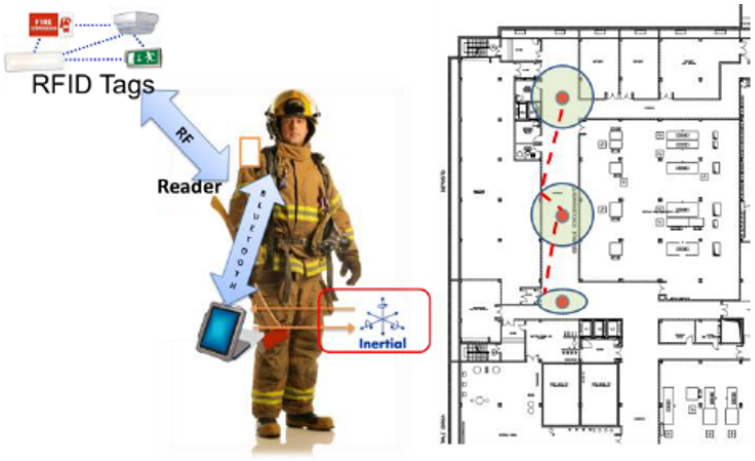

FIGURE 4.1: The HIPS general framework.

platform integrating a tri-axial accelerometer, a tri-axial gyroscope, a tri-axial magnetometer and a RFID reader) connected to a computation unit while PILDs correspond to RFID passive tags.

Concerning the inertial sensor placement, in chapters 2 and 3 we have illustrated as the position represent a typical design choice in HAR systems.

As stated in [106], the waist or trunk locations are probably the less intrusive IMU placements, and also the most reliable position for the heading estimation using gyroscopes or magnetometers. Locating the tracking device on one or more limbs may also limits the agility of the operator. For the above-mentioned reasons, in the HIPS the inertial platform is waist mounted; the pose of the inertial sensor is the same as for the DETECT, as illustrated in Figure 4.2.

The RFID reader together with the computation unit is placed on the left shoulder of the rescuer.

The strategy on which the HIPS relies provide for handling IMU data with the PDR algorithm to continuously estimate the rescuer position and for correcting it any times the rescuer is close enough to a PILD.

According to the REFIRE standard, the localization message is encoded in the user

[1]REFIRE (REference implementation of interoperable indoor location & communication systems for FIrst REsponders) is a two years project (2012-2013), co-funded by the European Commission, Directorate-General Home Affairs in the framework of the call "CIPS Action Grants 2010". Among partners, the REFIRE project includes the participation of the Italian Fire Corps. To mention that the HIPS architecture is currently used in the ongoing research project RISING (indooR localizatIon and building maintenance uSing radio frequency Identification and inertial NaviGation). The RISING project aims at refine on the HIPS paradigm to provide first responders an indoor positioning and situation awareness system, at the same time.

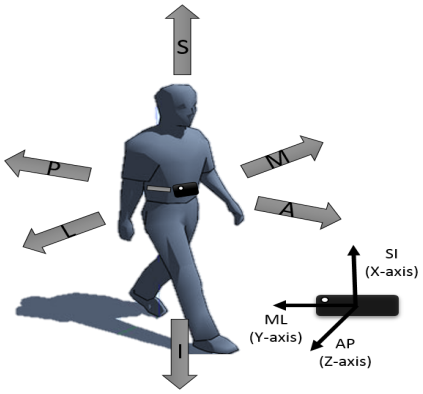

FIGURE 4.2: Local IMU coordinate frame and body-fixed coordinate frame poses. In the HIPS, we assume the two frame coincide: the IMU frame axes (x,y,z) are aligned along with the Superior-Inferior (SI), the Medio-Lateral (ML) and the Anterior-Posterior (AP) directions of the body segment, respectively.

memory of the RFID tag and is composed by seven fields. Users equipped with RFID readers can retrieve such information, which consist of:

- *REFIRE id*;
- *Geographical coordinates* provided adopting the WGS-84 standard for cartography, geodesy, and navigation;
- *Device classification* identifies the type of device (e.g., emergency lamp, sign, etc.) and its position in the emergency area (e.g., floor, mezzanine, corridor, etc.);
- *Tag classification* indicate the type of the tag (passive, semi-passive, or active);
- *Accuracy* is a data that characterizes the form of the electromagnetic field provided by the tag antenna;
- *Date* represents the last update of the information stored into the device.

During the mission, the rescuer is tracked by the algorithm running on the computation unit and sketched in Figure 4.3. The computation of the attitude and the position of the rescuer is addressed separately, so the *Sensory System* feeds both the *Attitude Filter* and the *Tracking System*.
The *Attitude Filter* is based on data retrieved from the inertial platform and computes the attitude of the rescuer with respect to a fixed Cartesian global reference frame (hereafter, called the navigation frame). The output of this filter is used by the *Tracking System* to produce the pose of the rescuer exploiting also data collected from both the inertial platform and PILDs. To this end, the *Tracking System* is further decomposed into a prediction-correction schema, according with the approach used in robotics localization, where both proprioceptive and exteroceptive sensors are jointly used.

It is worth noticing that all the filters run in a off-line fashion and the loops have different frequencies: the attitude computation depends on data retrieved from the gyroscope, the inertial prediction is based on the step-event detection, and the RFID refinement is based on PILD detection events, as it will be explained in the following section.

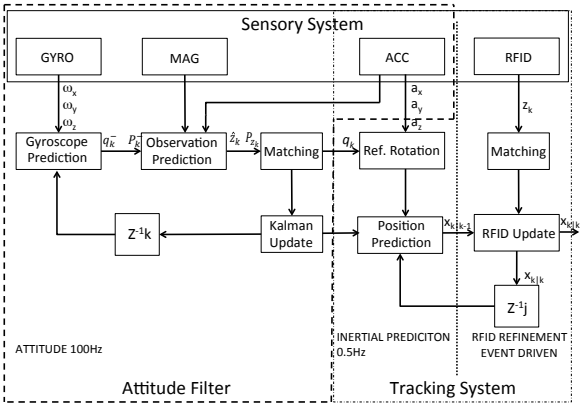

FIGURE 4.3: the HIPS architecture.

4.5 The Tracking System

As stated in Section 4.4, the Tracking System computes the user pose using a prediction-correction schema. In details:

- the *prediction phase* provides an estimate of the user pose by means of data retrieved from the IMU through the PDR approach;
- the *correction phase* uses data retrieved from PILDs, when available, to correct the pose estimate provided by the prediction phase.

4.6 The prediction phase

Concerning the PDR approach, Harle in [107] proposes a distinction between INSs and Step-and-Heading Systems (SHSs). An INS is a system that tracks position by estimating the full 2D trajectory of the sensor at any given moment. An SHS is specific to pedestrians, estimating position by accruing distance and heading vectors representing either steps or strides.
In this work we use the SHS approach for the 2D inertial localization. The fundamental cycle for a SHS is [107]:

1. identify subsets of the data corresponding to individual steps or strides;
2. estimate the length of the step;
3. estimate the step heading or change in heading.

Specifically, the accelerometer measurements retrieved from the IMU are used to implement the first and the second phase, known as *step detection* and *step length estimation*, respectively. The heading determination is simultaneously retrieved from the IMU through the *Attitude Filter* by fusing the information from gyroscopes, accelerometers, and magnetometers, as illustrated in Section 4.6.3.

Once all the information are available (i.e., the $j-th$ step event is detected, the corresponding step length s_j and heading $\bar{\theta}_j$ have been estimated), the 2D pedestrian motion propagation can be computed as follows:

$$\begin{aligned} \hat{p}_j &= \hat{p}_{j-1} + l_j \\ P_j^p &= P_{j-1}^p + Q_j^p \end{aligned} \tag{4.1}$$

where $\hat{p}_j$ is the current position estimate of the user with respect to the global reference frame, $\hat{p}_{j-1}$ is the previous position estimate, $l_j = [s_j cos\bar{\theta}_j, s_j sin\bar{\theta}_j]^T$ is the vector displacement, with $\bar{\theta}_j$ the average orientation during the sampling interval $[j-1, j]$ elapsing between two consecutive step events.
The second equation in 4.1 states the uncertainty of the PDR model for the pose update. Specifically, P_j^p represents the 2×2 error covariance matrix[2] associated with the corresponding pose p_j at step j, and $Q_j^p = l_j \; Q^p \; l_j^T$ with Q^p the 2×2 covariance matrix related to the PDR model uncertainty.
As a recursive approach, it is plane from the equation 4.1 that each time a step event is detected, the user position is updated within its uncertainty (P_j^p) with respect to the previous position estimate (p_{j-1}, P_{j-1}^p). To mention that the starting position of the operator has been assumed the same as the origin of the reference frame (the navigation frame, as illustrated in Section 4.6.3). To note that the error covariance matrix P_j^p apart from the recursive approach illustrated in equation 4.1, could be also updated according to a specific strategy adopted within the correction phase, as will be illustrated in Section 4.7.

Focusing on the prediction phase, different strategies have been proposed in the literature for step event detection and step length estimation. Following sections outline the strategies implemented.
The attitude filter and its derivation are illustrated in the Section 4.6.3. Experimental results concerning the prediction phase are illustrated in Section 4.6.4.

4.6.1 Step event detection

The first task of an SHS is the identification of steps or strides within the data. Different strategies have been proposed in the literature for this task and all the approaches use the acceleration data for the step identification [107, 106, 108, 109, 110, 111, 112, 113]. Depending on the position of the inertial sensor, these algorithms are usually classified into *stance detection* (the sensor is placed on the foot) and *step cycle detection* algorithms (the platform is mounted on elsewhere on the body other than feet) [107] .
The sensor position selected during the HIPS design has driven our investigation to the second category of algorithms. As stated in [107], these algorithms detect cycles in the sensor data caused by the repetitive motion of walking. This may involve searching for repeating data patterns or for repeating events (e.g. the heel-strike) and are well suited to step segmentation.
As part of HAR systems, SHS solutions firstly require the identification of the user activity (i.e., standing, level walking, etc.); once the walking activity has been discriminated, a dedicated algorithm can be exerted for counting the number of steps performed, known as *Step Counting*(SC) algorithm.
In this work, the identification of the activity under investigation (i.e. level walking) has been performed using a light version of DETECT (see Chapter 3), the L-DETECT. Specifically, it considers only the first two levels (Lev. 0 and Lev. 1) of the decision tree in order to identify which windows of the segmented signal pertains with the level walking activity.
After the classification, the windows identified as level walking undergo to a SC algorithm.

[2] As illustrated in Section 4.6.3, the error covariance matrix is common metric used to oint out the uncertainty related to an estimate.

In general, a SC algorithm aims to identify specific cues in the segmented acceleration signal for detecting the number of step performed. Different features have been proposed for detecting steps; peaks, zero crossing and signal autocorrelation represent the most used.
Next sections provide a description about the algorithms implemented for steps counting. The set of the proposed approaches hold both methodologies known from the literature that newly developed approaches. The selection of a specific SC algorithm for the HIPS has been fostered by results achieved during trials, as illustrated in Section 5.4.2. Nevertheless, the operating principle of each methods is graphically illustrated by means of some preliminary results.
To mention that in all the approaches is the vertical acceleration component (i.e., the SI component from Figure 4.2) the element under investigation. Concerning the ARC stages for the L-DETECT, the same parameter setting as described in Chapter 3 has been assumed.

Peak detection

Peak detection algorithms detect a step as a peak occurs in the SI acceleration signals. The heel strike is indeed associated with sharp changes to the vertical acceleration. Standard peak detection algorithms can be used to highlight potential strikes.
To note that each foot impact may generate multiple local peaks the nearer to the foot

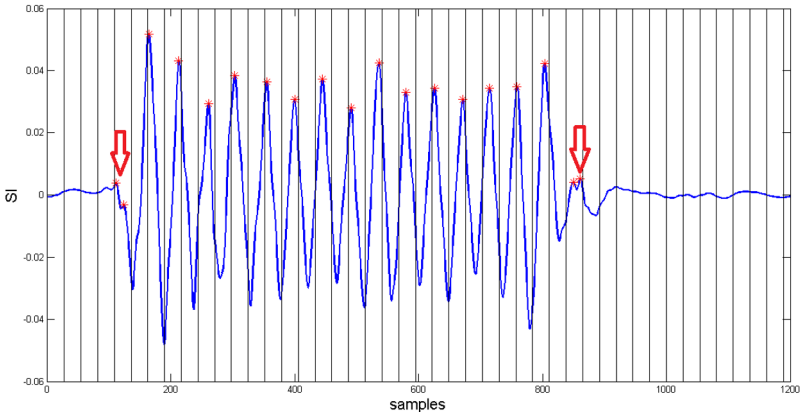

FIGURE 4.4: Step counting: the peak detection algorithm. In blue, the SI filtered and segmented acceleration component during a 15-steps trial. Red stars indicate peaks detected, red arrows indicate outliers.

it is sited, due to the higher forces resulting in sensor bounce.
Figure 4.4 shows the output achieved using a classic peak detection algorithm during a 15-steps level walking test.
Although its easy implementation and widespread diffusion, it is our opinion that the algorithm is not able to discriminate between peaks due to steps and outliers. Red arrows in Figure 4.4 indicate outliers (i.e., false positive), that is peaks non associated with step although they are not. This implies that the precision rate (see Chapter 3) within the test is about 80%.

For these reasons, peak detection algorithms are usually associated with other strategies that may significantly increase their complexity [107] as well as their identification accuracy.
Some solutions assume a threshold-based approach for selecting peaks associated with

steps. The threshold usually is fixed [114, 107] but in this work, we propose an adaptive approach.
Figure shows the outcome of the peak detection adaptive threshold-based approach. The threshold has been computed by averaging the SI samples within the window in which the step is detected. This methodology enables to achieve a precision of 100% for steps detection, as illustrated in Figure 4.5.

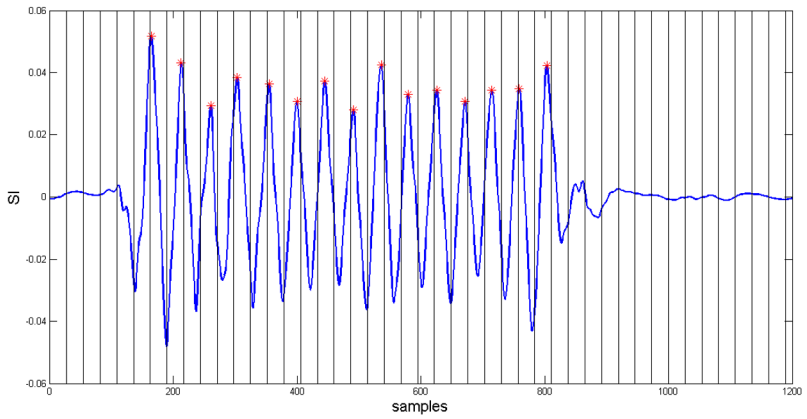

FIGURE 4.5: Step counting: the peak detection algorithm with adaptive threshold. In blue, the SI filtered and segmented acceleration component during a 15-steps trial. Red stars indicate peaks detected.

Zero crossings

A cheaper way to use for monitoring the cyclic property of the acceleration value is the zero crossings approach. This is indeed a popular choice for pedometers or activity monitors due to its simplicity [107].
Several algorithms have been presented in the literature for detecting zero crossings. In this work, the proposed strategy aims to detect a zero crossing (i.e., a step occurrence) when two consecutive samples of the SI acceleration component pass from negative to positive values. Figure 4.6 illustrates the results achieved using the zero crossings algorithm within the 15-steps trial. This method enables to achieve a good precision in steps counting, without requiring further constraints. For the trial illustrated in Figure 4.6, the precision is about 93%.

COM position in the sagittal plane

An alternative strategy for steps counting has been proposed by Goyal et al. in [93]. This step event detection scheme is based on the description of waist accelerometry given by Zijlstra [115]. It relies on the fact that each step even involves the rise and fall of the pelvis. The vertical displacement of the pelvis (i.e., COM) can be estimated by double integrating the SI acceleration component.
The vertical displacement thus obtained, however, has a large integration drift. In order to remove this drift, Goyal et al. propose to filter the signal using a zero-lag high-pass Butterworth filter with a cut-off frequency of 0.1 Hz.
Steps are detected as peaks in the resulting vertical displacement (see Figure 4.7). As

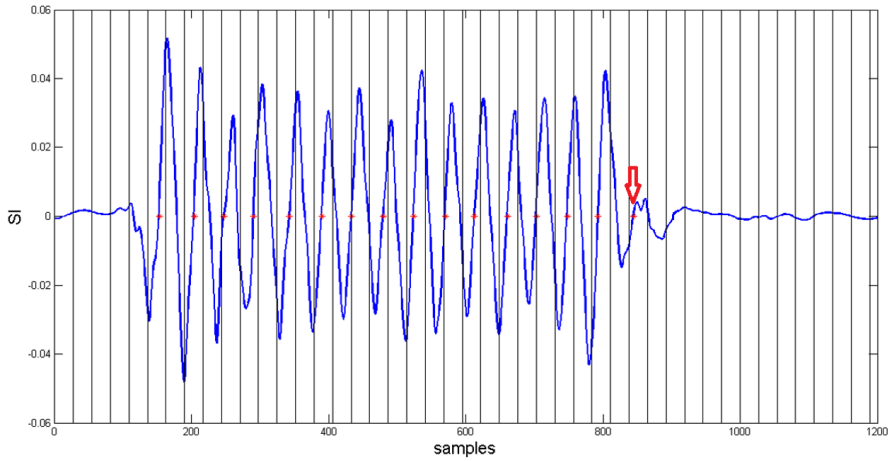

FIGURE 4.6: Step counting: the zero crossings detection algorithm. In blue, the SI filtered and segmented acceleration component during a 15-steps trial. Red stars indicate zero crossings detected, the red arrow indicates an outlier.

the numerical integration itself acts as a low-pass filter, the resulting curve is smooth and no further low pass filtering is required. Figure 4.8 shows the SC results using the

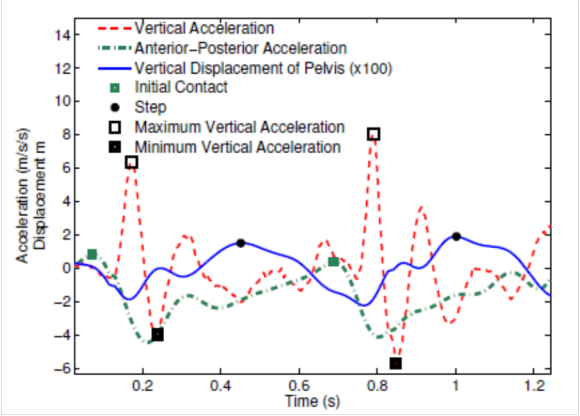

FIGURE 4.7: Step counting: methodology proposed by Goyal et. al in [93]. The vertical displacement is multiplied by 100 to make it comparable to SI and AP acceleration. (Source [93]).

method proposed by Goyal et al. within a 15-steps trial. To mention that as for other methods, the SI acceleration component undergoes to the L-DETECT before performing the double integration. The precision is about 88% for the 15-steps trial.

Normalised autocorrelation

Several researches [116, 113, 117] propose to use the accelerometer autocorrelation for SC.
In [117], Rai et al. proposed the Normalised Autocorrelation Step Counting (NASC),

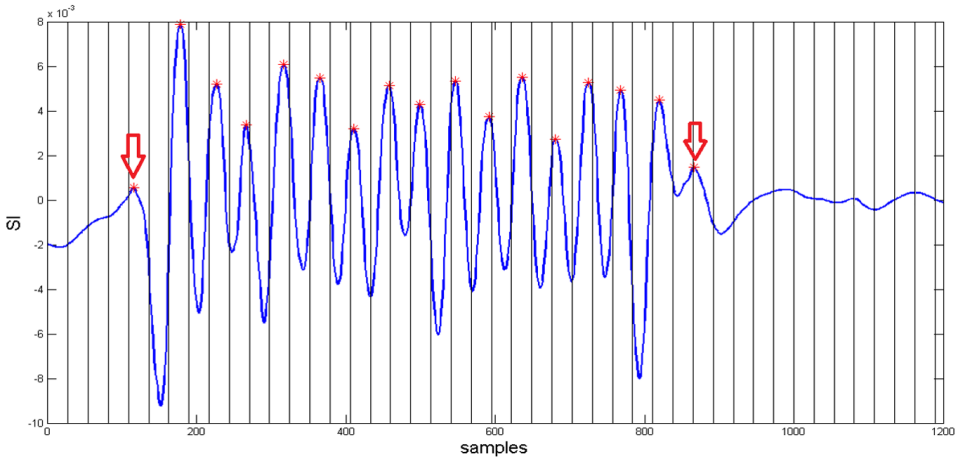

FIGURE 4.8: Step counting: methodology proposed by Goyal et. al in [93]. In blue, the SI filtered and segmented acceleration component during a 15-steps trial. Red stars indicate peaks detected, red arrows indicate outliers.

that is based on the intuition that if the user is walking, then the autocorrelation spikes at the correct periodicity of the walker.
Specifically, given the $a(n)$ acceleration signal corresponding to the SI component, the NASC computes the normalized auto-correlation for lag τ at the $m-th$ sample as:

$$\chi(m,\tau) = \frac{\Sigma_{k=0}^{k=\tau-1}\left[(a(m+k)-\mu(m,\tau))(a(m+k+\tau)-\mu(m+\tau,\tau))\right]}{\tau\ \sigma(m,\tau)\ \sigma(m+\tau,\tau)} \tag{4.2}$$

where $\mu(k,\tau)$ and $\sigma(k,\tau)$ are the mean and the standard deviation of the sequence of samples $a(k), a(k+1), \ldots, a(k+\tau-1)$.

When the person is walking and τ is exactly equal to the period of the acceleration pattern, the normalized auto-correlation is close to one. Since, the value of τ is not known a priori, NASC tries values of τ between τ_{min} and τ_{max} to find the value of τ for which $\chi(m,\tau)$ becomes maximum.
Once τ_{opt} has been retrieved, it gives the periodicity of the person walks (i.e., the time lag between to consecutive step).

Brajdic et al. in [113] propose an alternative NASC algorithm. They firstly assess if the user is walking by focusing on the SI acceleration component. Specifically, when a standard deviation threshold, σ_{thr}, is exceeded, they evaluate the normalised auto-correlation over a 2 s window for a series of appropriate time lags (τ_{min} to τ_{max}). Then, if the maximum of the auto-correlation computed with 4.2 exceeded a threshold, R_{thr}, the user was asserted to be walking. The walking state ended when the standard deviation fell back below σ_{thr}.
The steps counting is performed by computing the normalised autocorrelation as in equation 4.2 for rolling 2 s time windows. For each window, they take the time lag corresponding to the maximum autocorrelation as the stride period and the fractional steps computed. The step count was the sum of these fractional values.

Researchers in [113] do not mention to the value of the threshold used. At the same time, the method proposed in [117] is computational demanding and it has not given the expected result during the experimental trials.
For this reason, in this work we propose an alternative strategy that uses the Normalised Autocorrelation (NA) of the SI acceleration component for steps counting.

Specifically, as for previous methods the walking activity has been identified using the L-DETECT. Using the equation 4.2, the NA is then computed for the windows selected (i.e., in which the walking activity has been assessed), within the mean ($\overline{NA}_{walk}$) and the RMS (NA^{rms}_{walk}) values.
Given that the NA is an even function (see Figure 4.9), for the SC we consider only the

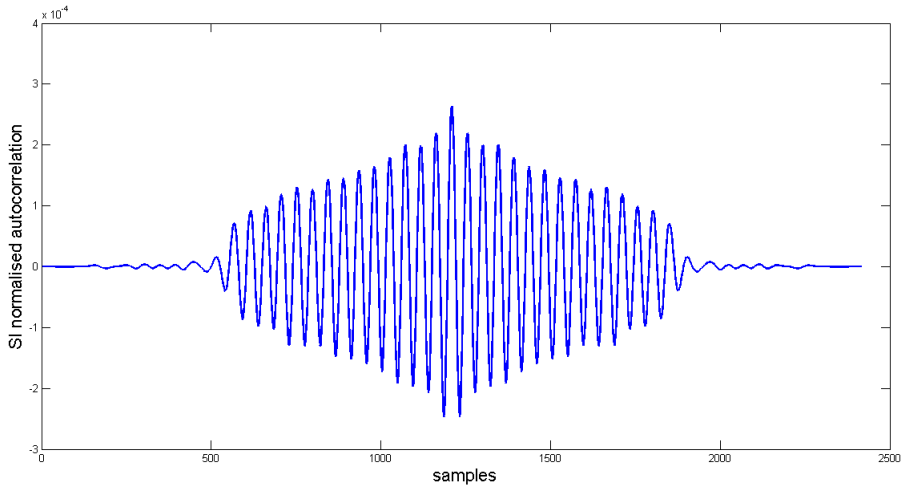

FIGURE 4.9: Normalised autocorrelation computed as illustrated in the equation 4.2 of the SI acceleration component during a 15-steps trial.

half of the NA (H-NA). A step occurs when a peak in the H-NA exceeds the threshold $step_{thr} = \overline{NA}_{walk} + NA^{rms}_{walk}$. To note that the $step_{thr}$ is not fixed but adaptive because it is computed each time on the current data arising from the equation 4.2. Figure 4.9 shows the NA of the SI component during the 15-steps trial. Figure 4.10 illustrates results for the steps count by means our proposed method for the H-NA; the sensitivity within the test is about 93%.

Peak detection & zero crossing

The last method we present for the steps counting combines two of the strategies above illustrated: the peak detection and zero crossing. To mention that it has been specifically design and actually it has not been yet proposed in the literature.
As for other methods, the SI filtered and segmented acceleration component undergoes to the L-DETECT. For the SI samples selected from the gait patterns identification algorithm, we use both the peaks detection and the zero crossing methods. Specifically, when a peak occurs in the SI, we check if the signal crosses also the zero in the close proximity of the peak itself. If it is the case, a step occurred.
To mention that the step count has not been performed on the SI samples pertaining to a single window, because the segmentation may split the two features (i.e., peak and zero crossing) between two adjacent windows (see Figure 4.11).
Figure 4.11 shows the result achieved in the 15-steps trial. The method is able to perfectly identify the 15 steps (sensitivity, specificity and precision are 100%).

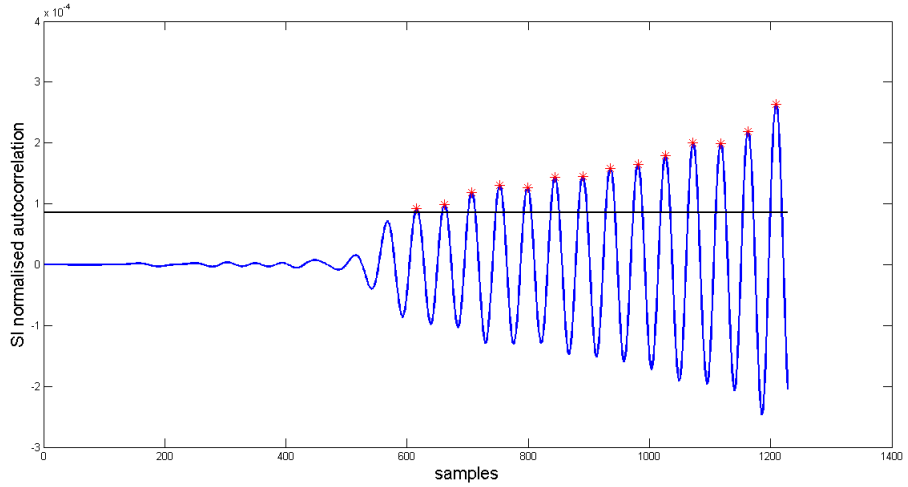

FIGURE 4.10: Step counting: using the normalised autocorrelation. In blue, the normalised autocorrelation of the SI filtered and segmented acceleration component during a 15-steps trial. Red stars indicate peaks detected and the black horizontal line concerns with the threshold $step_{thr}$.

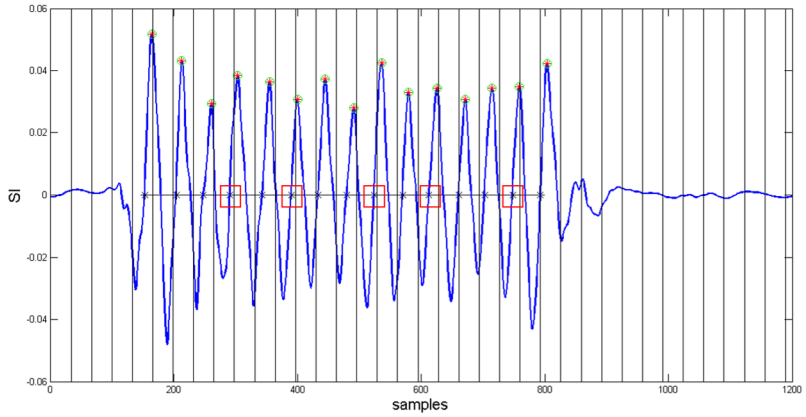

FIGURE 4.11: Step counting: using peak detection and zero crossing. In blue, the SI filtered and segmented acceleration component during a 15-steps trial. Red stars indicate peaks detected, black crosses indicate zero crossings and the green circle identify when a peak is discriminated as a step. Red squares show how the application of this strategy on the segmented signal may prove ineffective: peak and zero crossing pertaining the same step may indeed occur in adjacent window.

4.6.2 Step length estimation

Several step length estimation techniques have been devised for different applications. Levi and Judd have described a technique in which step length is modelled as a linear function of the step frequency [118]. Kim et al. have described a method that does not need to be calibrated for different users. However, their method assumes that the IMU is worn near the foot [119].
Zijlstra et al. have described an inverted pendulum model for the motion of pelvis during a step [115]. This method requires the leg length to be measured experimentally and is known to be sensitive to user calibration. Weinberg et al. [120] have proposed

an approximation of the popular inverted pendulum model described by Zijlstra et al. [115] that does not require knowledge of the leg length. In prior work, a comparison of several popular step length estimation schemes has revealed that the technique described by Wienberg et al. is best suited for a waist mounted IMU using generalized calibration values.
The method proposed by Weinberg et al., estimates the length of the $j-th$ step (s_j) performed by a user equipped with a waist-mounted IMU, from the corresponding vertical displacement of the pelvis (h_j), as illustrated in Figure 4.12. They have empiri-

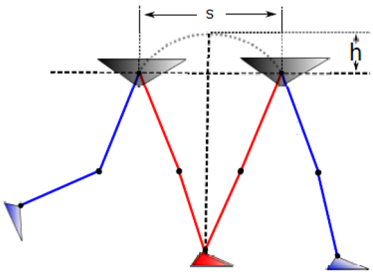

FIGURE 4.12: Motion of the pelvis during a step. Source [93].

cally demonstrated that the step length can be approximated as:

$$s_j = K \sqrt[4]{a^{SI}_{j,max} - a^{SI}_{j,min}} \tag{4.3}$$

where $a^{SI}_{j,max}$ and $a^{SI}_{j,min}$ denote the maximum and minimum vertical acceleration during the step, respectively, and K is a multiplication factor. K may vary among different individuals, and its value can be found out experimentally.

This method is definitely the most reliable and used among the research community for estimating the step length from waist accelerometry data. Although, different strategy may be used for extracting the information needed for the equation 4.3 from segmented data. The maximum and minimum vertical acceleration during a step may be indeed extracted from the same window or between adjacent windows.
The strategy adopted strictly depends upon the segmentation procedure: the modality (adjacent or overlapping windows) and the window size play a fundamental role in this context.
Given the option selected for the segmentation procedure (see Chapter 3), in this work we extract the information required for 4.3 using data from adjacent windows.
Figure 4.13 shows the result in the maximum and minimum acceleration samples identification that pertains within steps performed during a 15-steps trial.

Figure 4.14 shows the step length estimation for the 15-steps performed trial illustrated in Figure 4.13. To mention that during the trial the individual has travelled a total distance of about 9 m. The total distance estimated is about 8.6 m, with a percent error of about the 4.4%.
Results achieved during experimental trials for SC and estimation are illustrated in the Section 4.6.4.

4.6.3 The Attitude Filter

The orientation of a rigid body in the space with respect to reference frame, commonly refereed to as *attitude*, can be generally represented in three principal forms: Euler angles, quaternion, and Direction Cosine Matrix (DCM). The orientation in Euler form

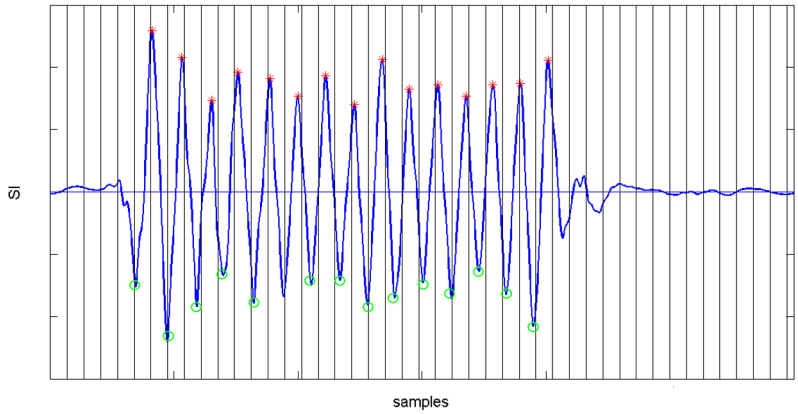

FIGURE 4.13: Step length estimation using the equation from Wienberg et al [120] and data extracted from adjacent windows. In blue, the SI filtered and segmented acceleration component during a 15-steps trial. For each detected step, green circles identify the minimum acceleration sample within the window while red stars indicate the maximum acceleration sample within the adjacent window.

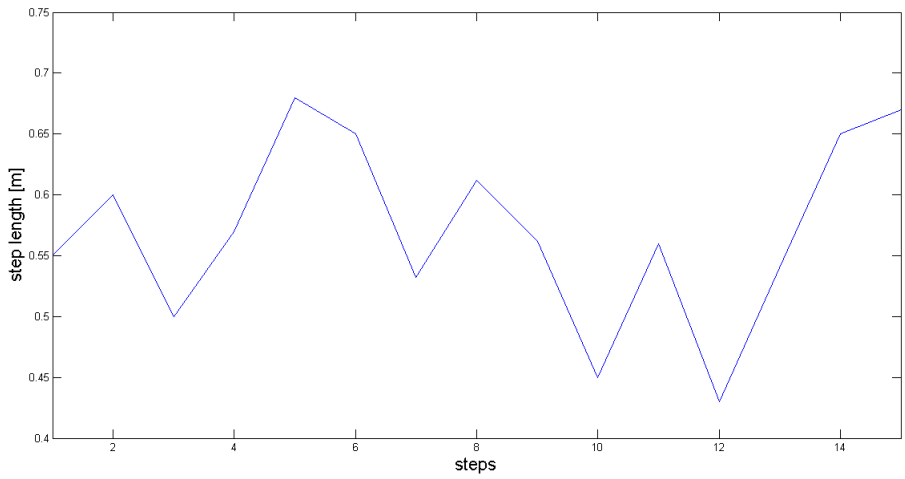

FIGURE 4.14: Step length estimation using the equation 4.3. The maximum and minimum acceleration samples for each step have been identified using the strategy illustrated in Figure 4.13.

is expressed using the three angles $\phi = \{\varphi, \vartheta, \psi\}$, known as *roll*, *pitch* and *yaw* angle, respectively (see Figure 4.15).

This representation is conceptually easy to understand, but may reach a singularity state commonly referred as "gimbal lock".
DCM and quaternion do not incur a singularity state but the DCM represents the orientation by a 3×3 matrix.
Furthermore, the quaternion representation offers a linear formulation of the orientation dynamics, as will be illustrated in Section 4.6.3. For these reasons, quaternions are usually the most used mathematics operators in the orientation estimation problem.

Apart form the specific representation used for the attitude, the accurate estimation of the orientation of a rigid body with respect to reference frame is a research common problem required for a wide range of applications. For the purpose of navigation, such

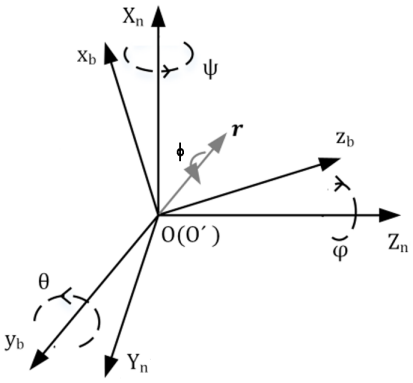

FIGURE 4.15: Representation of the Euler angles. Source [121]

estimation has employed high precision inertial and magnetic sensors. Nevertheless, as stated in previous chapters, the recent development of low-cost and light-weight IMU has allowed smaller and cheaper inertial sensors to be adopted for a wider range of applications and even in the daily use of consumer electronics.
Data provided by low-cost IMU is affected by high noise levels and time-varying biases (see Chapter 2).

Therefore, a sensor-fusion algorithm must be used to process the data to obtain a smooth and bias-free estimation of the orientation maintaining a low computational cost.

The problem of finding the optimal attitude estimation of an object in the space was formulated by Whaba in 1965 [122].
Many algorithmic solutions of Whaba's problem have been proposed. They are generally classified into two categories: deterministic and optimal, according to the popular definition by Wertz [123]. Deterministic algorithms use a minimal set of data and derive the attitude by solving non-linear equations, whereas optimal algorithms use more than a minimal set of measurements and compute the attitude by minimizing an appropriate cost function.
A very well known deterministic algorithm is the ThRee axIs Attitude Determination (TRIAD) [124]. It constructs two triads of orthonormal unit vectors by combining the normalized measurement of two non-parallel reference vectors and provides an estimation of the attitude matrix.
QUaternion ESTimator (QUEST) [124] is an optimal algorithm that produces the attitude estimation in quaternion form (see Section) given a set of 3D reference unit vectors in a fixed frame and their corresponding observations in the local frame.

Many other techniques have been proposed, such as singular value decomposition, polar decomposition, Euler-n, fast optimal matrix algorithm, and energy approach algorithm. All of them produce an optimal attitude estimation and they differ from each other in their computational speed. A complete survey and analysis of attitude estimation methods using vector observation is provided in [125, 126].

Nevertheless, as stated in [125], deterministic attitude-determination algorithms are not very frequent and their study is not extensive. Nonetheless, in IMU applications, only two sets of vector observations are provided, thus even the optimal approaches would have the same level of accuracy as a deterministic method [125].
In this kind of approaches, to obtain a better estimation of the orientation, acceleration

and magnetic field data are fused together with angular rate readings from a gyroscope. Although many approaches have been adopted for filtering gyroscope data with inertial measurements, the most commonly used techniques are Extended Kalman filtering (EKF).
Kalman filtering based techniques adopt a probabilistic determination of the state modelled as a Gaussian distribution given the system's model. They are widely used in aerospace applications, human motion analysis and robotics [125].

Quaternion-based orientation representation

As stated in Section 4.6.3, orientation by quaternions is usually the most used representation in the attitude estimation problem. These mathematical entities indeed need less computational effort in recursive updating and avoid the singularity issues that affect angular descriptors, like Euler angles.
Quaternions are defined as:

$$\mathbf{q} = [\eta, \epsilon]^T = [q_0, q_1, q_2, q_3]^T \tag{4.4}$$

where $\eta = cos\frac{\theta}{2} = q_0$ is the scalar part of the quaternion, $\epsilon = sin\frac{\theta}{2}\vec{r} = [q_1, q_2, q_3]^T$ is the vector part of the quaternion, θ is the $pitch$ angle, and $\vec{r} = [r_x, r_y, r_z]^T$ is the unit vector of a rotation axis with respect to a Cartesian reference frame $O{-}xyz$, as illustrated in Figure 4.16.
Given the generic quaternion $\mathbf{q}$, the quaternion conjugate $\mathbf{q}^* = [q_0, -q_1, -q_2, -q_3]^T$, is

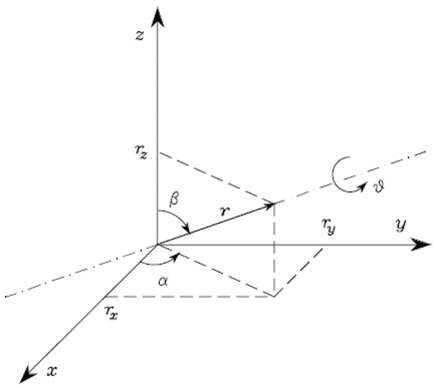

FIGURE 4.16: Generic rotation in the 3D space: rotation of an angle with respect to an axis. Source [121].

equivalent to the inverse quaternion and describes the inverse rotation. The orientation of a rigid body in the space is determined when the axis orientation of a coordinate frame attached to the body (the body frame, B) is specified with respect to an absolute coordinate system, usually named as the navigation frame N.
The generic pose of a point in the 3D space can be represents by a 3×1 column vector $\vec{v}(t)$, which components are generally functions of time t. If the $\vec{v}(t)^N$ is expressed in N, the corresponding representation with respect to the frame B, using the quaternion can be expressed as:

$$\vec{v}(t)_q^B = \mathbf{q}_N^B(t) \otimes \vec{v}(t)_q^N \otimes \mathbf{q}^{*B}{}_N(t) \tag{4.5}$$

where the symbol $\otimes$ indicates the quaternion multiplication[3], $\vec{v}(t)_q^B$ and $\vec{v}(t)_q^N$ are the observation vectors in the two reference frames written as pure quaternion[4].
The rotation described by equation 4.5, can be written in matrix form as:

$$\vec{x}^B = R(\mathbf{q}_N^B)\ \vec{x}(t)^N \tag{4.6}$$

where $R(\mathbf{q}_N^B)$[5], which belongs to the special orthogonal group *SO(3)*, is the DCM for the transformation from N to B, given in terms of the orientation quaternion $\mathbf{q}_B^N$. To note that the argument t has been omitted for the sake of the simplicity.
The rigid body angular motion obeys the vector differential equation:

$$\frac{d}{dt}q = \frac{1}{2}\ \mathbf{q} \times \vec{\omega} = \mathbf{\Omega}[\tilde{\omega}]\mathbf{q} \tag{4.7}$$

where $\mathbf{\Omega}[\tilde{\omega}]$ (hereafter indicated as $\mathbf{\Omega}$) is a 4×4 skew-symmetric matrix:

$$\mathbf{\Omega} = \frac{1}{2}\begin{bmatrix} 0 & -\omega_z & \omega_y & \omega_x \\ \omega_z & 0 & -\omega_x & \omega_y \\ -\omega_y & \omega_x & 0 & \omega_z \\ -\omega_x & -\omega_y & -\omega_z & 0 \end{bmatrix}^T \tag{4.8}$$

in which $\vec{\omega} = [\omega_x, \omega_y, \omega_z]^T$ represents the angular velocity measured in the body frame by the IMU, of B relative to N.
The discrete-time model corresponding to 4.7 is:

$$\begin{cases} \mathbf{q}_{k+1} = e^{(\mathbf{\Omega_k}\ \mathbf{\Delta t_k})}\ \mathbf{q}_k \\ \mathbf{q}_0 = q(0) \end{cases} \tag{4.9}$$

where $\Delta t_k = [t_{k-1}, t_k]$ is the sampling time interval. The quaternion $\mathbf{q}_k$ is computed at each sampling time k, starting from the initial condition $\mathbf{q}_0$.

The Kalman filter

The objective of this section is to provide some general remarks about the Kalman filter algorithm and how this algorithm can be applied to the attitude estimation problem. For a comprehensive dissertation about the topics, please refer to [127, 128, 129].

[3]For two generic quaternions, $\mathbf{q} = [q_0, q_1, q_2, q_3]^T$ and $\mathbf{p} = [p_0, p_1, p_2, p_3]^T$, the quaternion multiplication is defined as:

$$\mathbf{q} \otimes \mathbf{p} = \begin{bmatrix} p_0q_0 - p_1q_1 - p_2q_2 - p_3q_3 \\ p_0q_1 + p_1q_0 + p_2q_3 - p_3q_2 \\ p_0q_2 - p_1q_3 + p_2q_0 + p_3q_1 \\ p_0q_3 + p_1q_2 - p_2q_1 - p_3q_0 \end{bmatrix}$$

[4]$\vec{v}_q^B = [0,\ x^B,\ y^B,\ z^B]$, $\vec{v}_q^N = [0,\ x^N,\ y^N,\ z^N]$

[5]Given the two quaternions $\mathbf{q}_N^B = [q_0, q_1, q_2, q_3]^T$ and $\mathbf{q_N^B}^* = [q_0, -q_1, -q_2, -q_3]^T$, the DCM can be expressed as:

$$R(\mathbf{q}_B^N) = \begin{bmatrix} q_0^2 + q_1^2 - q_2^2 - q_3^2 & 2(q_1q_2 - q_0q_3) & 2(q_1q_3 - q_0q_2) \\ 2(q_1q_2 + q_0q_3) & q_0^2 - q_1^2 + q_2^2 - q_3^2 & 2(q_2q_3 - q_0q_1) \\ 2(q_1q_3 - q_0q_2) & 2(q_2q_3 + q_0q_1) & q_0^2 - q_1^2 + q_2^2 + q_3^2) \end{bmatrix}$$

Formally, the Kalman filter operates recursively on streams of noisy input data to produce a statistically optimal estimate of the underlying system state.
The algorithm works in a two-step process. In the *prediction* step, the Kalman filter produces estimates of the current state variables, along with their uncertainties. Once the outcome of the next measurement (in general corrupted with errors, including random noise) is observed, these estimates are updated using a weighted average, with more weight being given to estimates with higher certainty.
From a theoretical standpoint, the main assumption of the Kalman filter is that the underlying system is a linear dynamical system and that all error terms and measurements have a Gaussian distribution.
Extensions and generalizations to the method have also been developed, such as the EKF filter and the Unscented Kalman filter which are based upon non-linear systems.

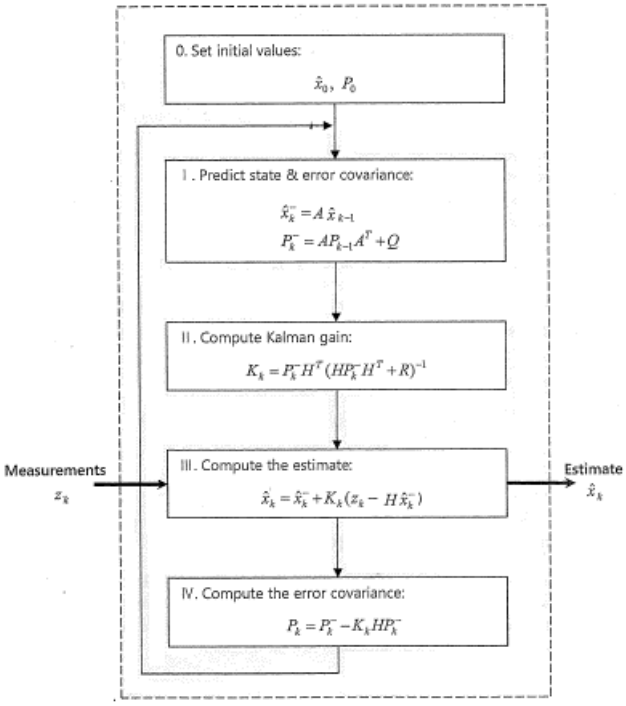

FIGURE 4.17: Main steps of the algorithm. Source [127].

The discrete form of the Kalman filter algorithm is illustrated in Figure 4.17. Known the system model (see below), the algorithm receives one input (measurements, $\vec{z}_k$) and returns one output (the state estimate, $\hat{x}_k$) and the corresponding error covariance associated with the estimate (P_k). Before going further with the dissertation, it is worth mentioning that the the error covariance P_k is a "measure" of the disparity, between the estimate provided by the Kalman filter ($\hat{x}_k$) and the true but unknown value ($\vec{x}_k$)[6]. In other words, the error covariance is a degree of the accuracy of the estimate, and if P_k is large, the error of the estimate is large as well.

The algorithm is divided into four main steps. Step I concerns with the *prediction* process, while Step II, III and IV are related to the *estimation* process. The Step 0 is the initialization step; it is performed once at the starting of the algorithm and requires the setting of the state variable (initial condition, $\vec{x}_0$) and of the error covariance associated

[6]Notation without the hat indicates the real value of the variable.

with the state variable (P_0).
Matrix A, H, Q, and R that compare in Figure represent the system model. They represent the dynamic of the system, and are known (A, H) or defined (Q, R) a priori:

$$\begin{cases} \vec{x}_{k+1} = A\,\vec{x}_k + \vec{w}_k \\ \vec{z}_k = H\,\vec{x}_k + \vec{v}_k \end{cases} \tag{4.10}$$

Equation 4.10 is the state space representation of the system model under investigation. As previously stated, $\vec{x}_k$ and $\vec{z}_k$ are two vectors ($n \times 1$ and $m \times 1$) concerning with the state variable (i.e., the physical quantity of interest) and the measurements. A is the $n \times n$ state transition matrix representing the dynamic of the system. H is the state-to-measurements matrix ($m \times n$) that shows the relationship between the measurement and the state variables. $\vec{w}_k$ and $\vec{v}_k$ are two vector ($n \times 1$ and $m \times 1$) representing the model noise and the measurement noise, respectively.
To mention that in the Kalman filter theory the noise is assumed to be a white process with a zero mean Gaussian distribution:

$$\vec{w}_k \sim N(0, Q)$$

$$\vec{v}_k \sim N(0, R)$$

where Q and R are a $n \times n$ and $m \times m$ matrix, representing the covariance matrix associated to the model and to the measurement noise, respectively. Given the hypothesis on the noise nature, these matrices are diagonals and the principal diagonal elements corresponds to the variance of each noise component.

Prediction The prediction corresponds to the Step I in Figure 4.17. The objective of this step is to produce the *predicted estimate* (or *a priori estimate*) of the state variables ($\hat{x}_k^-$) and the error covariance (P_k^-), based on the system model (A, Q) and the corresponding estimate[7] computed at the previous time step ($\hat{x}_{k-1}$, P_{k-1}).

Estimate The estimate process concerns with Step II, II and IV in Figure 4.17. Using the *a priori estimate* from the prediction step ($\hat{x}_k^-$, P_k^-), the current measurements from the sensors (z_k) and the system model (H, R), the estimation process produces the estimate of the state variables ($\hat{x}_k$) and of the covariance error (P_k), through the computation of the Kalman gain (K_k).
To understand the meaning of the Kalman gain, we can rewrite the equation corresponding to the Step III in Figure 4.17, as follows:

$$\begin{aligned} \hat{x}_k &= \hat{x}_k^- + K_k(\vec{z}_k - H\hat{x}_k^-) \\ &= (I - K_k H)\hat{x}_k^- + K_k\vec{z}_k \end{aligned} \tag{4.11}$$

It is clear from equation 4.11 that the state variable estimate is computed through a "weighted linear combination" of the prediction estimate ($\hat{x}_k^-$) and the sensor measurements ($\vec{z}_k$).
The weight is represented by the Kalman gain K_k, which strictly depends on the predicted error covariance (P_k^-) and the system model (H, R).
Nevertheless, H and R play a different role in the estimate process. H is indeed known from the system model, while R is not known a priori and it usually defined based on

[7] The output of the Kalman filter, that is the *estimate*, is also usually called the *a posteriori estimate*.

the experience about the process under investigation.
When R increases, it means that the measure model is not accurate and the corresponding measurements are not "reliable". As a consequence, the Kalman gain decreases ($K_k \propto R_{-1}$), and the contribution of the measurements to the estimate (equation 4.11) decreases as well. On the other hand, the contribution of the predicted estimate increases.
As stated, the Kalman gain depends also on the predicted error covariance (P_k^-), computed in the prediction step as follows:

$$P_k^- = AP_{k-1}A^T + Q$$

A and Q depend on the system model, but as in the previous case while A is known a priori from the dynamic of the system, Q is defined during the system model design and depends on the reliability of the system model itself. If the system model is imprecise, Q is large. As a consequence, P_k^- is large, the Kalman gain increases ($K_k \propto P_k^-$) and the estimate $\hat{x}_k$ is less affected by the prediction estimate that directly depends on the system model.

Nevertheless, the above assumes that the system and measurement model are linear. A strategy able to overcome such limitation is to use a slightly different modification of the Kalman filter, the well-know EKF.
For a non-linear system model, the state space representation can be expressed as follows:

$$\begin{cases} \vec{x}_{k+1} = f(\vec{x}_k) + \vec{w}_k \\ \vec{z}_k = h(\vec{x}_k) + \vec{v}_k \end{cases} \tag{4.12}$$

In other terms, the matrix A and H that compare in equation 4.10, have been replaced by non-linear function because the state variables ($\vec{x}_k$) and coefficients are not separable.
Nevertheless, the course of action illustrated for the classic Kalman filter are the same as for the extended form, as illustrated in Figure 4.18.

The only differences concern with Step I for the prediction, and with Step II and Step IV in the estimation. These steps assume the use of the corresponding Jacobian matrices ($\tilde{A}$, $\tilde{H}$) that represent the first-order Taylor-Mac Laurin expansion around the current state estimate ($\hat{x}_{k+1}$):

$$\tilde{A}_{k+1} = \frac{\partial f}{\partial \hat{x}_{k+1}}|_{\hat{x}_{k+1}}$$

$$\tilde{H}_{k+1} = \frac{\partial h}{\partial \vec{z}_{k+1}}|_{\hat{x}_{k+1}^-}$$

Quaternion-based EKF

In this section, the quaternion-based EKF for the attitude estimation is presented.
A part from the vector state, the proposed algorithm follows the one presented in [130] by Sabatini.
In the filter design, we assumed that navigation frame is fixed within the environment: its x-axis represents the vertical axis of the environment and the rescuer moves on the $(y - z)$ plane.
The orientation of the body frame of the IMU is the same as illustrated in Figure 4.2: the x, y and z-axis are aligned with the SI, ML and AP, direction respectively. In this

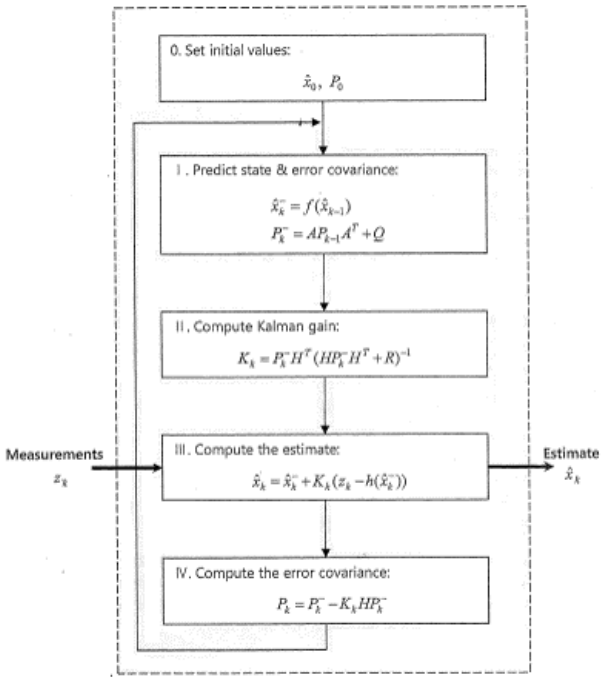

FIGURE 4.18: Main steps of the EKF algorithm. Source [127].

way, the gravity component is only along the x-axis and can be easily compensated.
At the starting time, we assume that the two reference frames have the same pose. Knowing the attitude of the body reference frame with respect to the navigation frame at the starting time, it is easy to compute the current IMU attitude by simple consecutive rotations.

In this work, the state vector $\vec{x}$ is represented by the quaternions $\mathbf{q}$. As illustrated in Section 4.6.3, the discrete time model, describing the dynamic of the state variable in the space state is:

$$\begin{cases} \hat{\mathbf{q}}_{k+1} = e^{(\mathbf{\Omega_k}\,\mathbf{\Delta t_k})}\,\hat{\mathbf{q}}_k = \mathbf{\Phi}(\vec{\omega}_k, \Delta t_k)\,\hat{\mathbf{q}}_k + \vec{w} \\ \mathbf{q}_0 = q(0) \end{cases} \tag{4.13}$$

where $\Delta t_k = [t_{k-1}, t_k]$ is the sampling time interval, and $\vec{\omega}_k$ is the angular velocity vectors measured by the gyroscope and $\vec{w}$ is a zero mean white noise process, with covariance matrix Q.
The quaternion $\hat{\mathbf{q}}_k$ is computed through the equation 4.13 at each sampling time k, starting from the initial condition $\mathbf{q}_0$. The initial condition $\mathbf{q}_0$ is computed from the acceleration measurements considering the user standing still at the beginning of the trial.

The measurement model is built by stacking the accelerometer and magnetometer measurement vectors as shown in the following equation:

$$\vec{z}_{k+1} = \begin{bmatrix} \vec{a}_{k+1} \\ \vec{m}_{k+1} \end{bmatrix} = f(\hat{x}_{k+1}) + \vec{v} \tag{4.14}$$

where $f(\cdot)$ is a non-linear function expressing the relation between the vector measurements and the state vector, and $\vec{v} = [\vec{v}^a, \vec{v}^m]^T$ are uncorrelated zero-mean white noise processes of covariance matrix R^a and R^m respectively. This two matrices can be combined into a single matrix:

$$R = \begin{bmatrix} R^a & \mathbf{0} \\ \mathbf{0} & R^m \end{bmatrix}$$

where $\mathbf{0}$ is the 3×3 null matrix.
To mention that in this work, we assume that the covariance matrices Q and R that represent a metric to convey the accuracy in the gyroscope, accelerometer and magnetometer measurements are constant matrices estimated through the calibration process illustrated in Chapter 2.
Concerning the measurement model, the acceleration in the body frame can be expressed as:

$$\hat{a}_{k+1} = f_a(\hat{\mathbf{q}}_{k+1}) = K_a R(\hat{\mathbf{q}}_N^B(k+1))\ \vec{g} + \vec{v}^a \tag{4.15}$$

where K_a is the scale factor matrix of the accelerometer (see Chapter 2), $\vec{g}$ is the gravity vector, and $R(\hat{\mathbf{q}}_N^B(k+1))$ is the rotation matrix from the navigation frame to the body reference frame, as illustrated in Section 4.6.3.
It is worth underlying that data from accelerometers can be used only when the rescuer is still, otherwise the gravity cannot be compensated. For this reason, a validation gate has been set up and the acceleration correction is performed only when $||\vec{a}_{k+1}|| - \vec{g} < \varepsilon_a$, where $||\cdot||$ is the Euclidean norm, and $\vec{a}_{k+1}$ is the acceleration measured by the IMU.
In a similar way, for the magnetometer we can write:

$$\hat{m}_{k+1} = f_m(\hat{q}_{k+1}) = K_m R(\hat{\mathbf{q}}_N^B(k+1))\ \vec{h} + \vec{v}^m \tag{4.16}$$

where K_m is the scale factor matrix of the magnetometer and $\vec{h}$ is the Earth magnetic field vector measured by the magnetometer in the navigation frame.
To prevent the use of magnetometer measures when affected by large magnetic disturbances, a matching test has been set up, so the update in the predicted estimate ($\hat{x}_{k+1}$) is performed only when $||\vec{m}_{k+1}|| - \vec{h} < \varepsilon_m$ and $||\vec{m}_{k+1} - \vec{m}_k|| < \varepsilon_{\Delta_m}$.

Given the non-linearity of the equation 4.14, the EKF approach requires that a first order Taylor expansion is carried out around the current state estimate by computing the Jacobian matrix:

$$F_{k+1} = \frac{\partial \vec{z}_{k+1}}{\partial \hat{x}_{k+1}} \mid_{\hat{x}_{k+1}^-} \tag{4.17}$$

For the sake of completeness, the EKF equations are summarized below:

- compute the predicted state estimate:

$$\hat{x_{k+1}}^- = \mathbf{\Phi}(\vec{\omega}_k, \Delta t_k)\ \hat{x}_k$$

- compute the predicted error covariance matrix:

$$P_{k+1}^- = \mathbf{\Phi}_k P_k \mathbf{\Phi}_k^T + Q$$

- compute the Kalman gain:

$$K_{k+1} = P_{k+1}^-\ F_{k+1}^T (F_{k+1}\ P_{k+1}^-\ F_{k+1}^T + R^{-1}$$

- compute the state estimate:

$$\hat{x}_{k+1} = \hat{x}_{k+1}^{-} + K_{k+1}(\vec{z}_{k+1} - f(\hat{x}_{k+1}^{-})$$

- compute the error covariance matrix estimate:

$$P_{k+1} = P_{k+1}^{-} - K_{k+1}F_{k+1}P_{k+1}^{-}$$

4.6.4 Results for the prediction phase

In this section are presented the results relative to the prediction phase. We firstly illustrate outcomes from the SC algorithms presented in Section 4.6.1 and for the step length estimation.
After we show results from the Quaternion-based EKF. The section closes with some main results achieved using the PDR algorithm presented in Section 4.6.

Data collection

During tests, the user is equipped with a waist-mounted IMU (see Figure 4.2). The data collection has been performed by using the InvenSense MPU-9150, described in Chapter 2.

A group of volunteers (15 subjects, 13 males, 12 females, average age 29.49 $\pm$ 7.75 years, average height 172.38 $\pm$ 6.76 cm, and average weight 70.46 $\pm$ 10.97 kg) were asked to perform different trials-set.

For SC and step length estimation validation, users performed a 15-steps trial, for a total travelled distance of about 9 m.

The validation of the algorithm for the orientation estimate through static and dynamic tests. The user equipped with the IMU were asked to stand still (static test) and to performs a half-square shaped path.

For the PDR validation, the same group have been asked to perform 2 tests:

- the forward and backward test. The user walks straight for 50 m, turn 180 deg and comeback on the same path.
- the turning test. The user walks straight for 50 m, turn 90 deg and then walks straight for about 50 m.

Step Counting

Table 4.1 shows results achieved during trial. As it is clear show from the results, the

TABLE 4.1: Results achieved during trial for the SC algorithms.

SC algorithm	AR
peak detection	74%
peak detection with adaptive threshold	94%
zero crossing	88%
COM position in sagittal plane	76%
normalised autocorrelation	82%
peak detection /& zero crossing	93%

implemented SC algorithms presents quite different accuracy rate, as illustrated in Section 4.6.1. Best results come from the peak detection with adaptive threshold SC algorithm, which presents the 94% of AR. For this reason, this algorithm has been selected for the Hybrid Indoor Positioning System (HIPS) and for the validation of the proposed algorithms for the prediction phase (i.e., step length estimation and PDR).

Step length estimation

The validation of the step length algorithm was carried out using the same trial set as for the SC algorithms. As stated in the previous section, the peak detection with adaptive threshold SC algorithm has been used for performing the step detection preliminary to the step length estimation.

Figure 4.19 illustrates the results achieved in the 15-step trials for each of the 15 sub-

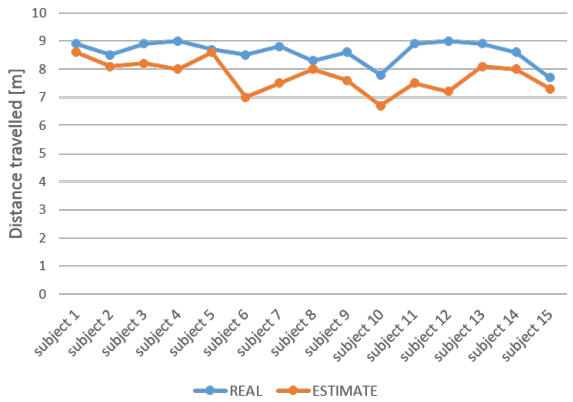

FIGURE 4.19: Comparison between the real (in blue) and the estimated (red) travelled distance in the 15-steps trial for the 15 subject, using the peak detection with adaptive threshold SC algorithm and the step length estimation strategy illustrated in equation 4.3.

ject. It is clear from the picture that the estimated travelled distance is usually shorter than the real one. This can be explained by the number of steps effectively estimated within each trial (see Figure 4.20), as well as assuming that the strategy proposed by Wienberg et al. is likely to underestimating the real step length.

Considering only the trial in which the number of steps has been properly detected,

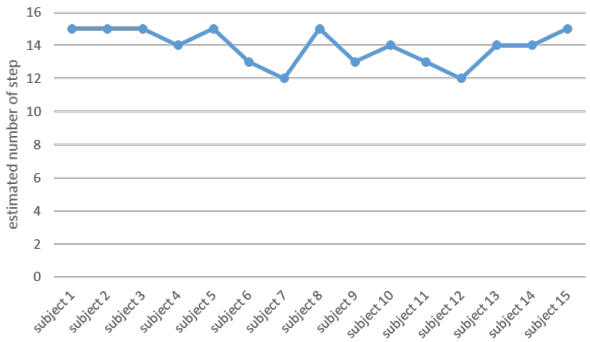

FIGURE 4.20: Number of steps estimated for each subject during the 15 steps trial, using the peak detection with adaptive threshold SC algorithm.

the percent error in the distance travelled is about the 4,8%. This result is perfectly in line with results exhibited in the literature on the topic.

Attitude estimation

Orientation estimation through quaternions is usually not intuitive to understand. For this reason, quaternions estimate computed by the EKF are converted into Euler angles, using the following relation:

$$\begin{cases} \varphi &= atan2(2q_2q_3 - 2q_0q_1, 2q_0^2 + 2q_3^2 - 1) \\ \vartheta &= -arcsin(2q_1q_1 + 2q_0q_2) \\ \psi &= atan2(2q_1q_2 - 2q_0q_3, 2q_0^2 + 2q_1^2 - 1) \end{cases}$$

where φ, ϑ and ψ are the roll, pitch and yaw representing the rotation angles with respect the z, the y and the x axis in the body reference frame (see Figure 4.2).
In this context, we analyse the results concerning the yaw angle. In the body reference frame, the yaw angle represents indeed the *heading* of the user, that is the direction in which the user is pointing during motion.

Figure 4.21 shows the results achieved during the static test from one volunteer. During the test, the user has been asked to wear the IMU and to stay still for about 30 sec.
The error in the heading estimation can be explained by considering the error affecting

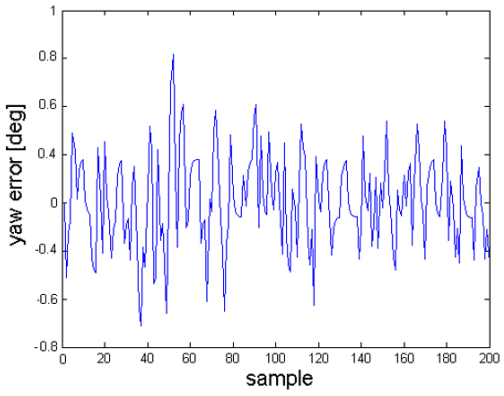

FIGURE 4.21: Yaw angle estimation error [deg] during the static test.

sensors and modelling simplification. The accelerometer and magnetometer measurement errors assumed in the equation 4.14 are much more complicated than what our model has described by a constant bias with zero mean Gaussian variable for each axis; especially for the magnetometer which may be seriously affected by external interferences.
Nevertheless, although not fully eliminated errors variations are small, which proves the accuracy and robustness of the attitude estimation algorithm.

In the walking test, we expect the roll and pitch angles are zero while the yaw angle depends on the user heading direction. In this trial, the volunteer walks along a U-turn shaped path: he/she walks straight, then turns right by 90 deg, walks again straight and finally turns right again by 90 deg.
Figure 4.22 illustrates the yaw angle during the test. The green line shows the ground truth of the heading direction (0, -90 deg, -180 deg). The red line shows the heading

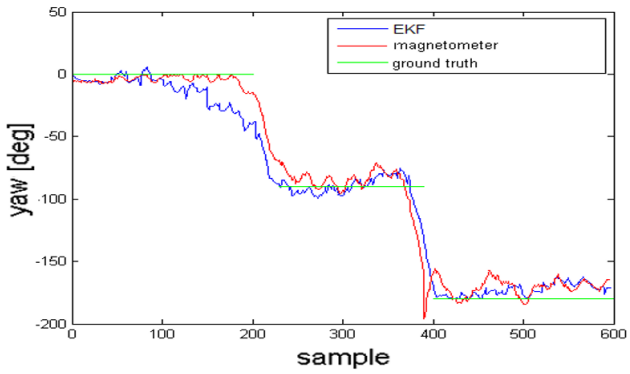

FIGURE 4.22: Yaw angle estimation [deg] during the dynamic test. In green the ground truth, in blue the estimation from the EKF, in red the output of the magnetometer.

provided by the magnetometer of the IMU. The EKF algorithm has comparable performance with respect to the magnetometer output, but at the same time is more robust with respect to potential magnetic interferences that may affect magnetometer output. To mention that the maximum error in the attitude estimate during trials did not exceed $8deg$.

PDR

Figure 4.23 shows the result achieved for one subject during the forward and backward test. The subjected performed 172 steps for a total distance travelled of about 100 m.

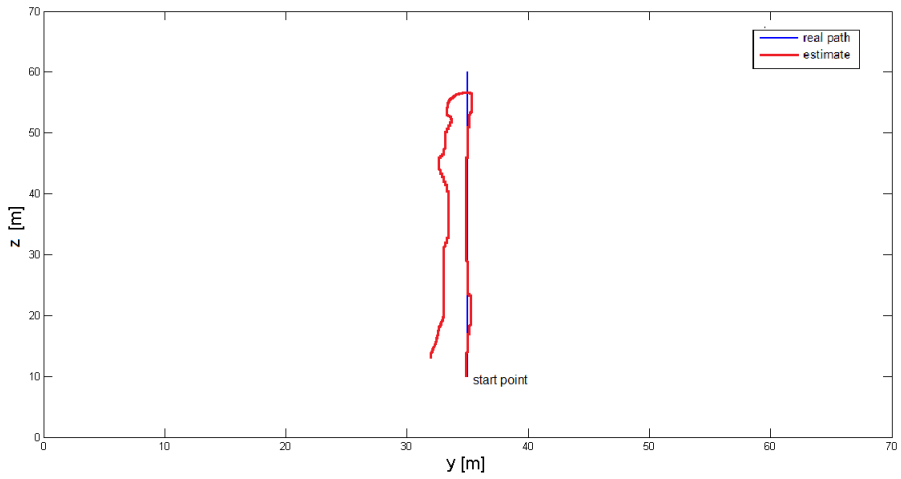

FIGURE 4.23: Forward and backward test: results achieved for one subject. In blue is represented the real path, red line shows the path estimated using the PDR.

The red line in Figure 4.23 represents the path estimated using the PDR algorithm (Section 4.6). It is clear from the figure that the total distance travelled provided by the PDR is underestimated (about 93 m). The relative error is about 7% and the position error computed as Euclidean distance that concern the ending point of the path is 4,7 m.
The relative error can be explained, as illustrated in previous results, by the effective

number of steps detected from the SC algorithm (161 steps detected, 172 steps performed) and the underestimation in the steps length.
To the position error contributes also the heading estimation. In the last part of path, the heading of the user appears to change and at the end of the path the user seems located in a different position respect the real one .
Almost the same behaviour is exhibited by tests performed by the other users.

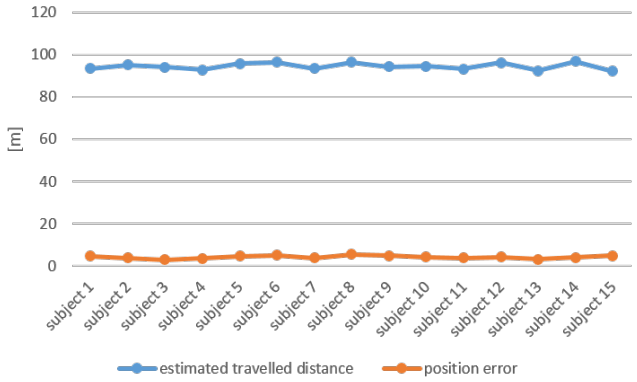

FIGURE 4.24: Forward and backward test. In blue the estimated distance travelled for each subject, red line shows the position error for each test performed.

Results from the turning tests for one volunteers are illustrated in Figure 4.25.
For the reasons exposed above, also in the turning test the estimated path is slightly different from the real one. For the test illustrated in Figure 4.25, the number of step performed is 168, while the one detected is 159. The relative error concerning the estimated distance is about 4.6%, while the position error corresponding to the end point of the path amounts to 6 m.
Figure 4.26 shows the result for all the performed tests.

4.7 The correction phase

As illustrated in previous sections, the output of the prediction phase represents a rough estimate of the user pose. Several sources of error may contribute to downgrade the estimate:

- sensors drift (constant and time-varying biases), electromagnetic and ferromagnetic interferences (that affect mainly gyroscope and magnetometer, respectively);
- FP and FN occurring from the SC algorithm;
- misleading steps length estimation;
- inaccuracy in the yaw estimation angle provided by the EKF.

To mention also that also the heading used for the pose estimate in the equation 4.1 may contribute to pose error estimation, given that is computed as the average yaw angle between two consecutive steps.
All the factors above may get the pose estimation worse, especially in long lasting mission. The different errors may indeed accumulate, causing a general misleading in the pose estimate.

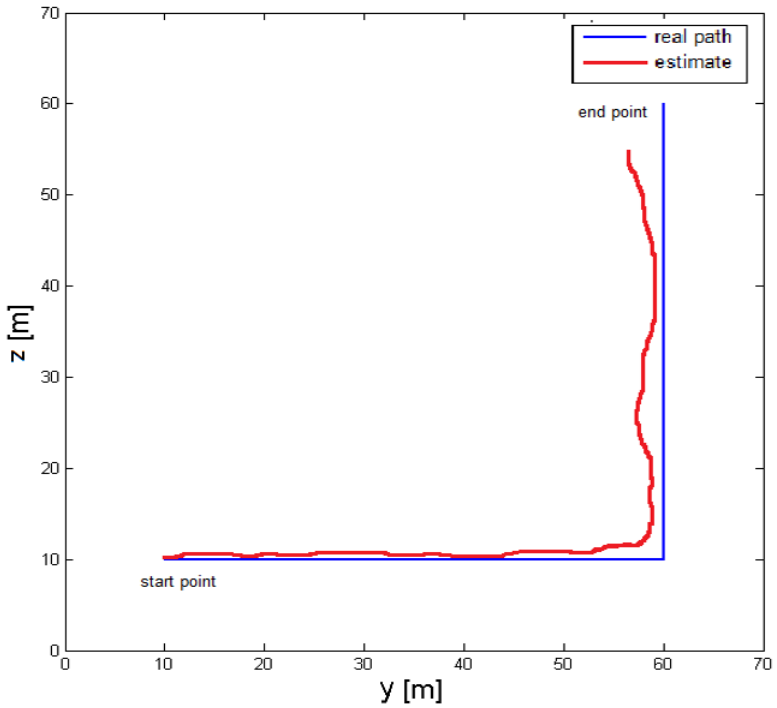

FIGURE 4.25: The turning test: results achieved for one subject. In blue is represented the real path, red line shows the path estimated using the PDR.

FIGURE 4.26: The turning test. In blue the estimated distance travelled for each subject, red line shows the position error for each test performed.

Nevertheless, the high-variable performance in the pose estimate offered by an inertial navigation system are virtually incompatible with first responders requirements: the position error in the pose determination should not exceed 5 m, since for safety reasons the user should be able to discriminate in which room is located.
One potential solution able to overcome the problem of the pose estimate concerns with using external references information supplied by exeroceptive sensors. This is the paradigm on which is based the correction phase of the HIPS. The correction phase aims indeed to refine the rough estimate provided by the prediction phase, by means of the RFID systems to have a hybrid system yields a position estimation having room

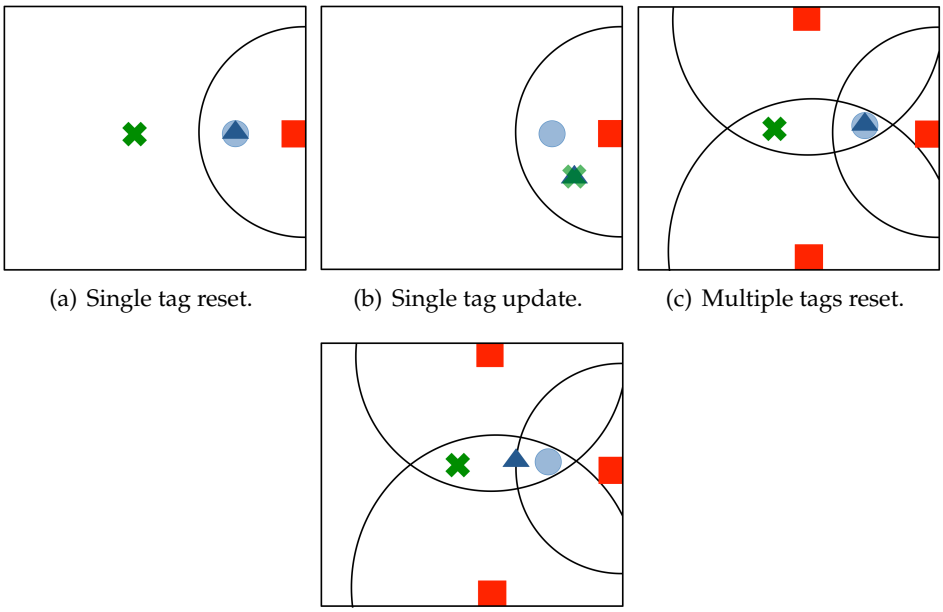

(a) Single tag reset. (b) Single tag update. (c) Multiple tags reset.

(d) Multiple tags update.

FIGURE 4.27: Correction strategies: the green cross indicates the rescuer position computed by the prediction step, red squares represents the position of the detected tags, blue dots are the center of the main radiation lobe (black line indicates their borders) of the detected tags, blue triangle represents the rescuer position after the correction phase.

level accuracy.
According to the REFIRE protocol illustrated in Section 4.4, a user equipped with a RFID reader is able to retrieve from tags installed into the environment information about their absolute position, and accuracy.

Specifically, the tag provides its own *Geographical Coordinates* and its *Accuracy* w_i. The *Geographical Coordinates* of a generic tag i are represented by a 2×1 vector $p^i_{tag} = [y^i_{tag}, z^i_{tag}]$ defining its position in the $(y - z)$ plane of the navigation frame, where the user is moving.
Given the shape of the tag main radiation lobe (retrieved from the RFID system assessment illustrated in Section 4.7.1), p^i_{tag} is used to define the center of the radiation lobe T^i that is exploited to update the position of the rescuer.
The *Accuracy* w_i represents the accuracy related to definition of the main radiation lobe shape for the $i - th$ tag, set during the RFID system assessment. It is expressed as numerical value $w_i \in [0.01, 1]$, where 0.01 means that the radiation lobe shape of the $i - th$ tag is perfectly compliant with the general shape defined during the system assessment.
Since no ranging technique is adopted in this work, only the position of the rescuer is corrected, due to observability issues. When a rescuer is in the main radiation lobe of the tag, the reader receives information from the tag and the rescuer's position is updated according with four strategies as shown in Figure 4.27. The first two strategies consider a single tag detection, specifically in the first one (see Figure 4.27(a)), the inertial prediction estimates the rescuers outside the radiation lobe of the perceived tag i

and the position and the accuracy are reset according with the following rules:

$$\begin{aligned} \hat{p}_j &= T^i \\ \hat{P}_j^p &= w_i \mathbf{I}_{2\times 2} \end{aligned} \tag{4.18}$$

where $\hat{p}_j$ represents the new current position and the covariance $\hat{P}_j^p$ is set according with the accuracy w_i provided by the tag.

In the second one (see Figure 4.27(b)), the rescuer position is estimated inside the main radiation lobe of the perceived tag i, in this case the pose is not updated but the accuracy is eventually bounded according to the follow equations:

$$\begin{aligned} \hat{p}_j &= \hat{p}_{j-1}^- \\ P_j^p &= \begin{cases} P_{j-1}^p & \textit{if} \quad \text{tr}[P_{j-1}^p] < w_i^2 \\ w_i \mathbf{I}_{2\times 2} & \text{otherwise.} \end{cases} \end{aligned} \tag{4.19}$$

where $\hat{p}_{j-1}^-$ is the user pose estimated by the prediction phase, and $\text{tr}[P_{j-1}^p]$ represents the Mean Squared Error (MSE) of the error covariance matrix, that is a common measure of the esteem quality.

In the last two cases, the rescuer is inside the main radiation lobe of r tags. If the inertial prediction locates the rescuer outside the radiation lobes (see Figure 4.27(c)), the position $\hat{p}_j$ is updated according to the following equations:

$$\begin{aligned} \hat{p}_j &= \bar{T}^i \\ P_j^p &= \textstyle\sum_{i=1}^r w_i (T^i - \bar{T}^j)(T^i - \bar{T}^j)^T \end{aligned} \tag{4.20}$$

where $\bar{T}^j$ is the average center of gravity of the tag radiation lobes.

Finally, when the inertial prediction locates the rescuer inside the radiation lobe of a subset of the r perceived tags, the position $\hat{p}_j$ is updated according to the following equations:

$$\begin{aligned} \hat{p}_j &= \hat{p}_{j-1}^- + L_j(T^j - [\hat{p}_{j-1}^-]_r) \\ P_j^p &= \begin{cases} P_j^p & \textit{if} \quad \text{tr}[P_{j-1}^p] < \text{tr}[S_j] \\ P_j^p – L_j S_j L_j^T & \text{otherwise} \end{cases} \end{aligned} \tag{4.21}$$

where T^j is the block vector of the coordinates retrieved from the r tags, $[\hat{p}_{j-1}^-]_r$ is a block vector stacking r times the coordinates of the position of the rescuer computed by the PDR, $\text{tr}[S_j]$ is the tags combined accuracy w_i, and L_j represents a gain. This gain is computed as:

$$L_j = P_{pz,j} S_j^{-1} \tag{4.22}$$

where:

$$P_{pz,j} = \sum_{i=1}^{r} w_i (T^i - p_{j-1}^-)(T^i - \bar{T}^j)^T \tag{4.23}$$

and S_j is:

$$S_j = \sum_{i=1}^{r} w_i (T^i - p_{j-1}^-)(T^i - p_{j-1}^-)^T. \tag{4.24}$$

It is worth noticing that the correction step is performed only on the perceived tags.

4.7.1 RFID system assessment

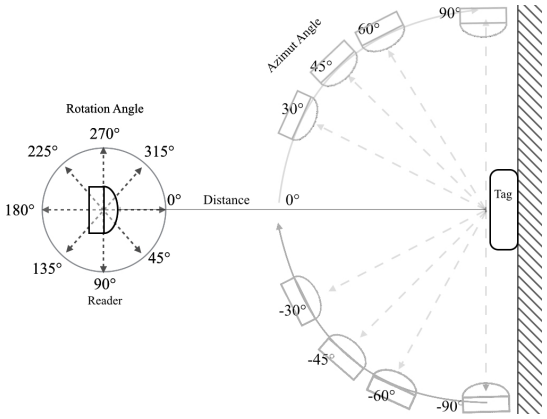

FIGURE 4.28: Parameters for static and dynamic tests.

The use of the RFID system for ILP tasks is challenging since it only provides information about the presence of tags in the environment. Moreover, most of the current RFID systems are developed for logistics applications, where high power antennas are used to detect tags equipped with small antennas. In the REFIRE framework, the opposite approach is foreseen, due to design constraints. The reader antenna is carried by the rescuer: it is small and low power to extend the battery life. The tags are embedded in the environment into emergencies signs and their size has been increased to host a big antenna.
Specifically, the reader selected in this study is the qID R1240I by CAEN. It is a mobile UHF RFID reader composed by two directional antennas (horizontal and vertical polarization) able to implement a semi-circular radiation lobe. The tag is the rugged Omni-ID Ultra passive equipped with a large reflective antenna.

To better understand the feasibility and the performance of the approach, a large number of trials has been carried out to outline the behaviour of the system under real operating scenarios, since the tags detection performances depends on environmental conditions (i.e., electromagnetic reflections, humidity, temperature, etc). Here only few are reported for the sake of space, however it is worth mentioning that a complete assessment for the adopted system has been carried out.

Preliminary tests have been performed to assess the operativeness of the selected RFID system in severe conditions, typically experienced during emergency scenarios. Specifically, from trials emerged that the RFID reader was able to retrieve information from RFID tags in presence of high temperature, smoke and high humidity.

For the system assessment, the following parameters have been used (see Figure 4.28):

d : represents the distance between the tag and the reader. It has been set in the range $[0 \div 350]\, cm$;

ϑ : is the azimuth angle between the two devices. When tag and reader are faced $\vartheta = 0$. Here, the following azimuth angles are considered during the assessment $\vartheta \in \{0, \pm 30\,\mathrm{deg}, \pm 45\,\mathrm{deg}, \pm 60\,\mathrm{deg}\, \pm 90\,\mathrm{deg}\}$;

φ : represents the rotation angle of the reader with respect to its vertical axis. For this parameter, the following value are considered $\varphi \in \{0, \pm 30\,\mathrm{deg}, \pm 45\,\mathrm{deg}, \pm 60\,\mathrm{deg}\, \pm 90\,\mathrm{deg}\}$;

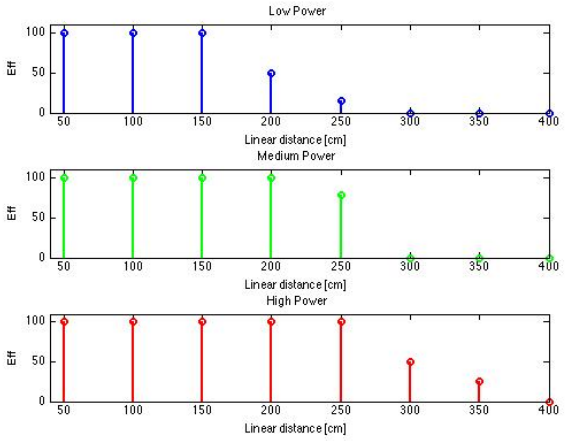

(a) RFID system efficiency for $h_T = 149\,cm$ and different values of e.

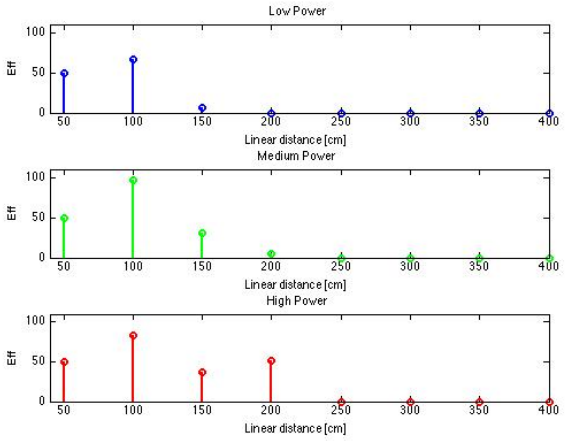

(b) RFID system efficiency for $h_T = 220\,cm$.

FIGURE 4.29: RFID efficiency vs distance d using different power level e (blue, green, and red are low, medium, and high power respectively).

h_T : represents the height of the RFID tag with respect to the ground; three different heights have been considered $h_T \in \{149, 187, 220\}\ cm$, according to the heights of the emergency signs;

h_R : is the height of the RFID reader; several heights have been considered according within the users;

e : represents the emission power of the reader. It can be set via the reader software with respect to the maximum power $12.5\,mW$ to high power (100%), medium power (66%) and low power (33%).

The tests performed can be split into two classes: *static* and *dynamic* tests. In these tests different indexes have been used to evaluate the efficiency of the system, as detailed below.

4.7.2 Static tests

The static tests aim to define the performance of the RFID system into indoor environments, when the reader is still. The main outcome of these tests concerns with the shape of the radiation lobe of the system in real operating conditions: tests, indeed, were performed in office-like environments, where reflections may warp the nominal radiation lobe.

During trials, the reader was fixed on a mobile platform and located in different position near a tag: tests performed in similar operating conditions have been averaged. In all the trials, for the reader a mean shoulder height is considered ($h_R = 140\,cm$).

The system efficiency η is defined as the percentage of the echoes sent by the reader and then reflected back by the passive tag, over the query sent by the reader itself:

$$\eta = \frac{n_e}{n_q} \times 100 \tag{4.25}$$

where n_e is the number of echoes detected and n_q the total number of query sent.

The first set of trials aimed at evaluating the performance of the system, using different power levels. These tests have been carried out by locating the reader in front of the tag (i.e., $\vartheta = 0$ and $\varphi = 0$) and moving forward and backward the mobile platform, in order to change the parameter d. Two different heights for the tag have been considered (i.e., $h_T \in \{149, 220\}\,cm$).
The outcome of the trials are illustrated in Figure 4.29. For $h_T = 149,\ cm$ both medium and higher power perform up to 250 cm, but medium power has a deeper cut-off. Using the low power, performances are degraded. In the case $h_T = 220,\ cm$ performances are less regular. This suggested us to set the height of the tag to $149\,cm$ and the power level to medium (to have a sharp cut-off and a longer battery life).
It is worth also noticing that the higher the difference $|h_T - h_R|$, the lower the efficiency.

The second set of trials were related to define the efficiency of the RFID system, considering different rotation angle φ. Table 4.2 presents the results having set $e = 66\%$, $h_T = 149\,cm$, $\vartheta = 0°$ and considering orientations and distances.

In the Table 4.2, the first column ($\varphi = 0°$) reports the same results of the test in Figure 4.29(a), since the devices are perfectly faced; the efficiency quickly decreases in the same way when the reader is rotated clockwise or counter-clockwise.
Some outlier are obtained when the reader is completely rotated ($\varphi = 135\,\mathrm{deg}$ and $\varphi = 180\,\mathrm{deg}$) due to reflections.

Finally, several tests have been carried out to characterize the efficiency behaviour when the value of the azimuth angle ϑ changes. A result of these tests is reported in Figure 4.30: the tag has a fixed location (i.e., the origin of the reference frame) and orientation, while the reader moves in the surroundings, changing the distance $d \in [0 \div 350]\,cm$.

The performed tests pointed out that in static conditions, the maximum range for the radiation lobe of the RFID system can be assumed $r = 250\,cm$ with a maximum angle of $\theta = \pm 30\,\mathrm{deg}$: the direction of the lobe strongly depends on the orientation of the tag.

4.7.3 Dynamic tests

The aim of the dynamic tests consisted in evaluating the performance of the RFID system during the user motion. Different scenarios have been considered: in the first set of trials, the door crossing test has been contemplated (Figure 4.31), in the second and

TABLE 4.2: Efficiency values [%]: distance [cm] vs rotation angle [deg]

φ	0	45 deg	90 deg	135 deg	180 deg	−135 deg	−90 deg	−45 deg
50	100	100	0	100	75	0	0	100
100	100	100	0	100	30	0	0	100
150	100	75	0	50	50	0	0	20
200	100	0	0	30	0	0	0	0
250	80	0	0	0	0	0	0	0
300	0	0	0	0	0	0	0	0

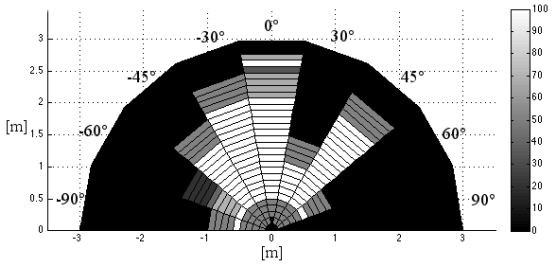

FIGURE 4.30: Percentage of successful readings.

third trial, we considered the user walking in an office-like environment (Figure 4.32, and Figure 4.33).

In all the trials, the power was set to $e = 66\%$, while the other parameters changed

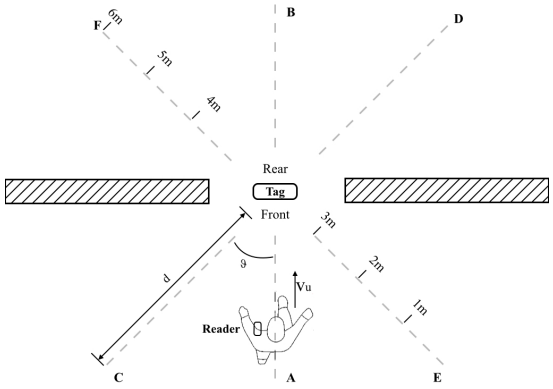

FIGURE 4.31: Door crossing tests.

during the test according to the walking path. For the sake of completeness, also the user speed v_u have been considered during tests.

To mention that in dynamic tests, the efficiency η becomes:

$$\eta = n_e \tag{4.26}$$

since the reader during the user motion is not always in a radiation lobe, so there is no need to consider the number of query sent by the reader.

In the first trial, the reader is placed on the left shoulder of the user that walks across a door along three different paths, as depicted in Figure 4.31. Trials outcome were averaged among users and approximated to the lower integer over 10 path executions. They are reported in Table 4.3: the number of detections during the forward walking

TABLE 4.3: Tag detections in door crossing tests

(a) $e = 66\%$ $v_u = 1\ m/s$

Path	1 m	2 m	3 m	TOT
AB	0	0	1	1
CD	0	1	2	3
EF	0	1	2	3
BA	0	0	1	1
DC	0	0	2	2
FE	0	0	0	0

(b) $e = 66\%$ $v_u = 2\ m/s$

Path	1 m	2 m	3 m	TOT
AB	0	0	1	1
CD	0	0	2	2
EF	0	0	1	1
BA	0	0	0	0
DC	0	0	0	0
FE	0	0	0	0

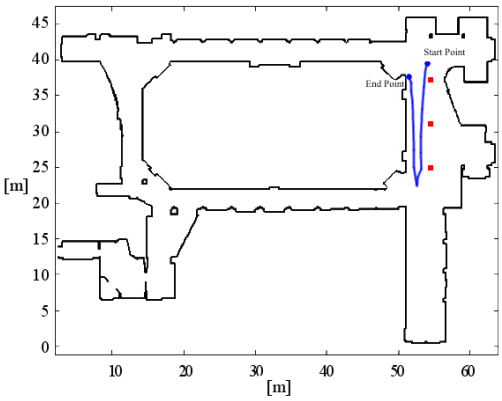

FIGURE 4.32: Corridor test: user path (blue solid line) and tags (red squares).

have been collected considering two different speed, $v_u = 1\,m/s$ and $v_u = 2\,m/s$.
As it is clear from the results achieved, a larger number of detection is retrieved walking at lower speed, since under this operating condition the reader is in the radiation lobe for a longer time, however some detections are available also at the higher speed. It is worth noticing that the results obtained during the crossing door trials are compliant with the static ones.
The tests emphasised that during the backward path, quite no detections were achieved. It can be explained considering that the user did not spent too much time in the lobe (probably less than 1 s), e.g. the user started moving very close to the tag and/or he/she moved very fast.

In the second trials the user walks along a corridor, forward and backward, as shown in Figure 4.32: the overall length of the path is $l = 34\,m$, the user speed is about $v_u = 1\,m/s$. The reader is placed on the left shoulder of the user, considering $h_R = 140\,cm$.. Three tags used in the experiment; they are located on columns, at height

TABLE 4.4: Tag Detections in Corridor Test

Forward			Backward		
Tag n.1	**Tag n.2**	**Tag n.3**	**Tag n.3**	**Tag n.2**	**Tag n.1**
2	9	0	3	9	0

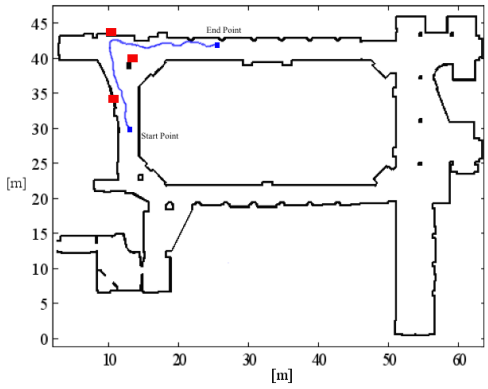

FIGURE 4.33: Open space test: user path (blue solid line) and tags (red squares).

TABLE 4.5: Tag detections in the open space test

Tag n.1	Tag n.2	Tag n.3
11	0	5

$h_T = 220\,cm$. Their orientation with respect to the vertical x-axis of the global reference frame is $\varphi_T = 12deg$ $\varphi_T = 15deg$, and $\varphi_T = 30deg$ for the first, second and third tag, respectively. In Table 4.4, the detection of the reader during the test is reported. It is worth noticing that the detection number of the second tag is greater with respect to the others, due to the presence of metal door reflecting the electromagnetic signal.

In the third dynamic test a forward path in an open space is performed as shown in Figure 4.33. The user walking along a $26\,m$ long path, the speed is constant $v_u = 1m/s$ and he/she wears the RFID reader on the left shoulder. Three tags are considered: they have the same orientation with respect the x-axis of the global reference frame $\varphi_T = 0$, however they are located at different height, $h_T = 149\,cm$, $h_T = 187\,cm$, and $h_T = 220\,cm$ for the first, second and third tag, respectively.

The number of echoes retrieved during the experiment from each tag is reported in Table 4.5. The second tag is not detected since the radiation lobe of the RFID reader does not intersect the radiation lobe of the tags.

4.8 Experimental Results

Several experimental tests have been carried out to prove the effectiveness of the HIPS in different indoor scenarios. Here only an office like scenario is considered for sake of space. The testing environment is composed by an office-like environment: a long ring-shaped corridor bounds by rooms. This environment has been selected for its

closed-loop layout, that allows a better assessment of the performance of the localization algorithm.

During the experimental trials, the rescuer is equipped with a waist-worn InvenSense MPU-9150 device connected to a laptop PC by high speed USB. The CAEN RFID reader is connected to the same laptop via Bluetooth. The sampling frequency of the IMU is 100 Hz, the one of RFID reader is 5 Hz, and a step is detected at $\sim$1 Hz. To this end, a synchronization procedure is performed for data alignment. In these trials, the RFID system detection area is computed according to the results shown in Figure 4.30, so the main radiation lobe is supposed to have a range of $r = 250\ cm$. A MATLAB toolbox have been developed to pre-process the data and implement the HIPS algorithm. The first trial represents a penetrating mission along the corridor. The user executes

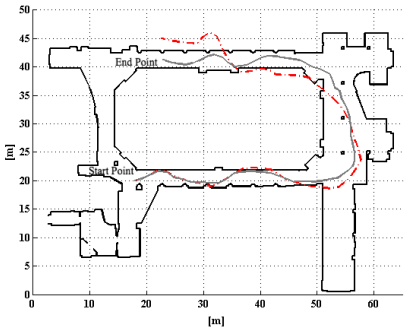

(a) Real path (solid gray line) and inertial prediction estimate (dot–dashed red line)

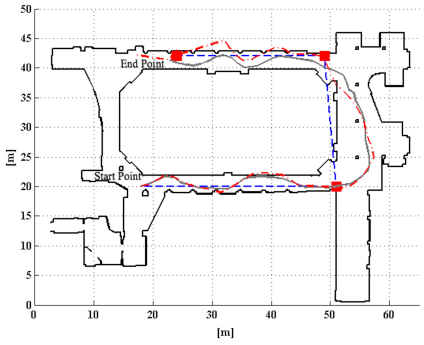

(b) Estimated path using 3 tags: HIPS estimate (dot–dashed red line).

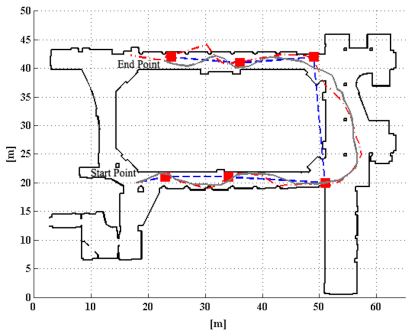

(c) Estimated path using 6 tags: HIPS estimate (dot–dashed red line).

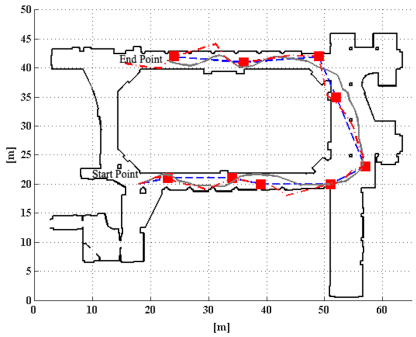

(d) Estimated path using 9 tags: HIPS estimate (dot–dashed red line).

FIGURE 4.34: Indoor results in office like environment: real path (solid gray line), **tag tracking (dashed blue line).**

140 steps travelling an overall distance of about 110 m. The objective of this trial is to determine the optimal number of tags to be used for improving the localization accuracy. Several configurations have been examined for assessing the impact of RFID corrections: according to this approach, a trade off between accuracy and the deployment overhead needs to be found.
To this end, an increasing number of tags, ranging from 3 to 9 and deployed in the environment, is considered. The results of the experiments are depicted in Figure 4.34, where the tag-based position estimate is compared with respect to the HIPS one. Specifically, Figure 4.34(a) shows the path of the rescuer computed by the PDR without integrating RFID corrections and the real path. It can be noticed that the PDR is not suitable

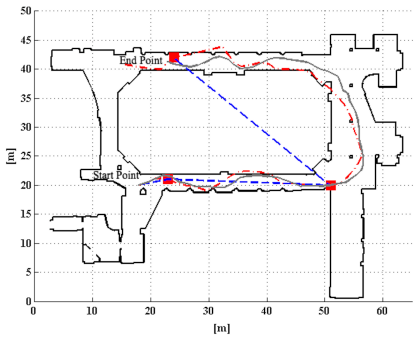

FIGURE 4.35: Estimated path using 3 tags (sub–optimal deployment): real path (solid gray line), tag tracking (dashed blue line), HIPS estimate (dot–dashed red line), and tag (red squares).

by itself: the positioning error grows along the path and, at the end of the experiment, the accuracy is highly downgraded. Using HIPS with 3 tags located in optimal positions (see Figure 4.34(b)), the PDR estimate is remarkably improved and the target performance (i.e., position accuracy at room level) is achieved. Exploiting the same set-up, the path retrieved using only tags information cannot be considered reliable. In this case, the user position during the path between two RFID is completely lost and the position accuracy is limited. For a position estimate accuracy comparable to the one arising from the HIPS but using only the RFID system, we should use nine tags.

For understanding the relevance of the tags deployment for the position correction, a sub-optimal set-up is shown in Figure 4.35: the performance of the HIPS is downgraded and the RFID-based system is not able to provide a reliable position estimate. It is worth noticing that the maximum number of tags represents the actual number and position of emergency signs in the real environment.

The second test has been performed considering the closed-loop path depicted in Figure 4.36. The rescuer executed 382 steps and the overall distance travelled is $\sim$220 m. In this trial, the objective is to determine the performance of the HIPS approach considering a closed-loops task. To this end, a fixed number of tags (6) is deployed in the environment and 6 check points are considered. The Euclidean distance between the check points and the estimated ones (i.e., the positioning error) has been used as performance index. According with Figure 4.36(a), as for tests in Figure 4.34, the positioning error arising from the PDR approach grows along the path and at the end the accuracy is highly downgraded.

To reduce the position error, the correction step resets the position of the user according with the rules described in Section 4.7. As illustrated in Table 4.6, after the correction step the error decreased significantly. After the pose correction, the maximum position error (3.4 m) fits the system requirements: it is able to provide the user pose with room-level accuracy ($\sim$5 m error).

To mention, that in all the trials the residual error after the position correction arises from the heading estimation: tags do not provide information about the orientation and the user attitude can not be updated during the correction phase. As a consequence, the residual bias resulting from the heading estimation affects the estimate, downgrading the overall results.

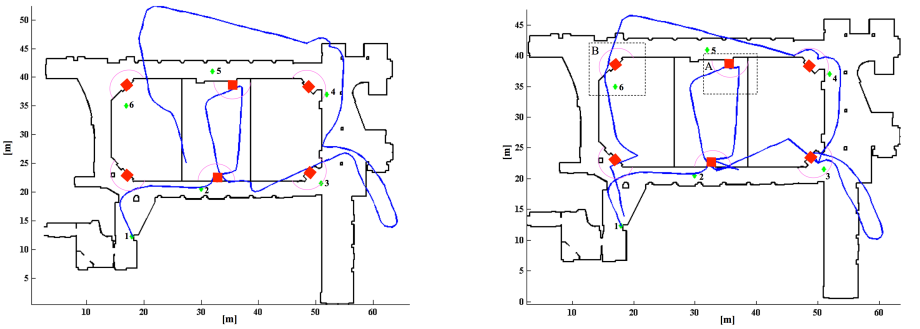

(a) Inertial prediction estimate (solid blue line).

(b) HIPS estimate (solid blue line) using 6 tags (red squares).

FIGURE 4.36: Indoor results in an office-like environment: the performed path (solid blue line), tags position (red squares), the radiation lobe (magenta circle) and check points (green diamond).

TABLE 4.6: Prediction and correction Euclidean errors $[m]$

	1°	2°	3°	4°	5°	6°	1°
Prediction	0	0.4	6.0	4.0	9.0	14.8	14.0
Correction	0	0.4	1.4	1.7	2.8	3.4	1.6

4.9 Conclusion

In this chapter we presented the HIPS, a hybrid indoor positioning system for deep indoor localization. The proposed approach is based on well-known localization schema adopted in robotics: both proprioceptive and exteroceptive sensors are exploited. The proprioceptive sensor, a 6-DoF IMU, is used to provide a rough position estimate of the operator by means of the PDR approach. The RIFD technology has been selected as the exteroceptive system to refine the prediction estimate provided by the proprioceptive approach. This approach allows to suitably reduce the drift error in the pose estimate by achieving a room level accuracy.

Chapter 5

Sporadic ADLs Detection using Inertial Sensing

Within the increasing of life expectancy, falls are becoming a major risk among the elderly community. Although falls present a sporadic nature, falls occurrence increases with age.
In this Chapter we present the FALLEN, an inertial-based fall detection algorithm. Section 5.1 illustrates the current state of the art in the HAR system for fall detection. The innovative approach on which is based FALLEN is presented in Section 5.2. The main peculiarities of the ARC pertaining to FALLEN are discussed in Section 5.3.
Section 5.4.2 illustrates results achieved by means experimental trials. Section 5.5 concludes the Chapter.

5.1 Background & motivations

Falls are defined as the inadvertent settling down of a body on the ground, floor or other lower level. The prevalence of falls is very common among the elderly. The World Health Organization reported that 28%−35% of people aged 65 years and above, fall each year and the rate increases to 32%−42% for those over 70 years of age. Those who are vulnerable to falls also include those suffering from neurological diseases (e.g., epilepsy and dementia), which commonly occur in older people. Living alone itself increases the risk of falls for community elders.
As sporadic human activity, falls are usually isolated event, nevertheless the prevalence of falls is very common among the elderly and increases with age.
Falls can potentially cause severe physical injuries and can reduce the independence of older individuals through dramatic psychological consequences [131]. Moreover, most dramatic effects resulting from falls are usually not related with falls themselves, but with long laying periods (i.e., remaining on the floor for prolonged periods after a fall) which lead to an increased risk of pneumonias, pressure ulcers and even death. These findings call for the development and use of assistive devices for fall detection. Early detection and treatment of falls represent key strategies to be employed in reducing fall-related injuries and preventing their consequences, thus reducing the risk of long laying periods and admissions to nursing homes.

A number of fall-detection algorithms and methods do currently exist, but none of these solutions is universally accepted [131]. One major problem with existing products is that they have deficiencies that hinder pervasive fall detection solutions [132]. Although rather efficient, these devices are usually costly, could need maintenance and have bounded maximum distance between the sensor and the base, limiting the detection within small indoor environments.
Typical fall detection systems present a detection component, which objective concerns

with determining whether there has been falling through the analysis of human movement patterns, such as speed variations and/or body posture changes.
Depending on the nature of the detection component, fall detection technologies can be currently classified into three main categories: video surveillance, audio-vibration-based identification and wearable detection devices [131].
A fall detection system based on video surveillance usually uses one or several RGB/depth cameras to capture the target's movements. The system determines the image characteristics of falls through specific image processing algorithms, thereby distinguishes between falls and typical ADLs (i.e. basic self-care tasks such as, e.g., walking, see Chapter 2). Although several video surveillance solutions have been proposed in literature [131], such approaches have limitations on pervasive detection, affordability and acceptability. Video-based solutions for fall management can indeed be used only in indoor structured environments; moreover users privacy may be compromised.
Audio-vibration-based identification solutions try detecting fall events by analysing audio signals frequency vibration caused by shocks on the floor. Although these solutions do not compromise patients' privacy, as in the previous case the detection area is limited within the monitoring environment, which is costly to build up.
Very good candidates to overcome the aforementioned limitations are represented by fall detection solutions based on MEMS sensors. IMUs and Smart-Phones (SPs) can be used as wearable sensors for long-term analysis in fall detection management. Typical fall detection systems that use IMUs and SPs try to detect the occurrence of fall events by extracting features from the output signal/s of the sensor/s and then discriminating falls from typical ADLs.
As self-contained devices, SPs present a mature hardware and software environment for pervasive fall detection systems development [132]. SP based systems for fall detection can operate almost everywhere since mobile phones are highly portable, integrate all the necessary components and their communication services usually present vast coverage. Moreover, recent data illustrate the increasing popularity of SPs also within elderly people: they indeed might prefer to have a single tool with self-contained fall detection functionality than to carry a separate fall detection device.
Nevertheless, mobile-based solutions are calling for even less complex and lowest computational power algorithms. For this reason most SP-based solutions use Threshold-Based Algorithms (TBAs) [132]. According to [131], the tri-axial accelerometer is the most used sensor in IMU/SP-based fall detection applications. However, solely data from accelerometers are commonly not able to effective discriminate between falls and typical ADLs presenting similar acceleration patterns (e.g., running or laying on the back).

5.2 Research goals & contributions

To overcome the limitations of typical fall detection solutions, in this work we propose a fall detection TBA, the FALLEN (FALL dEtectioN algorithm) that integrates accelerometer and gyroscope data retrieved from a waist-mounted inertial sensor (IMU, SP) (see Figure 5.1).

The matching between features extracted from these two sensors (i.e., the magnitude vector of the acceleration and variations of the user's attitude) allows differentiating falls from ADLs presenting similar acceleration patterns, increasing the overall

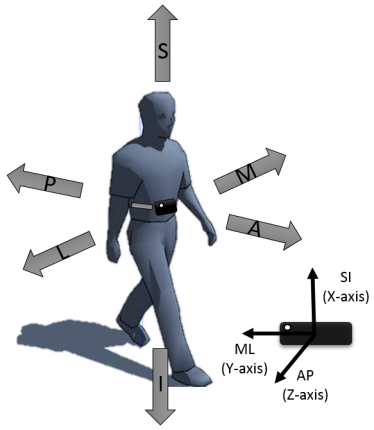

FIGURE 5.1: Local inertial sensing coordinate frame and body-fixed coordinate frame. The local inertial sensing frame axes (x,y,z) are aligned along with the Superior-Inferior (SI), the Medio-Lateral (ML) and the Anterior-Posterior (AP) directions of the body segment, respectively.

system's accuracy without affecting its computational load.
To mention that our proposed method of fusing features retrieved from different sensors (accelerometer and gyroscope) for fall detection is the first time that is proposed in literature.
As illustrated in [133, 134, 135, 132, 136, 137, 138, 139, 131], the typical fall detection solutions mostly use TBAs based on a specific feature, the instantaneous acceleration Signal Magnitude Vector (SVM). Nevertheless, SVM could be not sufficient for optimal fall discrimination, increasing the occurrence of False Positives (FPs) and False Negatives (FNs) or leading to the implementation of more sophisticated classifiers in order to increase the system accuracy. This is especially true with specific ADLs presenting fall-like acceleration patterns, such as laying on the back or running. To overcome the aforementioned limitations without affecting the system's computational burden, we investigated an alternative fall detection solution combining the classical approach with the instantaneous variation of the user's attitude by means of data retrieved from the inertial sensor.
The attitude defines the current orientation of the user wearing the sensor, with respect to a global reference frame. Sudden changes in time of the user's orientation in combination with abrupt variations of the acceleration SVM can be a clear sign that a fall occurred (see Figure 5.2).
To mention that the attitude of the user has been defined by means Euler angle, using an Extended Kalman Filter that fuses data retrieved by accelerometer, gyroscope and magnetometer, as illustrated in Chapter 4.

To validate the effectiveness of the proposed solution, extensive trials have been conducted by users presenting different anthropomorphic features. During experiments, both an IMU and a SP have been used as detectors, which have been attached to the waist of the user to capture movement data, as illustrated in Figure 5.1.

5.3 The FALLEN

In this section, we present an overview of the proposed fall detection algorithm. As part of HAR systems, inertial-based fall detection solutions follow the typical course

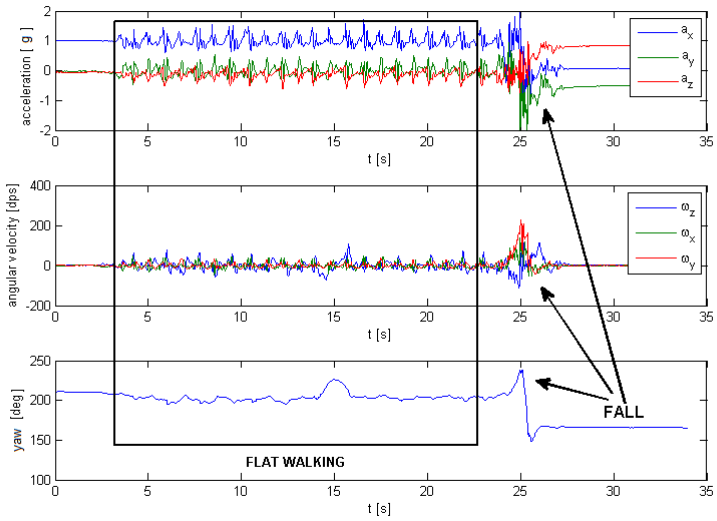

FIGURE 5.2: Superior-Inferior (a_x), Medio-Lateral (a_y) and Antero-Posterior (a_z) accelerations, angular velocities (w_x, w_y and w_z) and the yaw angle of a user equipped with a waist-mounted inertial sensor, during flat walking and a fall.

of action of the ARC illustrated in Chapter 2: data collection, segmentation, features extraction and classification (see Figure 5.3). Stated that a comprehensive description

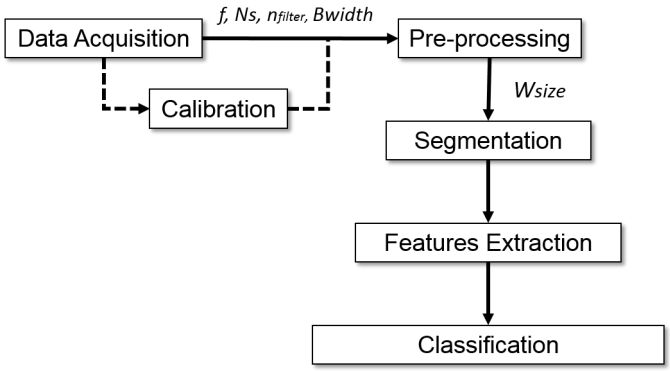

FIGURE 5.3: Steps of the typical ARC.

about the different stages composing the ARC have been provided in Chapter 2 and Chapter 3, the following briefly illustrates the specific design option selected for the FALLEN.

5.3.1 Preprocessing

Accelerometer data stream are used to compute the SVM, one of the two features used in the FALLEN. Preliminary to the features extraction and classification, the accelerometer signal undergoes to a preprocessing step.
This operation is not implemented also on gyroscope and magnetometer data because the EKF approach used for retrieving attitude information has its own intrinsic filtering and smoothing procedure.

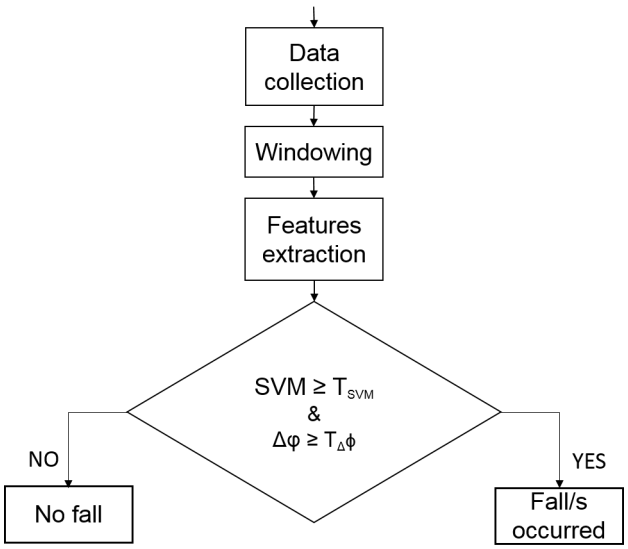

FIGURE 5.4: General architecture of the FALLEN.

As regards acceleration, the procedure used for data preprocessing is the same illustrated for the DETECT algorithm in Chapter 3.
Specifically, we use a two stage filter: a MAF filter with length $l = 20$, and a 5-th order band-pass Butterworth filter with lower and upper cut-off frequencies set to 0.5 Hz and 6 Hz, respectively ($Bwidth = 5.5Hz$).

5.3.2 Windowing

Fixed Non-overlapping Sliding Window approach has been selected for segmenting acceleration and attitude data.
The selection of the window size usually represents an essential design parameter in HAR systems. Nevertheless, when dealing with sporadic activity the length of the window does not longer represent a crucial requirement. Given the typical short duration of a fall, it indeed should mean to heavily segment the signal reducing the window length to fractions of a second. Nevertheless, this could lead to increment the algorithm computational burden.
A the same time, we should also account for the sporadic nature of the activity itself.
Given the above, for the FALLEN the window length is set to $W_{size} = 5s$. Experimental trials showed that this design choice enables to discriminate falls, when occurring, without affecting the algorithm complexity.

5.3.3 Features & classification

Figure 5.4 and Algorithm 1 outline the main steps of the FALLEN.
To detect falls, we extract features from each window. As stated, features extracted in our TBA include the values of the acceleration SVM and the attitude change rate, computed as difference between adjacent elements of the Euler angles. As stated in Chapter 4, the orientation in Euler form is expressed using the three angles $\phi = \{\varphi, \vartheta, \psi\}$, known as *roll*, *pitch* and *yaw* angle. For the sake of completeness, let $i = 1, 2, ..., l$ be the number of samples in each window with $N_s^{acc} = W_{size} * f_{acc}$, where f_{acc} is the acquisition frequency of the accelerometer. For the ith sample, $SVM(i)$ is defined as the square root of the summation of the squared acceleration signals of each axis:

$$SVM(i) = \sqrt{a_x^2(i) + a_y^2(i) + a_z^2(i)}, i = 1, ..., l.$$

Algorithm 1 TBA for fall-detection

1: $FallCount = 0$
2: **while** $FallCount = 0$ **do**
3: **collect data** $\vec{a}, \vec{\omega}, \phi$
4: FILTERING
5: $\vec{a}_{MovAverage} = MovingAverageFilter(\vec{a})$
6: $\vec{a}_{filter} = ButterworthFilter(\vec{a}_{MovAverage}, Bwidth)$
7: WINDOWING
8: $SVM = Windowing(\vec{a}_{filter})$ {set of N_s^{acc} samples}
9: $h = Windowing(\phi)$ {set of N_s^{gyro} samples}
10: FEATURES EXTRACTION
11: **compute** $MaxSVM$, $Max\Delta\phi$ {features for the current window}
12: DISCRIMINATION
13: **if** $MaxSVM \geq T_{SVM}$ **and** $Max\Delta h \geq T_{\Delta\phi}$ **then**
14: $FallCount = 1$
15: **else**
16: $FallCount = 0$
17: **end if**
18: **end while**

Concerning the attitude, the sampling rate is defined by the acquisition frequency of the gyroscope (see Chapter 4). Assuming N_s^{gyro} samples for each window, with $N_s^gyro = W_{size} * f_{gyro}$ and f_{gyro} the gyroscope acquisition frequency, the feature related to the jth sample of the $i-th$ Euler angle can be computes as follows:

$$\Delta(i) = \phi(j)^i - \phi(j-1)^i, j = 1, ..., k-1.$$

where ϕ^i represents the roll (φ), pitch (ϑ) and yaw (ψ) angle for $i = 1, 2, 3$, respectively. Notice that, the f_{gyro} is usually lower than f_{acc} and the gap depends on the acquisition sensor.
Once features are extracted, the algorithm computes the maximum values of both features in the current window (*MaxSVM* and *Max*$\Delta\phi$ in Algorithm1). *MaxSVM* and *Max*$\Delta\phi$ are then compared with specific fixed thresholds (T_{SVM} and $T_{\Delta\phi}$, respectively), defined using experimental data. If both features get over their own threshold, a fall occurred. Otherwise, the algorithm goes on with data collection, windowing, features extraction and discrimination.

5.4 System evaluation

We evaluate the effectiveness of the proposed solution with an extensive experimental activity. In this section, we first introduce how the data were collected; then, we present the system's performances.
According to the common practice familiar with the HAR field, the FALLEN performances will be presented using the metrics presented in Chapter 3.

5.4.1 Data collection

To check the effectiveness of the proposed solution, several experimental tests have been performed by a group of volunteers. Participants (16 subjects, 8 males, 8 females, average age 22 $\pm$ 0.76 years, average height 172.38 $\pm$ 6.76 cm, and average weight 70.46 $\pm$ 10.97 kg) were asked to perform two different trials-set (I and II), for a total number of 32 tests. The first trial-set (I) concerned with typical ADLs, while the second set (II) mixed both ADLs and falls. Typical ADLs were sitting on a chair, laying on the back and four walking patterns. Walking patterns were, specifically, flat walking, walking up/down stairs, jumping and running. Each pattern has been performed by subjects at normal speed in indoor environments; each trial took usually from 1 to 3 minutes.
In the second trial-set (II), subjects simulated falls while performing typical ADLs (the same ADLs as the trial-set I). To generalize the fall-detection problem, in the trial-set II we instructed participants to attempt that each fall was different from the others (for user's specific posture, fall's different direction). During both trials-set, participants wore both sensors (IMU and SP) on their waist using an ad-hoc belt that integrated the devices with minimum interferences with user's activities.

Data collection has been performed using the InvenSense MPU-9150 and the Nexus 5. Concerning the IMU, data storing have been carried out connecting the IMU via Bluetooth to a laptop PC. Data logging from the SP has been performed using the Sensor Insider Pro Android app [58] that enables to import data directly in MATLAB.

5.4.2 Experimental results

We measured the detection performances of the proposed algorithm in terms of True Positive (TP)/FN and True Negative (TN)/FP rates.
To compare the detection accuracy of the proposed solution with respect to traditional fall-detection algorithms, we processed trials dataset I and II with two TBAs that used respectively *SVM* and *SVM & $\Delta\phi$* thresholds for fall discrimination.
Table 5.1 summarizes the achieved results.
Experimental results show that the TBA based on the solely *SVM* presents a sensitivity of 100%, a specificity of 72,5% and an overall detection accuracy of about 83%. Better performance were achieved using a TBA combining both information from accelerometer and gyroscope. In this case, falls and ADLs are perfectly discriminated, with a detection accuracy of 100%.
Experimental results show as some subjects can exhibit fall-like acceleration patterns during typical ADLs. Specifically, these behaviour is especially true during activities such as running or laying on the back. Nevertheless, these activities are not usually related with large instantaneous changing in the user's orientation. The time-variation of the user's attitude during typical ADLs is usually quite smooth. The combination of information retrieved from accelerometer and gyroscope can help specialists to detect simultaneous quick variations of user's acceleration and orientation, increasing the system capability to discriminate falls from ADLs.

TABLE 5.1: Performance comparison of detection tests.

	SVM				SVM & Δh			
	TP	TN	FP	FN	TP	TN	FP	FN
FLAT WALKING (I)		7				7		
FLAT WALKING (II)	7				7			
UP/DOWN STAIRS (I)		2				2		
UP/DOWN STAIRS (II)	2				2			
JUMP (I)		2				2		
JUMP (II)	2				2			
RUNNING (I)			3			3		
RUNNING (II)	3				3			
LAYING THE BACK (I)			2			2		
SITTING ON A CHAIR (I)		2						

5.5 Conclusion

In this Chapter, we proposed a pervasive fall detection TBA using data retrieved from a waist worn inertial sensor. The simultaneous use of features extracted from accelerometer and gyroscope sensors enables the algorithm to detect falls from ADLs presenting fall-like acceleration patterns, increasing the system accuracy with respect to traditional approaches that use only accelerometer data. However, the performance increase does not affect the system computational load, making the proposed solution compliant for the implementation on mobile platforms.

Chapter 6

Concluding remarks

This dissertation presented novel methods aimed at supporting the improvement over the state of the art in the inertial-based HAR field.
A first contribution of this work concerns with an innovative inertial-based solution for the gait assessment. The availability of tracking services for monitoring the walking activity may prove useful for promoting healthier lifestyles, preventing unhealthy habits, detecting anomalous behaviours or monitoring conditions.
Given the primary role played by this topic in several application domains, in the last few years several solutions have been proposed in the literature for addressing the gait assessment by means of inertial sensors. High dimension features vectors (typical length $15 \div 57$) and complex classifiers are usually exerted for addressing the gait patterns classification.
The concurrent advent of the new mobile era contributed to get this topic more intriguing and challenging at the same time. Pervasive solutions for long term tracking are indeed usually in contrast with typical mobile platform requirements. Limiting memory demanding, power consumption, computational time and complexity are just some of the main specifications required by long-term monitoring. As it is clear, these demands are merely incompatible with classic-fashioned approaches for gait assessment.
According to these findings, in this dissertation we proposed the DETECT. Limiting the number of features and using a light classifier, the DETECT is able to provide a high classification accuracy while matching the afore-mentioned requirements.
In compliance with the typical course of actions pertaining to a HAR system, we illustrated the main features of each stage of the DETECT ARC. Accelerometry data retrieved from a waist-mounted IMU are then firstly preprocessed. According to experimental facts, we use a two stage filter: a moving average filter (length = 20), and a Butterworth filter in cascade (lower and upper cut-off frequencies set to 0.5 Hz and 6 Hz, respectively) enabled reducing noises and outliers without affecting computation time and classification accuracy.
Concerning the segmentation technique, we proposed the sliding window approach with FNWS and window-size of $0.54s$. Experimental outcomes showed indeed how the overlapping approach may increase the FP/FN rates and compromise the computational time of the algorithm at the same time. Although the feature extraction is usually performed on a single-window data, in this work we introduced the notion of *motion segments*. A motion segment is a macro-window, that is a set of unclassified consecutive windows arising from the Lev. 1 of the decision tree. Introduced in the DETECT training phase, this concept enabled avoiding potential misclassification when dynamic patterns are mixed.
The selection of specific features and a peculiar classifier in general represents the two main design options for a HAR system. Experimental outcomes led us to select a 4 four level decision tree and 3 features: the variance, the peak amplitude and the derivative

trend.
Despite its simplicity, the feasibility of the proposed approach has been demonstrated by extensive experimental trials. Tests performed by a group of volunteers showed an overall classification accuracy exceeding the 91% for continuous applications. DETECT perfectly discriminates standing and level walking patterns; the misclassification increases in case of stair patterns but the mean misclassification rate for both patterns does not exceed the 8%. In addition, the test duration does not affect the algorithm performances making the DETECT perfectly compliant with long term applications.

A second contribution discussed in this work pertains to a hybrid personal indoor positioning system, the HIPS. Through a comprehensive dissertation about the current state of the art in the Indoor Localization and Positioning (ILP) field, we illustrated that classic approaches exerting the use of proprioceptive or exteroceptive sensors are not able to provide a position estimate with a satisfactory accuracy. Nevertheless, limiting the position error is essential when the ILP task is addressed into emergency scenarios. By means of the HIPS, we have demonstrated that the synergistic use of proprioceptive and exteroceptive technologies enables limiting the positioning error to room level. The user position estimate provided by the HIPS founds on the well-known prediction-correction schema used in robotics for pose estimation. For the prediction phase, we proposed the PDR approach based on a step-heading system, that estimate the user pose by accruing the length of each step and the corresponding heading. Five methods for step detection and counting have been proposed and experimental facts showed as the peak detection with adaptive threshold algorithm is the most effective approach (the detection accuracy exceeds the 94%). Then, we presented the step length estimation algorithm, that uses data extracted from adjacent windows of the vertical acceleration component to provide the estimate of each step performed by the user. Experimental data showed that the maximum percent error in the length estimate does not exceed the 4.4%.
In this work, the heading of the user has been computed fusing data retrieved from the inertial sensor, by means of a quaternion-based EKF. Data arising from trials demonstrated the validity of the attitude filter in tracking the user orientation. The maximum percent error in the orientation estimate is indeed below 8 deg.
Combining the step counting algorithm, the step length estimation and the attitude filter in the PDR approach, we were able to estimate continuously the user pose. Nevertheless, we stated that different sources of error may contribute to deteriorate the accuracy of the estimate provided by the inertial navigation. At the same time, the inertial sensor is internal referenced so it has no means to reset potential errors. As a consequence, the position error grows unbounded along the path and the system may provide a complete misleading estimate of the user pose.
In this work, we proposed to use a hybrid approach to solve potential issues arising from the inertial navigation. In the HIPS architecture, RFID passive tags disseminated into the working environment are used to collect their absolute geographical position with respect to a global reference frame. The correction on the inertial navigation pose estimate is performed using data retrieved from tag/s each time the user is in the its/their radiation lobe/s. Depending on the number of the tags detected, we proposed a specific correction strategy for the definition of the user pose "update". The characterization of the RFID system went hand-in-hand with the correction strategy. Beside the correction strategy design, an extensive RFID system assessment in real operating scenarios has been performed. Experimental facts showed that the system (reader-tag) radiation lobe shape strictly depends on the environmental layout, reader-tag relative pose, and potential interferences. Nevertheless, we were able to asses that in normal

operating conditions the radiation lobe is semicircular-shaped with a radius of about 250 cm. Given potential variability that may affect the radiation lobe shape, we associate to each tag an accuracy (w_i) defined during the assessment.
Finally, we illustrated the validity of the HIPS by means of experimental tests in a real-operating scenario. We considered both open and closed loop paths and a different number of tags deployed into the environment, in order to asses how many tags are sufficient to perform an effective position correction. Experimental facts demonstrated that the maximum position error (3.4 m) provided by the HIPS with a limited number of tags is perfectly compliant with the user requirement (position error less than 5 m), thus justifying the validity of the proposed approach.

A third and final novel result presented in this thesis is the design of an inertial-based algorithm for fall detection. Within the increasing of the life expectancy, fall are becoming a major risk among the elderly community. In order to reduce potential long lying periods arising after falls, we proposed the use of an innovative approach able to detect falls by means of data retrieved from a waist-mounted IMU. We illustrated as classic inertial-based methods for fall detection usually exert only data from accelerometer for detecting falls. Nevertheless, feature extracted from accelerometry data stream are usually ineffective in differentiating falls from specific ADLs (i.e., laying on the back, running). To overcome this limitation, we proposed to use features extracted from both accelerometer and gyroscope sensors. Experimental trials showed the effectiveness of the proposed approach with respect to classical methods.

6.1 Scientific publications

6.1.1 Journal papers

De Cillis, F., De Maggio, M. C., Pragliola, C., & Setola, R. (2013). Analysis of criminal and terrorist related episodes in railway infrastructure scenarios. Journal of Homeland Security and Emergency Management, 10(2), 447-476.

Marrone, S., Nardone, R., Tedesco, A., D'Amore, P., Vittorini, V., Setola, R., **De Cillis F.**, & Mazzocca, N. (2013). Vulnerability modeling and analysis for critical infrastructure protection applications. International Journal of Critical Infrastructure Protection, 6(3), 217-227.

De Cillis, F., Sforza, A., & Sterle, C. (2013). Optimal location of flow intercepting facilities to improve security in urban areas. International Journal of System of Systems Engineering, 4(3-4), 222-242.

6.1.2 Conference papers

De Cillis F., Inderst F., Pascucci F., Tesei M., Setola R., "Uso di dispositivi wearable e tecnologia RFID per migliorare la conoscenza dei luoghi di intervento Sistema di localizzazione utenti ambienti indoor", In Soccorso, sicurezza ed evoluzione tecnologica – Istituto Superiore Antincendio, Rome, October 15th – 16th 2015, Rome, Italy.

De Cillis F., Hernantes J., Sarriegi J. M., Pascucci F., Inderst F., Setola R., "RISING:

Radio Frequency Identification and inertial navigation for indoor localization in emergency management and building maintenance," In TIEMS 2015, The International Management Society Annual Conference, September 30th – October 2nd 2015, Rome, Italy.

De Simio F., **De Cillis F.**, Fumagalli G., De Maggio M.C., van de Beek S., Dawson J., Dawson L., and Setola R., "Strategies to improve Critical Infrastructures Robustness against the IEMI threat: a Review of relevant Standards and Guidelines on the topic", In CRITIS 2015, the 10th International Conference on Critical Information Infrastructures Security, Protection and Resilience, October 13th – 15th, 2014 – Berlin, Germany.

De Cillis, F.; De Simio, F.; Guido, F.; Incalzi, R.A.; Setola, R., "Fall-detection solution for mobile platforms using accelerometer and gyroscope data," in Engineering in Medicine and Biology Society (EMBC), 2015 37th Annual International Conference of the IEEE , vol., no., pp.3727-3730, 25-29 Aug. 2015.

De Cillis F., De Simio F., Inderst F., Faramondi L., Pascucci F., and Setola R. "Improving Situational Awareness for First Responders," In Proceedings of CRITIS 2014, the 9th International Conference on Critical Information Infrastructures Security, Protection and Resilience, October 13th – 15th, 2014 – Limassol, Cyprus.

De Cillis, F.; De Simio, F.; Faramondi, L.; Inderst, F.; Pascucci, F.; Setola, R., "Indoor positioning system using walking pattern classification," in Control and Automation (MED), 2014 22nd Mediterranean Conference of , vol., no., pp.511-516, 16-19 June 2014.

De Cillis, F.; Oliva, G.; Pascucci, F.; Setola, R.; Tesei, M., "On field gesture-based human-robot interface for emergency responders," in Safety, Security, and Rescue Robotics (SSRR), 2013 IEEE International Symposium on , vol., no., pp.1-6, 21-26 Oct. 2013.

Pascucci F., Setola R., **De Cillis F.**, Inderst F., Delprato U., Marsella S., Marzoli M., Petracca M., Vari M., and Cristaldi M., "REFIRE: A Reference Implementation for Deep Indoor Localization," In Future Security 2013, the 8th Security Research Conference, September 17th – 19th, 2013 – Berlin, Germany.

Sforza A., Sterle C., D'Amore P., Tedesco A., **De Cillis F.**, and Setola R., "Optimization Models in a Smart Tool for the Railway Infrastructure Protection", In Lectures Notes on Computer Science, Proceedings of CRITIS 2013, the 8th International Conference on Critical Information Infrastructures Security, Protection and Resilience, vol. 8328, no., pp. 191-196.

Bibliography

[1] Andreas Bulling, Ulf Blanke, and Bernt Schiele. "A Tutorial on Human Activity Recognition Using Body-worn Inertial Sensors". In: *ACM Comput. Surv.* 46.3 (Jan. 2014), 33:1–33:33. ISSN: 0360-0300. DOI: 10.1145/2499621.

[2] Lara Allet et al. "Wearable Systems for Monitoring Mobility-Related Activities in Chronic Disease: A Systematic Review". In: *Sensors* 10.10 (2010), p. 9026. ISSN: 1424-8220.

[3] Michael B. del Rosario, Stephen J. Redmond, and Nigel H. Lovell. "Tracking the Evolution of Smartphone Sensing for Monitoring Human Movement". In: *Sensors* 15.8 (2015), p. 18901. ISSN: 1424-8220.

[4] C.V.C. Bouten et al. "A triaxial accelerometer and portable data processing unit for the assessment of daily physical activity". In: *Biomedical Engineering, IEEE Transactions on* 44.3 (1997), pp. 136–147. ISSN: 0018-9294. DOI: 10.1109/10.554760.

[5] Inaki Maurtua et al. "A Wearable Computing Prototype for supporting training activities in Automotive Production". In: *Applied Wearable Computing (IFAWC), 2007 4th International Forum on*. 2007, pp. 1–12.

[6] G. Ogris et al. "Using a complex multi-modal on-body sensor system for activity spotting". In: *Wearable Computers, 2008. ISWC 2008. 12th IEEE International Symposium on*. 2008, pp. 55–62. DOI: 10.1109/ISWC.2008.4911585.

[7] R. Meziane et al. "Safer hybrid workspace using human-robot interaction while sharing production activities". In: *Robotic and Sensors Environments (ROSE), 2014 IEEE International Symposium on*. 2014, pp. 37–42. DOI: 10.1109/ROSE.2014.6952980.

[8] Kai Kunze et al. "Towards Recognizing Tai Chi Â¿ An Initial Experiment Using Wearable Sensors". In: *Applied Wearable Computing (IFAWC), 2006 3rd International Forum on*. 2006, pp. 1–6.

[9] Sidney Katz. "Assessing Self-maintenance: Activities of Daily Living, Mobility, and Instrumental Activities of Daily Living". In: *Journal of the American Geriatrics Society* 31.12 (1983), pp. 721–727. ISSN: 1532-5415. DOI: 10.1111/j.1532-5415.1983.tb03391.x.

[10] Hao Xia et al. "Using Smart Phone Sensors to Detect Transportation Modes". In: *Sensors* 14.11 (2014), p. 20843. ISSN: 1424-8220. DOI: 10.3390/s141120843.

[11] Oresti Banos et al. "Window Size Impact in Human Activity Recognition". In: *Sensors* 14.4 (2014), p. 6474. ISSN: 1424-8220. DOI: 10.3390/s140406474.

[12] Sebastijan Sprager and Matjaz B. Juric. "Inertial Sensor-Based Gait Recognition: A Review". In: *Sensors* 15.9 (2015), p. 22089. ISSN: 1424-8220.

[13] Deng Zhongliang et al. "Situation and development tendency of indoor positioning". In: *Communications, China* 10.3 (2013), pp. 42–55.

[14] Michalis Vrigkas, Christophoros Nikou, and Ioannis Kakadiaris. "A Review of Human Activity Recognition Methods". In: *Frontiers in Robotics and AI* 2.28 (2015). ISSN: 2296-9144. DOI: 10.3389/frobt.2015.00028.

[15] D.M Gavrila. "The Visual Analysis of Human Movement: A Survey". In: *Computer Vision and Image Understanding* 73.1 (1999), pp. 82 –98. ISSN: 1077-3142. DOI: http://dx.doi.org/10.1006/cviu.1998.0716.

[16] J.K. Aggarwal and Q. Cai. "Human Motion Analysis: A Review". In: *Computer Vision and Image Understanding* 73.3 (1999), pp. 428 –440. ISSN: 1077-3142.

[17] Liang Wang, Weiming Hu, and Tieniu Tan. "Recent developments in human motion analysis". In: *Pattern Recognition* 36.3 (2003), pp. 585 –601. ISSN: 0031-3203. DOI: http://dx.doi.org/10.1016/S0031-3203(02)00100-0.

[18] J.K. Aggarwal and M.S. Ryoo. "Human Activity Analysis: A Review". In: *ACM Comput. Surv.* 43.3 (Apr. 2011), 16:1–16:43. ISSN: 0360-0300. DOI: 10.1145/1922649.1922653.

[19] Yang Yang, I. Saleemi, and M. Shah. "Discovering Motion Primitives for Unsupervised Grouping and One-Shot Learning of Human Actions, Gestures, and Expressions". In: *Pattern Analysis and Machine Intelligence, IEEE Transactions on* 35.7 (2013), pp. 1635–1648. ISSN: 0162-8828. DOI: 10.1109/TPAMI.2012.253.

[20] Bingbing Ni et al. "Motion Part Regularization: Improving action recognition via trajectory group selection". In: *Computer Vision and Pattern Recognition (CVPR), 2015 IEEE Conference on*. 2015, pp. 3698–3706. DOI: 10.1109/CVPR.2015.7298993.

[21] A. Patron-Perez et al. "Structured Learning of Human Interactions in TV Shows". In: *Pattern Analysis and Machine Intelligence, IEEE Transactions on* 34.12 (2012), pp. 2441–2453. ISSN: 0162-8828. DOI: 10.1109/TPAMI.2012.24.

[22] KN Tran et al. "Activity analysis in crowded environments using social cues for group discovery and human interaction modeling". In: *Pattern Recognition Letters* 44 (2014), pp. 49–57.

[23] Hector P Martinez, Georgios N Yannakakis, and John Hallam. "Don't classify ratings of affect; rank them!" In: *Affective Computing, IEEE Transactions on* 5.3 (2014), pp. 314–326.

[24] Tian Lan, Leonid Sigal, and Greg Mori. "Social roles in hierarchical models for human activity recognition". In: *Computer Vision and Pattern Recognition (CVPR), 2012 IEEE Conference on*. IEEE. 2012, pp. 1354–1361.

[25] J. R. Hall et al. "Biomarkers of basic activities of daily living in Alzheimer's disease". In: *Journal of Alzheimer's Disease* 31.2 (2012), pp. 429–437.

[26] Janet Fricke. *Activities of Daily Living*. Center for International Rehabilitation Research Information and Exchange (CIRRIE). 2008. URL: http://cirrie.buffalo.edu/encyclopedia/en/article/37/.

[27] Ferhat Attal et al. "Physical Human Activity Recognition Using Wearable Sensors". In: *Sensors* 15.12 (2015), p. 29858. ISSN: 1424-8220.

[28] Akin Avci et al. "Activity Recognition Using Inertial Sensing for Healthcare, Wellbeing and Sports Applications: A Survey". In: *Architecture of Computing Systems (ARCS), 2010 23rd International Conference on*. 2010, pp. 1–10.

[29] Muhammad Shoaib et al. "A Survey of Online Activity Recognition Using Mobile Phones". In: *Sensors* 15.1 (2015), p. 2059. ISSN: 1424-8220.

[30] O.D. Lara and M.A. Labrador. "A Survey on Human Activity Recognition using Wearable Sensors". In: *Communications Surveys Tutorials, IEEE* 15.3 (2013), pp. 1192–1209. ISSN: 1553-877X. DOI: 10.1109/SURV.2012.110112.00192.

[31] Mingjing Yang et al. "Statistical and Machine Learning Approach to Assessing the Environmental Impact on Walking Patterns". In: *Data Mining Workshop (ICDMW), 2014 IEEE International Conference on*. 2014, pp. 231–235. DOI: 10.1109/ICDMW.2014.169.

[32] N.H. Lovell et al. "Accelerometry Based Classification of Walking Patterns Using Time-frequency Analysis". In: *Engineering in Medicine and Biology Society, 2007. EMBS 2007. 29th Annual International Conference of the IEEE*. 2007, pp. 4899–4902. DOI: 10.1109/IEMBS.2007.4353438.

[33] R.K. Ibrahim et al. "Time-Frequency Based Features for Classification of Walking Patterns". In: *Digital Signal Processing, 2007 15th International Conference on*. 2007, pp. 187–190. DOI: 10.1109/ICDSP.2007.4288550.

[34] Wei-Chih Hung et al. "Activity Recognition with sensors on mobile devices". In: *Machine Learning and Cybernetics (ICMLC), 2014 International Conference on*. Vol. 2. 2014, pp. 449–454. DOI: 10.1109/ICMLC.2014.7009650.

[35] Sebastian D. Bersch et al. "Sensor Data Acquisition and Processing Parameters for Human Activity Classification". In: *Sensors* 14.3 (2014), p. 4239. ISSN: 1424-8220.

[36] Sekine et al. "Classification of waist-acceleration signals in a continuous walking record". In: *Med. Eng. Phys.* 22 (2000), pp. 285–291.

[37] M.N. Nyan et al. "Classification of gait patterns in the time frequency domain". In: *Journal of Biomechanics* 39.14 (2006), pp. 2647 –2656. ISSN: 0021-9290. DOI: http://dx.doi.org/10.1016/j.jbiomech.2005.08.014.

[38] Donald J Patterson et al. "Fine-grained activity recognition by aggregating abstract object usage". In: *Wearable Computers, 2005. Proceedings. Ninth IEEE International Symposium on*. IEEE. 2005, pp. 44–51.

[39] Tim Van Kasteren et al. "Accurate activity recognition in a home setting". In: *Proceedings of the 10th international conference on Ubiquitous computing*. ACM. 2008, pp. 1–9.

[40] M. Dash and H. Liu. "Feature selection for classification". In: *Intelligent Data Analysis* 1 (1997), pp. 131 –156. ISSN: 1088-467X. DOI: http://dx.doi.org/10.1016/S1088-467X(97)00008-5.

[41] Peter H Veltink et al. "Detection of static and dynamic activities using uniaxial accelerometers". In: *Rehabilitation Engineering, IEEE Transactions on* 4.4 (1996), pp. 375–385.

[42] A. et al. Godfrey. "Direct measurement of human movement by accelerometry". In: *Medical Engineering and Physics* 30.10 (2008), pp. 1364 –1386.

[43] Jhun-Ying Yang, Jeen-Shing Wang, and Yen-Ping Chen. "Using acceleration measurements for activity recognition: An effective learning algorithm for constructing neural classifiers". In: *Pattern recognition letters* 29.16 (2008), pp. 2213–2220.

[44] Shuangquan Wang et al. "Human activity recognition with user-free accelerometers in the sensor networks". In: *Neural Networks and Brain, 2005. ICNN&B'05. International Conference on*. Vol. 2. IEEE. 2005, pp. 1212–1217.

[45] B. Najafi et al. "Ambulatory system for human motion analysis using a kinematic sensor: monitoring of daily physical activity in the elderly". In: *Biomedical Engineering, IEEE Transactions on* 50.6 (2003), pp. 711–723. ISSN: 0018-9294. DOI: 10.1109/TBME.2003.812189.

[46] E. Sejdic et al. "A Comprehensive Assessment of Gait Accelerometry Signals in Time, Frequency and Time-Frequency Domains". In: *Neural Systems and Rehabilitation Engineering, IEEE Transactions on* 22.3 (2014), pp. 603–612. ISSN: 1534-4320. DOI: 10.1109/TNSRE.2013.2265887.

[47] Ning Wang et al. "Accelerometry based classification of gait patterns using empirical mode decomposition". In: *Acoustics, Speech and Signal Processing, 2008. ICASSP 2008. IEEE International Conference on*. 2008, pp. 617–620. DOI: 10.1109/ICASSP.2008.4517685.

[48] Ning Wang et al. "Feature extraction using an AM-FM model for gait pattern classification". In: *Biomedical Circuits and Systems Conference, 2008. BioCAS 2008. IEEE*. 2008, pp. 25–28. DOI: 10.1109/BIOCAS.2008.4696865.

[49] AK Bourke, JV O'brien, and GM Lyons. "Evaluation of a threshold-based tri-axial accelerometer fall detection algorithm". In: *Gait & posture* 26.2 (2007), pp. 194–199.

[50] Ling Bao and Stephen S. Intille. "Activity recognition from user-annotated acceleration data". In: Springer, 2004, pp. 1–17.

[51] Oliver J. Woodman. *An introduction to inertial navigation*. Tech. rep. University of Cambridge - Computer Laboratory, 2007.

[52] Faisal Mohd-Yasin, DJ Nagel, and CE Korman. "Noise in MEMS". In: *Measurement Science and Technology* 21.1 (2010), p. 012001.

[53] Luca Ricci. "On inertial sensing of motion: validation, calibration and tracking with wearable devices in robotics and biomedical applications". PhD thesis. Università Campus Bio-Medico di Roma, 2015.

[54] A. Kozlov, I. Sazonov, and N. Vavilova. "IMU calibration on a low grade turntable: Embedded estimation of the instrument displacement from the axis of rotation". In: *Inertial Sensors and Systems (ISISS), 2014 International Symposium on*. 2014, pp. 1–4. DOI: 10.1109/ISISS.2014.6782525.

[55] D. Tedaldi, A. Pretto, and E. Menegatti. "A robust and easy to implement method for IMU calibration without external equipments". In: *Robotics and Automation (ICRA), 2014 IEEE International Conference on*. 2014, pp. 3042–3049. DOI: 10.1109/ICRA.2014.6907297.

[56] B.V. Reddy, L. Pavithra, and G. Satheesh Reddy. "Automation of strapdown IMU calibration using LabVIEW". In: *Intelligent Control and Automation (WCICA), 2014 11th World Congress on*. 2014, pp. 5147–5151. DOI: 10.1109/WCICA.2014.7053591.

[57] Michael J Caruso. "Applications of magnetoresistive sensors in navigation systems". In: *SAE transactions* 106 (1997), pp. 1092–1098.

[58] URL: https://play.google.com/store/apps/details?id=com.lucanatech.sensorinsider.pro&hl=en.

[59] Ning Wang et al. "Can Triaxial Accelerometry Accurately Recognize Inclined Walking Terrains?" In: *Biomedical Engineering, IEEE Transactions on* 57.10 (2010), pp. 2506–2516. ISSN: 0018-9294. DOI: 10.1109/TBME.2010.2049357.

[60] Qing Zhang et al. "Activity of Daily Living assessment through wireless sensor data". In: *Engineering in Medicine and Biology Society (EMBC), 2014 36th Annual International Conference of the IEEE*. 2014, pp. 1752–1755. DOI: 10.1109/EMBC.2014.6943947.

[61] R.K. Ibrahim et al. "Gait patterns classification using spectral features". In: *Signals and Systems Conference, 2008. (ISSC 2008). IET Irish*. 2008, pp. 98–102.

[62] Clemens Lombriser et al. "On-body Activity Recognition in a Dynamic Sensor Network". In: *Proceedings of the ICST 2Nd International Conference on Body Area Networks*. BodyNets '07. Florence, Italy: ICST (Institute for Computer Sciences, Social-Informatics and Telecommunications Engineering), 2007, pp. 171–176. ISBN: 978-963-06-2193-9. URL: http://dl.acm.org/citation.cfm?id=1460232.1460249.

[63] Susanna Pirttikangas, Kaori Fujinami, and Tatsuo Nakajima. "Feature Selection and Activity Recognition from Wearable Sensors". English. In: *Ubiquitous Computing Systems*. Ed. by HeeYong Youn, Minkoo Kim, and Hiroyuki Morikawa. Vol. 4239. Lecture Notes in Computer Science. Springer Berlin Heidelberg, 2006, pp. 516–527. ISBN: 978-3-540-46287-3. DOI: 10.1007/11890348_39.

[64] P. Kugler et al. "Automatic recognition of Parkinson's disease using surface electromyography during standardized gait tests". In: *Engineering in Medicine and Biology Society (EMBC), 2013 35th Annual International Conference of the IEEE*. 2013, pp. 5781–5784. DOI: 10.1109/EMBC.2013.6610865.

[65] J. Parkka et al. "Activity classification using realistic data from wearable sensors". In: *Information Technology in Biomedicine, IEEE Transactions on* 10.1 (2006), pp. 119–128. ISSN: 1089-7771. DOI: 10.1109/TITB.2005.856863.

[66] Pierre Barralon, Norbert Noury, and Nicolas Vuillerme. "Classification of daily physical activities from a single kinematic sensor". In: *Engineering in Medicine and Biology Society, 2005. IEEE-EMBS 2005. 27th Annual International Conference of the*. IEEE. 2006, pp. 2447–2450.

[67] D.M. Karantonis et al. "Implementation of a real-time human movement classifier using a triaxial accelerometer for ambulatory monitoring". In: *Information Technology in Biomedicine, IEEE Transactions on* 10.1 (2006), pp. 156–167. ISSN: 1089-7771. DOI: 10.1109/TITB.2005.856864.

[68] E.A. Heinz et al. "Using Wearable Sensors for Real-Time Recognition Tasks in Games of Martial Arts - An Initial Experiment". In: *Computational Intelligence and Games, 2006 IEEE Symposium on*. 2006, pp. 98–102. DOI: 10.1109/CIG.2006.311687.

[69] James Dougherty, Ron Kohavi, and Mehran Sahami. "Supervised and Unsupervised Discretization of Continuous Features". In: *MACHINE LEARNING: PROCEEDINGS OF THE TWELFTH INTERNATIONAL CONFERENCE*. Morgan Kaufmann, 1995, pp. 194–202.

[70] Roozbeh Jafari et al. "Physical Activity Monitoring for Assisted Living at Home". English. In: *4th International Workshop on Wearable and Implantable Body Sensor Networks (BSN 2007)*. Ed. by Steffen Leonhardt, Thomas Falck, and Petri. Vol. 13. IFMBE Proceedings. Springer Berlin Heidelberg, 2007, pp. 213–219. ISBN: 978-3-540-70993-0. DOI: 10.1007/978-3-540-70994-7_37.

[71] Nishkam Ravi et al. "Activity Recognition from Accelerometer Data". In: *Proceedings of the 17th Conference on Innovative Applications of Artificial Intelligence - Volume 3*. IAAI'05. Pittsburgh, Pennsylvania: AAAI Press, 2005, pp. 1541–1546. ISBN: 1-57735-236-x. URL: http://dl.acm.org/citation.cfm?id=1620092.1620107.

[72] Jonathan Lester, Tanzeem Choudhury, and Gaetano Borriello. "A Practical Approach to Recognizing Physical Activities". English. In: *Pervasive Computing*. Ed. by KennethP. Fishkin et al. Vol. 3968. Lecture Notes in Computer Science. Springer Berlin Heidelberg, 2006, pp. 1–16. ISBN: 978-3-540-33894-9. DOI: 10.1007/11748625_1.

[73] Felicity R Allen et al. "An adapted gaussian mixture model approach to accelerometry based movement classification using time-domain features". In: *Engineering in Medicine and Biology Society, 2006. EMBS'06. 28th Annual International Conference of the IEEE*. IEEE. 2006, pp. 3600–3603.

[74] David Perrin Susan J. Shultz Peggy Houglum. *Examination of muskoskeletal injuries. 2nd Ed.* Ed. by Human Kinetics. North Carolina, 2005.

[75] Christopher L. Vaughan. "Theories of bipedal walking: an odyssey". In: *Journal of Biomechanics* 36.4 (2003), pp. 513–523.

[76] J. London. *The clinical orthopedic assessment guide. 2nd Ed.* Ed. by Kansas. Human Kinetics, 2008.

[77] Samantha M Reid et al. "Knee biomechanics of alternate stair ambulation patterns". In: *Medicine and science in sports and exercise* 39.11 (2007), p. 2005.

[78] Sadiq J Abbas and Zahraa M Abdulhassan. "Kinematic Analysis of Human Climbing up and Down Stairs at Different Inclinations". In: *Engineering &Techology Journal* 31.8 (2013), p. 201.

[79] Alison C Novak et al. "Stair negotiation alters stability in older adults". In: *Lower Extremity Review* (2010).

[80] Jeen-Shing Wang et al. "Walking Pattern Classification and Walking Distance Estimation Algorithms Using Gait Phase Information". In: *Biomedical Engineering, IEEE Transactions on* 59.10 (2012), pp. 2884–2892. ISSN: 0018-9294. DOI: 10.1109/TBME.2012.2212245.

[81] Emanuele Trucco and Konstantinos Plakas. "Video tracking: a concise survey". In: *Oceanic Engineering, IEEE Journal of* 31.2 (2006), pp. 520–529.

[82] Sanchez. *STeAM: Sensor Tracking and Mapping*. Microsoft Indoor Localization Competition - IPSN 2015. 2015. URL: http://research.microsoft.com/en-US/eventsindoorloccompetition2015/ipsn_sanchez.pdf.

[83] Qiang Yang, Sinno Jialin Pan, and Vincent Wenchen Zheng. "Estimating location using wi-fi". In: *IEEE Intelligent Systems* 1 (2008), pp. 8–13.

[84] Chai Jihong. "Patient positioning system in hospital based on zigbee". In: *Intelligent Computation and Bio-Medical Instrumentation (ICBMI), 2011 International Conference on*. IEEE. 2011, pp. 159–162.

[85] Chun-Jung Lin et al. "Application of intelligent agent and RFID technology fo indoor position: Safety of kindergarten as example". In: *Machine Learning and Cybernetics (ICMLC), 2010 International Conference on*. Vol. 5. IEEE. 2010, pp. 2571–2576.

[86] Mohamed M Saad et al. "High-accuracy reference-free ultrasonic location estimation". In: *Instrumentation and Measurement, IEEE Transactions on* 61.6 (2012), pp. 1561–1570.

[87] Zhu Xiao et al. "Development and prospect of ultra-wideband localization research and application". In: *Dianzi Xuebao(Acta Electronica Sinica)* 39.1 (2011), pp. 133–141.

[88] Sheng Zhou and John K Pollard. "Position measurement using Bluetooth". In: *Consumer Electronics, IEEE Transactions on* 52.2 (2006), pp. 555–558.

[89] Daniel Hauschildt and Nicolaj Kirchhof. "Advances in thermal infrared localization: Challenges and solutions". In: *Indoor Positioning and Indoor Navigation (IPIN), 2010 International Conference on*. IEEE. 2010, pp. 1–8.

[90] Jouni Rantakokko et al. "Accurate and reliable soldier and first responder indoor positioning: multisensor systems and cooperative localization". In: *Wireless Communications, IEEE* 18.2 (2011), pp. 10–18.

[91] Joel A Hesch et al. "A Laser-aided Inertial Navigation System (L-INS) for human localization in unknown indoor environments". In: *Robotics and Automation (ICRA), 2010 IEEE International Conference on*. IEEE. 2010, pp. 5376–5382.

[92] Rainer Mautz. "Combination of indoor and outdoor positioning". In: *1st International Conference on Machine Control & Guidance*. Citeseer. 2008.

[93] Pragun Goyal et al. "Strap-down pedestrian dead-reckoning system". In: vol. 2. 2011, p. 3.

[94] Rainer Mautz. "Indoor positioning technologies". PhD thesis. Habilitationsschrift ETH Zürich, 2012, 2012.

[95] Jari Saarinen et al. "Rescue personnel localization system". In: *Safety, Security and Rescue Robotics, Workshop, 2005 IEEE International*. IEEE. 2005, pp. 218–223.

[96] DL Smith et al. "The Station Uniform Shirt: Does it play a role beyond appearance?" In: *Firehouse magazine* (2013).

[97] MM Atia, MJ Korenberg, and A Noureldin. "Particle-Filter-Based WiFi-Aided Reduced Inertial Sensors Navigation System for Indoor and GPS-Denied Environments". In: *International Journal of Navigation and Observation* 2012 (2012).

[98] Y Li and C Rizos. "Triple Integration of GPS, Locata and INS for Seamless Integrated Navigation in Urban Environments [Z]". In: *Proceedings of 2010 International Symposium on Inertial Technology and Navigation, NanJing*. Citeseer. 2010.

[99] Chris Rizos et al. "Experimental results of Locata: A high accuracy indoor positioning system". In: *Indoor Positioning and Indoor Navigation (IPIN), 2010 International Conference on*. IEEE. 2010, pp. 1–7.

[100] Markus Klann et al. "Lifenet: an ad-hoc sensor network and wearable system to provide firefighters with navigation support". In: (2007).

[101] Valérie Renaudin et al. "Indoor navigation of emergency agents". In: *European Journal of Navigation* 5.3 (2007), pp. 36–45.

[102] Federica Pascucci and Roberto Setola. "An adaptive localization system for first responders". In: *Proceedings of the 1st International Conference on Wireless Technologies for Humanitarian Relief*. ACM. 2011, pp. 109–114.

[103] Federica Pascucci and Roberto Setola. "An indoor localization framework for hybrid rescue teams". In: *Proceedings of the 18th IFAC World Congress*. 2011.

[104] Nan Li et al. "A BIM centered indoor localization algorithm to support building fire emergency response operations". In: *Automation in Construction* 42 (2014), pp. 78–89.

[105] Luıs Pinto et al. "On-the-Fly Deployment of Wireless Sensor Networks for Indoor Assisted Guidance". In: ().

[106] Antonio R Jimenez et al. "A comparison of pedestrian dead-reckoning algorithms using a low-cost MEMS IMU". In: *Intelligent Signal Processing, 2009. WISP 2009. IEEE International Symposium on*. IEEE. 2009, pp. 37–42.

[107] Robert Harle. "A survey of indoor inertial positioning systems for pedestrians". In: *Communications Surveys & Tutorials, IEEE* 15.3 (2013), pp. 1281–1293.

[108] Antonio R Jiménez, Francisco Zampella, and Fernando Seco. "Improving inertial pedestrian dead-reckoning by detecting unmodified switched-on lamps in buildings". In: *Sensors* 14.1 (2014), pp. 731–769.

[109] Jiuchao Qian et al. "Vector graph assisted pedestrian dead reckoning using an unconstrained smartphone". In: *Sensors* 15.3 (2015), pp. 5032–5057.

[110] Oleg Mezentsev, Jussi Collin, and Gerard Lachapelle. "Pedestrian Dead Reckoning–A Solution to Navigation in GPS Signal Degraded Areas?" In: *Geomatica* 59.2 (2005), pp. 175–182.

[111] Xuebing Yuan et al. "Indoor pedestrian navigation using miniaturized low-cost MEMS inertial measurement units". In: *Position, Location and Navigation Symposium-PLANS 2014, 2014 IEEE/ION*. IEEE. 2014, pp. 487–492.

[112] Wonho Kang and Youngnam Han. "SmartPDR: smartphone-based pedestrian dead reckoning for indoor localization". In: *Sensors Journal, IEEE* 15.5 (2015), pp. 2906–2916.

[113] Agata Brajdic and Robert Harle. "Walk detection and step counting on unconstrained smartphones". In: *Proceedings of the 2013 ACM international joint conference on Pervasive and ubiquitous computing*. ACM. 2013, pp. 225–234.

[114] Valérie Renaudin, Melania Susi, and Gérard Lachapelle. "Step length estimation using handheld inertial sensors". In: vol. 12. 7. Molecular Diversity Preservation International, 2012, pp. 8507–8525.

[115] Wiebren Zijlstra. "Assessment of spatio-temporal parameters during unconstrained walking". In: *European journal of applied physiology* 92.1-2 (2004), pp. 39–44.

[116] Rolf Moe-Nilssen and Jorunn L Helbostad. "Estimation of gait cycle characteristics by trunk accelerometry". In: *Journal of biomechanics* 37.1 (2004), pp. 121–126.

[117] Anshul Rai et al. "Zee: zero-effort crowdsourcing for indoor localization". In: *Proceedings of the 18th annual international conference on Mobile computing and networking*. ACM. 2012, pp. 293–304.

[118] Robert W Levi and Thomas Judd. "Dead reckoning navigational system using accelerometer to measure foot impacts". Pat. US Patent 5,583,776. 1996.

[119] Jeong Won Kim et al. "A step, stride and heading determination for the pedestrian navigation system". In: *Positioning* 1.08 (2004), p. 0.

[120] Harvey Weinberg. "Using the ADXL202 in pedometer and personal navigation applications". In: *Analog Devices AN-602 application note* 2.2 (2002), pp. 1–6.

[121] et al. Siciliano Bruno. *Robotics: modelling, planning and control*. Ed. by Springer Science & Business Media. 2010.

[122] G Whaba. "A least squares estimate of spacecraft attitude". In: *SIAM Review* 7.3 (1965), p. 409.

[123] Malcolm D Shuster and WAYNE F Dellinger. "Spacecraft attitude determination and control". In: *Fundamentals of Space Systems* (1994), pp. 236–325.

[124] Malcolm David Shuster and SD Oh. "Three-axis attitude determination from vector observations". In: *Journal of Guidance, Control, and Dynamics* 4.1 (1981), pp. 70–77.

[125] Roberto G Valenti, Ivan Dryanovski, and Jizhong Xiao. "Keeping a Good Attitude: A Quaternion-Based Orientation Filter for IMUs and MARGs". In: *Sensors* 15.8 (2015), pp. 19302–19330.

[126] F Landis Markley and Daniele Mortari. "Quaternion attitude estimation using vector observations." In: *Journal of the Astronautical Sciences* 48.2 (2000), pp. 359–380.

[127] Phil Kim and Lynn Huh. *Kalman filter for beginners: with MATLAB examples*. CreateSpace, 2011.

[128] Anton J Haug. *Bayesian estimation and tracking: a practical guide*. John Wiley & Sons, 2012.

[129] Dimitri P Bertsekas et al. *Dynamic programming and optimal control*. Vol. 1. 2. Athena Scientific Belmont, MA, 1995.

[130] Angelo Maria Sabatini. "Estimating Three-Dimensional Orientation of Human Body Parts by Inertial/Magnetic Sensing". In: *Sensors* 11.2 (2011), p. 1489. ISSN: 1424-8220.

[131] Mohammad Ashfak Habib et al. "Smartphone-based solutions for fall detection and prevention: challenges and open issues". In: *Sensors* 14.4 (2014), pp. 7181–7208.

[132] Jiangpeng Dai et al. "PerFallD: A pervasive fall detection system using mobile phones". In: *Pervasive Computing and Communications Workshops (PERCOM Workshops), 2010 8th IEEE International Conference on*. IEEE. 2010, pp. 292–297.

[133] Mark V Albert et al. "Fall classification by machine learning using mobile phones". In: *PloS one* 7.5 (2012).

[134] Jian Liu et al. "Patterns of bipedal walking on tri-axial acceleration signals and their use in identifying falling risk of older people". In: *Computer and Information Technology, 2006. CIT'06. The Sixth IEEE International Conference on*. IEEE. 2006, pp. 205–205.

[135] Alan K Bourke et al. "Design and test of a long-term fall detection system incorporated into a custom vest for the elderly". In: (2008).

[136] Jiangpeng Dai et al. "Mobile phone-based pervasive fall detection". In: *Personal and ubiquitous computing* 14.7 (2010), pp. 633–643.

[137] Yanjun Li et al. "Accelerometer-based fall detection sensor system for the elderly". In: *Cloud Computing and Intelligent Systems (CCIS), 2012 IEEE 2nd International Conference on*. Vol. 3. IEEE. 2012, pp. 1216–1220.

[138] Wang Ye and Bai Xiang-yu. "Research of fall detection and alarm applications for the elderly". In: *Mechatronic Sciences, Electric Engineering and Computer (MEC), Proceedings 2013 International Conference on*. IEEE. 2013, pp. 615–619.

[139] Miao Yu et al. "An online one class support vector machine-based person-specific fall detection system for monitoring an elderly individual in a room environment". In: *Biomedical and Health Informatics, IEEE Journal of* 17.6 (2013), pp. 1002–1014.